Electrical Transport Properties of Ultrathin Amorphous Bismuth Films near the Superconductor-Insulator Transition

A DISSERTATION

SUBMITTED TO THE FACULTY OF THE GRADUATE SCHOOL

OF THE UNIVERSITY OF MINNESOTA

BY

Yen-Hsiang Lin

IN PARTIAL FULFILLMENT OF THE REQUIREMENTS

FOR THE DEGREE OF

Doctor of Philosophy

Allen M. Goldman, Advisor

August, 2011

Acknowledgements

There are many people who have earned my appreciation for their contribution to this research project and to my life in the past six years. I would specially give my thanks to: Allen Goldman, my mentor. Your enthusiasm, patience, and knowledge set up a role model of an outstanding scientist. Your advising is life-long lasting for me. My parents and my brother. Thank you all for the endless support and encouragement, which is not only for the last six years but started since I was born. Hsiang-Yi Karen Yang, my wife. Your unconditional love supports me through all the difficulties in the past few years. Professor Alex Kamenev, Beth Stadler, and James Kakalios for serving on my oral committee. The entire condensed matter faculty for very useful courses, advice and encouragement. Many current and former members of the Goldman group, each of whom contributed advice, support, and/or direct help for this project. Kevin Parendo and Sarwa Tan, who patiently taught and helped me to start in the field. Yu Chen, and Stephen Synder for your help with AFM and useful discussions. Jack Hellerstedt for processing STO substrates. Alexey Kobrinsikii, Javia Garcia-Barriocanal, Xiang Leng, JJ Nelson Yeonbae Lee, Joseph Kindey, IlanaPercher for useful discussions. Lastly, the members of the physics Machine Shop, especially Carl Johnson, Jon Kilgore, and William Voje, with their efforts in machining to improve the experimental equipment and in supplying liquid helium to run the experiment. To all my friends in Minnesota for making my life joyful.

Dedication

To those who held me up over the years

Abstract

A combination of thickness- and perpendicular magnetic field- tuning of SI transitions has been performed on quench-deposited homogeneous *a*-Bi thin films with a 14.67 Angstrom *a*-Sb underlayer. Transport properties, including measurements of resistance and of I-V characteristics have been studied in both the insulating and superconducting regimes. In the insulating regime, the resistance exhibits an Arrhenius type of conduction and the magnetoresistance (MR) exhibits a peak in perpendicular magnetic field. Furthermore, a possible quantum phase transition is found in the insulating regime. Presumably this transition is between the Bose and Fermi insulators discussed in the literature. The I-V characteristics exhibit strong non-linearities in the insulating regime at low temperatures. These non-linear curves can be well described by a heating model involving the decoupling of the electronic and phononic degrees of freedom at low temperatures. On the conductive or superconducting side of the transition, the transport properties are found to be remarkably similar to those of an overdamped random Josephson junction array, and vortex dynamics dominates the conductive behavior in both zero and non-zero magnetic fields. These observations suggest that isolated superconducting islands or localized Cooper pairs exist in both the insulating and conductive regimes. An AFM scan of the last film in the sequence has revealed that this series of films although continuous, has thickness variations on a mesoscopic length scale. Therefore, it is not surprising that there may be superconducting islands. The AFM scan also suggests that some of the thick, nominal granular films grown by quench condensed deposition are directly connected with large thickness variations. These insulating granular films also exhibit an Arrhenius type conduction at low temperatures, which reveals the existence of a hard gap in the electronic density of states, which is consistent with the theory of Feigel'man et al.. However, the activation energy of the Arrhenius type conduction found in the thickness tuning homogeneous a-Bi films doesn't follow this model. Therefore, the model may not completely explain the hard gap.

Contents

List of Tables

List of Figures

Chapter 1

Introduction

The electrical transport properties of two-dimensional (2D) electron systems have been studied extensively for a number of years. Such investigations provide an opportunity to study a wide variety of quantum phenomena. With improvements in technology and instrumentation, different regimes of electrical transport are found in the limit of zero temperature in various 2D thin films. These observations reveal the existence of different quantum mechanical ground states. By changing some parameter of a system, transitions between ground states in the limit of zero temperature can be realized. These transitions between different ground states and their critical behaviors are one of the active fields in contemporary condensed matter physics.

Superconductivity in 2D and quasi-2D systems has been of interest because of the possibility of quantum critical behavior and because of connections to the 2D aspects of superconductivity in high-critical-temperature (high-T_c) cuprates.

Experimentally, ultra-thin superconducting films can be fabricated by quench-condensed deposition, which is the thermal evaporation of material onto liquid helium cooled substrates. Films grown with this technique can be disordered on

an atomic scale, when deposited on a substrate precoated with a thin a-Ge or a-Sb[1]. These films are often referred to as homogeneous amorphous films, as they are only disordered on an atomic scale. On the other hand, films grown by directly depositing the metal onto the substrate will exhibit mesoscopic disorder, and are referred to as granular films. Previous work found that the homogeneous amorphous films can exhibit a superconductor-insulator (SI) transition by tuning either film thickness, external magnetic fields, or the density of electrons[3, 4].

Recently the application of a magnetic field perpendicular to the film plane has been the most extensively used tuning parameter in the study of SI transitions. There are reports of large magnetoresistance peaks in the insulating regime of superconducting films in perpendicular magnetic fields [6, 7, 8, 9]. Although this effect was first observed and interpreted as evidence of a Bose insulating regime by Paalanen, Hebard, and Ruel [10] almost two decades ago, recent experiments have displayed enhancements of resistance by many more orders of magnitude. In addition to the appearance of a giant magnetoresistance peak, other phenomena have also been reported near the perpendicular magnetic field tuned SI transition. The resistance vs temperature, $R(T)$, follows an Arrhenius type conduction form[7, 9, 13]:

$$R = R_0 exp(T_0/T) \tag{1.1}$$

This is instead of the variable range hopping form usually found in a disordered electron system. The current-voltage (I-V) characteristics are also found to be very non-linear in this regime[11, 12]. It has been suggested that these strange phenomena are related to a possible special insulating state, perhaps a superinsulator.

These recent investigations have been carried out on films of amorphous InO_x and polycrystalline TiN ranging in thickness from tens to hundreds of Angstroms, and on nano-honeycomb patterned amorphous Bi films. In work on much thinner films prepared by quench-condensation, which are homogeneously disordered, and which exhibit a direct perpendicular field driven SI transition[14], a peak in resistance vs. perpendicular magnetic field in the insulating regime, has never been observed over the range of parameter space explored. Also, the conductivity on the insulating side of the SI transition is found to be describable by the models of variable range hopping or quantum corrected metals[4, 14]. The tacit assumption that all homogeneously disordered films should exhibit properties, which are the same as those of InO_x and TiN, may not be the case.

In most previous work on quench-condensed homogeneous films, normal resistances were very close to the critical values associated with thickness- or charge-tuned SI transitions. The present work was motivated by the desire to discern whether a peak in the magnetoresistance, Arrhenius type conduction and non-linear I-V characteristics were ever observable in homogeneously disordered, quench-evaporated films of metals. Transport properties were measured over a wide range of tuning parameters to see if the above mentioned phenomenon could be found in regimes away from criticality. The tuning parameters chosen for this study were thickness and perpendicular magnetic fields.

The main complication is that the microstructure and transport properties of these quench-condensed films will irreversibly be changed when they been warmed up. The work requires an apparatus that permits quench-condensed depositions and *in situ* measurements while applying different tuning parameters. Hernandez

et al. built up a system to achieve this goal[15] and Parendo made further modifications to improve the thermal contact and lower the noise background[16]. In the present work the system was further modified to apply perpendicular magnetic fields using a sample rotator. The noise background was further reduced as will be described in Chapter 2.

This dissertation mainly reports the results of investigations of a series of sequentially quench-deposited a-Bi films with a nominal 14.67Å thick a-Sb underlayer. The resistance vs. temperature, $R(T)$, in zero field with various thicknesses is shown in Fig. 1.1. The nominal film thicknesses range are from 19.94Å to 23.42Å with increments between successive films of 0.2Å on average. It is worth noting that there are differences between this set of films and those of previous work. Firstly, the underlayer of a-Sb is nearly 5Å thicker than those used in previous work. The films are thicker when they have measurable resistance at temperatures below 1K. The progression through the critical regime is very rapid, occurring over only a 0.2Å increment of thickness. The resistance at criticality measured at 300mK changes by 4 orders of magnitude. Although the information close to criticality, as tuned by thickness, for this set of films is missing, the data are still useful for the investigation of transport properties in perpendicular magnetic fields. The $R(T)$ curves don't exhibit local minimum in any one of the films at low temperature, which is a common feature of the behavior of granular films. This suggests that these films are not granular.

The data in Fig. 1.1 can be divided into two categories determined by the sign of dR/dT at low temperature. The negative signs correspond to the insulating branch and the positive signs are the superconducting branch. On both branches, we studied the transport properties in zero field and when perpendicular magnetic

fields were applied. We found a magnetoresistance peak with films that were sufficiently thick on the insulating branch. The curves of $R(T)$ of all the films in both zero and non-zero fields at low temperature all exhibited Arrhenius type conduction. They even exhibited a possible quantum phase transition with using magnetoresistance as the observable quantity. This phenomenon will be discussed in Chapter 3.

All the I-V characteristics on the insulating branch were very non-linear at the lowest temperatures. In Chapter 4, we describe a heating model involving the decoupling of the electrons and phonons. It can be used to describe our data. This indicates that the non-linearities of I-V curves in this series of a-Bi films are caused by heating of the carriers. This heating model also provides a quantitative way to estimate the electron temperature as a function of measuring current.

On the superconducting branch, the transport properties of the films in zero or non-zero field are similar to those of a random Josephson junction array (JJA). This will be discussed in Chapter 5. The conductivity can be described by thermally activated vortex motion, while quantum tunneling dominates at low temperature. In this chapter, we also report on the surface character as determined by an atomic force microscopic (AFM) scan. It suggests that the films are well connected, but with a 13% thickness variation on mesoscopic length scales. This may explain the difference between this series of films and those of previous work on quench-condensed homogeneous films.

In Chapter 7, we further discuss the Arrhenius type conduction that is found in granular films of different metals. A hard gap model proposed by Feigel'man *et al.* can described the activation energy variation of thickness-tuned granular films. Although the model appears to explain the Arrhenius conduction of granular films,

it cannot explain the activation energy in this series of homogeneous a-Bi films.

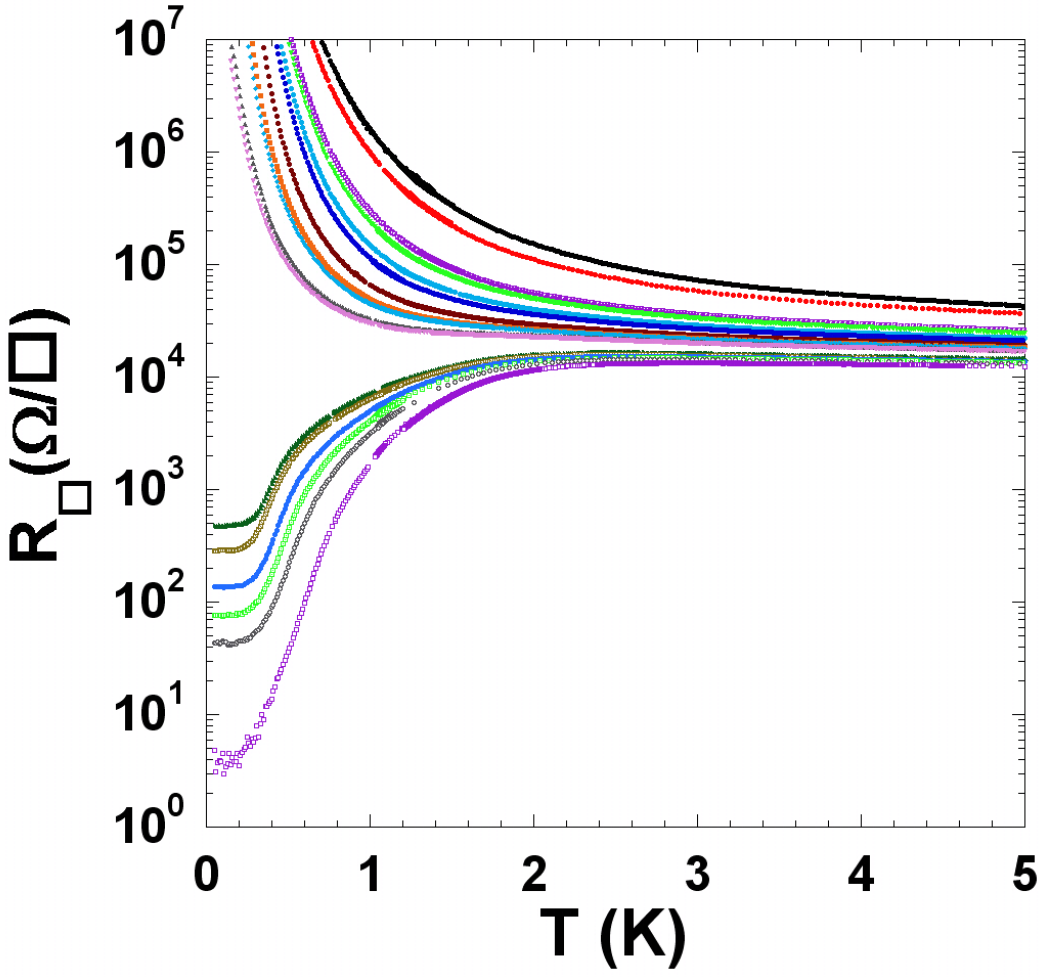

Figure 1.1: Resistance vs temperature of a series of sequentially quench deposited a-Bi films with a 14.67Å a-Sb underlayer. The thicknesses are 19.94Å(top), 20.16Å, 20.36Å, 20.53Å, 20.71Å, 20.91Å, 21.12Å, 21.38Å, 21.58Å, 21.80Å, 22.01Å, 22.24Å, 22.36Å, 22.63Å, 22.89Å, 23.15Å to 23.42Å(bottom).

Chapter 2

Experimental Apparatus and Techniques

2.1 Introduction

The quasi-two dimensional SI transition has been studied for more than two decades. Many different tuning methods had been used to explore the transition such as varying the thickness of the films or applying the external magnetic field, and changing the carrier concentration. New discoveries have been made as temperatures have been lowered, magnetic fields have been increased, and the orientation of magnetic fields has been varied.

We used the quench-condensation technique to grow ultrathin amorphous films. This involves the deposition of films onto cooled substrates as introduced by Shal'nikov[18]. In order to obtain reliable data one must perform the deposition with precision, carefully tracking film history, and maintaining a consistently clean vacuum environment. Without well-controlled vacuum conditions and a

well-controlled substrate temperature, substantial unknown variations of structure will be introduced. The microstructure of the resultant films strongly affects their electrical transport properties. The quench-deposition technique has been well developed for growing homogenous or granular quasi-two dimensional single element films[19, 3, 4] in last two decades.

Based on an earlier configuration of the instruments, we invested a substantial effort into extending the "phase space" of sample properties and performing more precise measurements. In this chapter, the combination of a dilution refrigerator and a deposition system will be described. The rotator for changing sample orientation, and the steps taken to reduce background noise will be discussed next. The last part of the chapter consists of a description of the sample preparation procedures and the determination of the geometric correction factor for resistance measurements.

2.2 Dilution Refrigerator and UHV Deposition System

The difficulty with this approach to sample preparation and characterization is that the films need to stay at temperatures lower than a characteristic temperature during the full course of measurements in order for their structure and properties to remain stable. The microstructure of the films and the transport mechanism will be changed significantly if they are warmed above this material dependent temperature. For amorphous Bismuth (a-Bi), which is the main material in this study, films crystallize as a semi-metal above 18K and no longer exhibit superconductivity at low temperatures[21]. Therefore, all processing and measurements of a-Bi must be kept below this temperature.

Hernandez *et al.* built a system to achieve this goal[15] and Parendo made further modifications to improve the thermal contact and noise background[16]. A schematic of the system from these works is shown on Fig. 2.1. The three main parts of the system are the Oxford Kelvinox 400 dilution refrigerator, an ultrahigh vacuum (UHV) thermal molecular beam epitaxy (MBE) deposition system, and a liquid helium flow-through cryostat. This combination allows for the electrical transport properties of films to be studied *in situ*, without warming or removing them from vacuum. The dilution refrigerator has a cooling power of 400μW at 100mK and a base temperature of approximately 0.004K. The $Nb-Ti$ superconducting magnet has a maximum field of 13 Tesla. The vacuum condition of the MBE system is maintained by 220l/s ion pump in a pressure range of $8 \times 10^{-10} \sim 1 \times 10^{-9}$torr. The distance between source and substrate is designed to be two feet, which ensures that the inhomogeneity in vapor flux at the sample due to geometry is less than one part in 10^4. The film thickness is monitored by quartz crystal microbalance (QCM) during the deposition. During the deposition, the liquid helium flow-though cryostat can maintain the temperature of the sample below 8K.

2.3 Sample Holder and Rotator

The original geometry of the superconducting magnet results in fields applied parallel to the plane of the sample. In order to study transport properties with different orientations of the external magnetic field, a device to change the direction of the sample, while maintaining its temperature below 10K is required. This has been achieved by modifying the sample holder and the transfer siphon. On the sample holder, a specially designed screw with a hollow ring at its end was

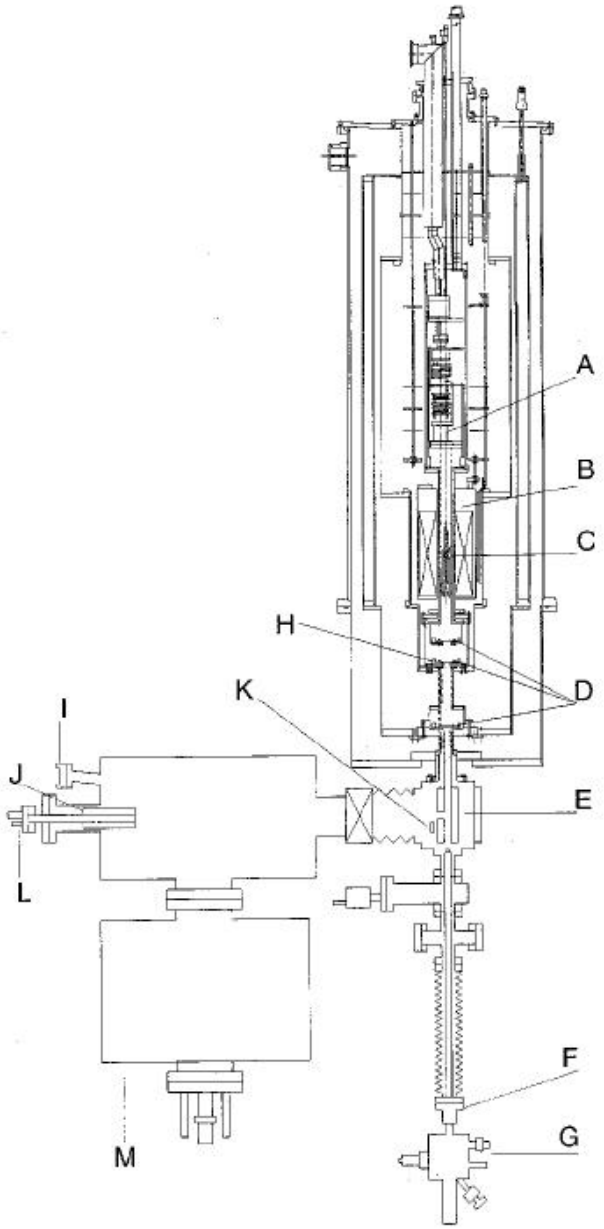

Figure 2.1: Schematic of the bottom-loading dilution refrigerator and the attached ultra-high vacuum deposition system. Including (A) the mixing chamber, (B) the superconducting solenoid, (C) the sample holder, (D) the radiation doors at 50mK(top), 4K, and 77K(bottom), (E) the liquid nitrogen shroud, (F) the rotatable ferrofluidic feedthrough, (G) the transfer siphon, (H) the sample holder keyway, (I) the window, (J) the second liquid nitrogen shroud, (K) the quartz crystal monitor, (L) the thermal evaporation cell, (M) the ion pump chamber. (Adapted from Ref.[15])

attached to the sample platform through a joint pin. The center of the platform was fixed to the sample holder as the rotation axis, and the platform could be rotated as long as the screw could be moved up or down with respect to the platform. The other end of the screw is engaged to a knuckle joint, which is extended to the bottom of the sample holder. The knuckle joint can be rotated relative to the sample holder and therefore is able to move the screw up or down. The screw is specially tapped so that it will no longer move up (down) when the platform is parallel (perpendicular) to the external magnetic field direction. The bottom end of the knuckle joint is connected to a cylinder sleeve with a key at its center.

The transfer siphon is a hollow tube, through which a long fiber glass driving rod is fit. This driving rod sticks out of the transfer siphon through an O-ring sealing port and is attached to a rotator dial. This design allows the driving rod to rotate and move up and down freely. A fork pin is attached to the end of the driving rod. The fork pin is fit inside of a bass adapter, which contains copper rollers to contact with the fork pin. These rollers inside the adopter allow the fork pin to be freely rotated, controlled by the driving rod. This adapter is directly screwed onto the top of the transfer siphon to cool down the fork pin. The fork pin can engage with the key of the cylinder sleeve without heating up the sample once it is cooled down to liquid helium temperature by the flow-though cryostat. Then, the sample platform can be rotated by rotating the dial at the bottom of the siphon.

During tests, several calibrated resistance thermometers were attached to the sample holder at different positions. We found that the sample holder and rotator could be cooled down to 14K using only the flow-though cryostat. Although this is already below the temperature at which amorphous Bismuth crystallizes, we

performed rotation when the sample holder was attached to the dilution refrigerator. We found that the cooling power from the dilution refrigerator could cool the sample below 4K during the entire process of rotation.

The other part of the sample holder and wiring to the dilution refrigerator preserved the original design of Hernandez and Parendo[15, 16]. This retains the consistency of the experiments and allows for new results to be compared with earlier ones.

2.4 Reduction of Background Noise

The combination of the dilution refrigerator and UHV deposition chamber introduced new problems. First, the deposition system contains electrical noise sources such as a turbo pump and ion pumps. These external sources of noise directly affect the electrical measurements. Furthermore, the Joule heating due to these noise sources will cause failure of the films to cool. Also, the complex electrical connections of the measurements and the deposition process will generate ground loops and therefore introduced unexpected noise. So, the reduction of background noise is crucial for the performance of precise electrical transport measurements at low temperature.

In order to separate the electrical connections of all of the pumps in the system from the measurement apparatus, we installed two isolators from CeramTec company. Each one is consist of an insulating ceramic ring with two conflat flanges at the two ends. These isolators directly break the electrical connection between the pumps and refrigerator and also remove the ground loop coming from the pumps.

All of the measurement instruments and the gas handling system for the mixture are controlled by computer through a GPIB connection. We use a GPIB-120A

isolator from National Instruments to isolate the measurement instruments from the computer. The power for all of the measurement instruments is connected through an isolation transformer. Finally, the dilution refrigerator and the measurement instruments are grounded through a grounding point to the clean power ground, which is isolated from the main ground.

With these efforts, the noise level was reduced at both in low and high frequencies. In order to test this, we compared the power spectral density (PSD) to that of a test resistance of around 30Ω. The PSD was obtained by two different methods in two different frequency ranges. The PSDs below 1Hz were obtained by taking a Fourier transform of a timed sampling of a voltage signal recorded by Keithley 2182A voltmeter, while the ones in the high frequency range were measured directly using an HP 3561A Dynamic Signal Analyzer. The comparison of PSD before and after the modification in low and high frequency ranges is shown in Figs. 2.2a and 2.2b respectively. In Fig. 2.2a, there are many low frequency noise peaks before the isolation was installed. Typically, these low frequency noise peaks came from mechanical vibration, which may be generated by the pumps. Also, the white noise PSD is reduced to $10^{-16}V^2/Hz$. In Fig. 2.2b, the noise peaks of 60Hz and their modulations are significant, which may come from the ground loops. After isolation and proper grounding, all the peaks were greatly reduced and the background noise level was lowered by two orders of magnitude.

2.5 Normal Cycle of Sample Preparation and Measurement

The dilution refrigerator, its dewars, and the UHV system were normally assembled during the normal cycle of sample preparation and measurement. With the bottom loading fridge, a freshly prepared substrate can be loaded even when the

dilution unit is cooled to 4K. Therefore, the refrigerator is usually maintained at low temperature. For the preparation of a new sample, wires must be attached to the substrate, and the substrate must be attached to the sample holder. Then the sample holder must be inserted into the inner vacuum space on the end of a transfer siphon. By cooling the flow-through cryostat, the sample can be attached to the dilution refrigerator. Then the deposition processes for tuning thickness can be performed by moving the sample back onto the transfer siphon and depositing onto it while it is in the UHV chamber. When a film is grown to a desired thickness, the sample platform can be rotated while the sample holder is still engaged with the dilution refrigerator. Then, the refrigerator can be cooled to its base temperature and measurements can be made. These processes of measurement, deposition, and rotation of the sample direction can be alternated at will. Therefore, the transport properties can be explore within the "phase space" of different thicknesses, directions and magnitudes of magnetic fields, and temperatures. At the end of a run the sample can either be removed from vacuum while the system is cold and under vacuum, or removed after having been warmed slowly. For samples whose surfaces were characterized the entire system was gradually warmed up in order to preserve the surface structure from changing which could happen with rapid warming.

2.6 Preparing the System for Cooling

To prepare the dilution refrigerator for cooling, the outer vacuum chamber (OVC) between the liquid nitrogen jacket and the outer world was pumped by using a Pfeiffer Balzers TPU 520M turbomolecular pump. Next, the inner vacuum chamber (IVC) that separates the dilution unit from the liquid helium dewar

was evacuated from the top port. The deposition chamber was first pumped by Leybold Trivac D4B mechanical rotary pump to about 60 mtorr. Then a 160l/s Leybold Turbovac 151C turbomolecular pump was turned on, and the system was pumped to about 10^{-6} torr. At this pressure, the system was then baked at temperatures between $100°C$ and $250°C$ to liberate adsorbed water vapor from the metal surfaces, taking care not to harm any non-metallic components. Both Knudsen effusion cells (K-cells) used for thermal deposition were heated for half an hour at temperatures of $50°C$ higher than the temperatures used for deposition. Baking was discontinued when the vacuum stabilized. The pressure falls and eventually reaches a minimum. Then, a 220 l/s ion pump was turned on. The pressure in the system will fall to a value in the range of 10^{-9} torr with the radiation doors closed. A check for leaks was usually performed by using a Stanford Research Systems Residual Gas Analyzer (RGA).

The dilution refrigerator was first cooled to 77 K by adding liquid nitrogen into the liquid helium space. A $5cm^3$ volume of 1 atmosphere pressure helium exchange gas was added, which will cool the dilution refrigerator to the same temperature as the bath by conduction. The magnet and dilution refrigerator were then cooled overnight to ensure that they are fully cooled to 77K.

The liquid nitrogen was then removed the next day. Liquid helium was then used to cool the liquid helium bath. When the mixing chamber and still of the fridge were near 10K, the exchange gas was removed by opening the doors of the deposition hexagonal chamber and pumping from the top port. When the pressure recorded by the RGA is stable, the 1K pot of the dilution unit can be cooled down to 1.4 to 1.7K. Then, the refrigerator is ready to engage with the sample holder and film deposition can proceed.

2.7 Sample Preparation and Deposition

The substrates were epi-polished (100) $SrTiO_3$ (STO) wafers which were purchased from Princeton Scientific Company. These substrates were 1/4 inches square, and 300μm thick. Although the manufacturer claimed the epi-polished side of these substrates had as R_{rms} roughness of less than 10nm, it has been reported that smoothness could be greatly improved by chemical etching and annealing[22, 23, 24]. The substrates that were used in this study were all cleaned first with acetone to remove organic contamination and then pre-annealed in a tube furnace with an O_2/O_3 atmosphere for two hours at 680°C to remove other contamination. After being cleaned, these substrates were soaked in DI water for thirty minutes. The H_2O reacts with SrO on the crystal surface and forms $Sr(OH)_2$ but TiO_2 is relative stable. Then the substrates were immersed in J. T. Baker 10:1 Buffer Oxide Etch(BOE), an aqueous $NH_4 - HF$ etch, for 20 seconds. This process removes the $Sr(OH)_2$ from the surface layer. Then, a final anneal of six hours in an O_2/O_3 atmosphere at 780°C was carried out to reconstruct the TiO_2 terminated surface. The annealing process promoted the formation of terraces on the surface with unit-cell step heights. A typical AFM scan of the treated substrates is shown in Fig. 2.3. One can clearly see the terrace structures with a width of around 200nm and a step height of around 3Å. This treatment provided substrates with atomic level smoothness, which is crucial for the growth of ultrathin films with thicknesses of around 10Å.

After treatment, 100Å thick Pt electrodes were deposited through an Al physical mask to form a four-probe arrangement, as shown in Fig. 2.4. The gaps between the electrodes were 0.5 mm, and the section where a film will eventually

be grown was 2.5mm long and 0.5mm wide. Schematics of the masks used to deposit Pt leads and the films are shown in Figs. 2.4a and 2.4b. The configurations are exactly the same as those used in the work of Hernandez and Parendo[15, 16], so that results can be directly compared.

The substrate was then attached to the sample holder with a very thin layer of Apiezon N-Grease. The N-Grease provides thermal contact between the sample holder and the substrate. The electrodes were connected to 4 mil diameter Cu wires with HML insulation, by low temperature Indium solder. The other ends of the wires were soldered to the appropriate sections of the All-Flex circuit of the sample holder, which was connected to the commutator rings on the top of the sample holder. The physical mask through which the film is deposited was then placed onto the sample holder. The outermost mask was then attached.

The sample holder must then be transferred onto the dilution refrigerator and cooled before any depositions. The sample holder is first screwed onto the transfer siphon and tightened with 40 inch-lbs of torque to ensure good thermal contact when cooling the siphon. Then, the sample holder can be cooled by the flow-though cryostat and engaged with the dilution refrigerator. The refrigerator and the sample holder then can be cooled down by condensing and circulating the $^3He/^4He$ mixture. At this point, the whole system is ready for deposition of a film.

Films were grown thermally by heating solid source materials with a K-cell. The source materials consist of 99.9999% pure Sb and 99.999% pure Bi shot. The vapor streams of these materials are aimed at a substrate that is cooled to at least liquid helium temperatures. The deposition rates for both materials can be controlled in around 0.08 ± 0.005Å/sec, which requires K-cell temperatures

of 710°C for Sb and 750°C for Bi. The presence or absence of an amorphous Sb (a-Sb) underlayer results in different morphologies. Directly depositing a-Bi onto bare substrates results in films with mesoscale clusters, which are often referred to as granular films. Films of a-Bi deposited onto an underlayer of (a-Sb) are believed to be disordered on a microscopic, rather than a mesoscopic length scale. In this study, we found that the thickness of the underlayer may also affect the morphology, and a comparison of films with different morphologies will be discussed later. The major part of this work is based on a-Bi films with 14.67Å a-Sb underlayer. After a film is deposited, it can be brought back to the dilution refrigerator to carry out transport measurements.

2.8 Measurement Techniques and Geometric Correct Factor

Transport properties of these films were measured using a standard four-terminal technique by injecting a bias current from a Keithley 6221 current source and by measuring voltage with a 2182A Keithley nanovoltmeter. The starting point involved first identifying the linear regime of the I-V characteristic, and two bias currents were chosen in this regime. The resistance was then measured by measuring voltage at these two bias currents and computing the slope. Temperatures of the dilution refrigerator are measured using a Picowatt AVS-47A resistance bridge. The temperatures of the samples have been shown to be in good thermal equilibrium with the dilution unit down to 60mK[16]. Measurements below 1K were taken by setting the temperature of the dilution refrigerator with TS-530 temperature controller within a 0.5 mK precision. Above 1K, a temperature range where the dilution refrigerator cannot be stabilized, resistance measurements were

taken by slowly cooling down at a rate of about 0.05K per minute. The external magnetic field was controlled by IPS 120-10 magnet power supply with a precision of 1 Gauss and at fields of up to 13 Tesla. The rate of change of external magnetic field was kept below 0.1 Tesla/minute to avoid the heating from Eddy currents.

Due to the geometry of the sample, the measured resistance of the film R_m needed to be corrected to obtain the sheet resistance $R_\square$. For films of this study, this correction was a constant scaling factor g, such that $R_\square = g \cdot R_m$. We obtained the correction factor g by two different methods. One was by a finite element analysis using the student version of QuickField software, which yielded 0.538. The other method involved performing a two-terminal measurement on the current leads of a film going through a superconducting transition by varying temperature. As shown in Fig. 2.4b, the sample resistance of between two current leads should be five times of sheet resistance. When the film is superconducting at low temperature, the measured resistance comes from the contact resistance and resistance in the circuit. The transition temperature range is around 1K and we assume the contact resistance doesn't change in this temperature regime. Above the transition, we thus can obtain the sheet resistance by subtracting the contact resistance and then divided by five. By comparing the four-terminal measurement with this sheet resistance, we obtained a geometric correction factor of 5.4, which is in agreement with the results of the finite element analysis. All the measured resistance were corrected by $g = 0.538$ in order to compare with theoretical models.

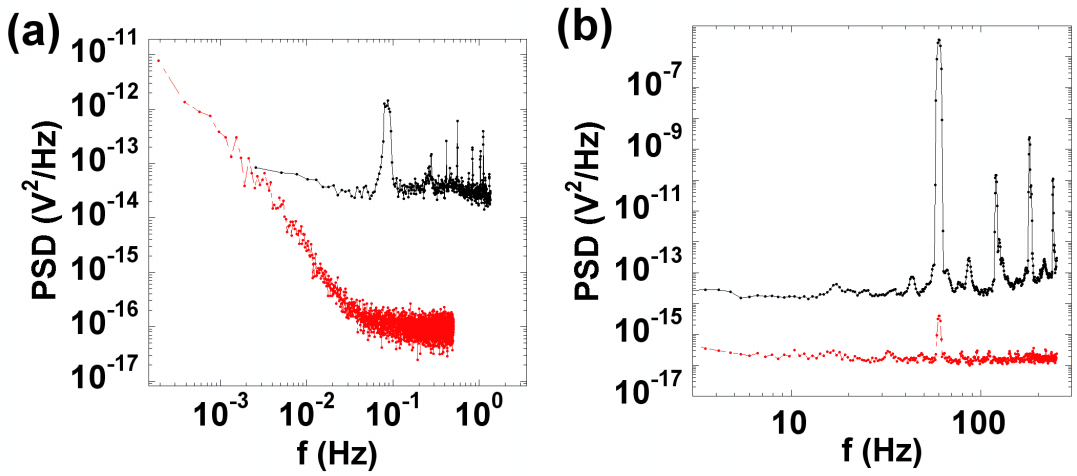

Figure 2.2: Comparison of PSD before(top) and after(bottom) installing the isolator and removing ground loops in frequency range of (a) below 1Hz and (b) $2 \sim 200$Hz.

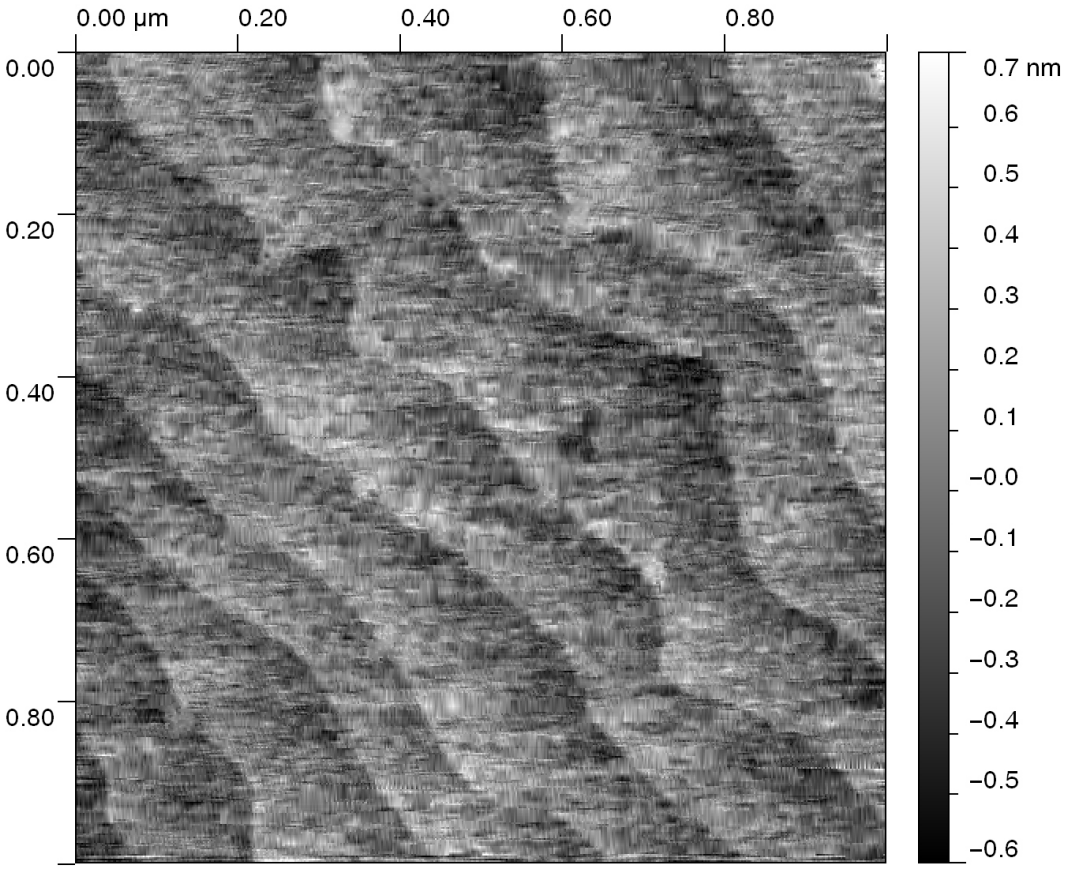

Figure 2.3: A $1\mu m \times 1\mu m$ AFM scan of a treated STO substrate. The treatment procedure is described in the text. It clearly shows a TiO_2 terminated[22] terrace structure.

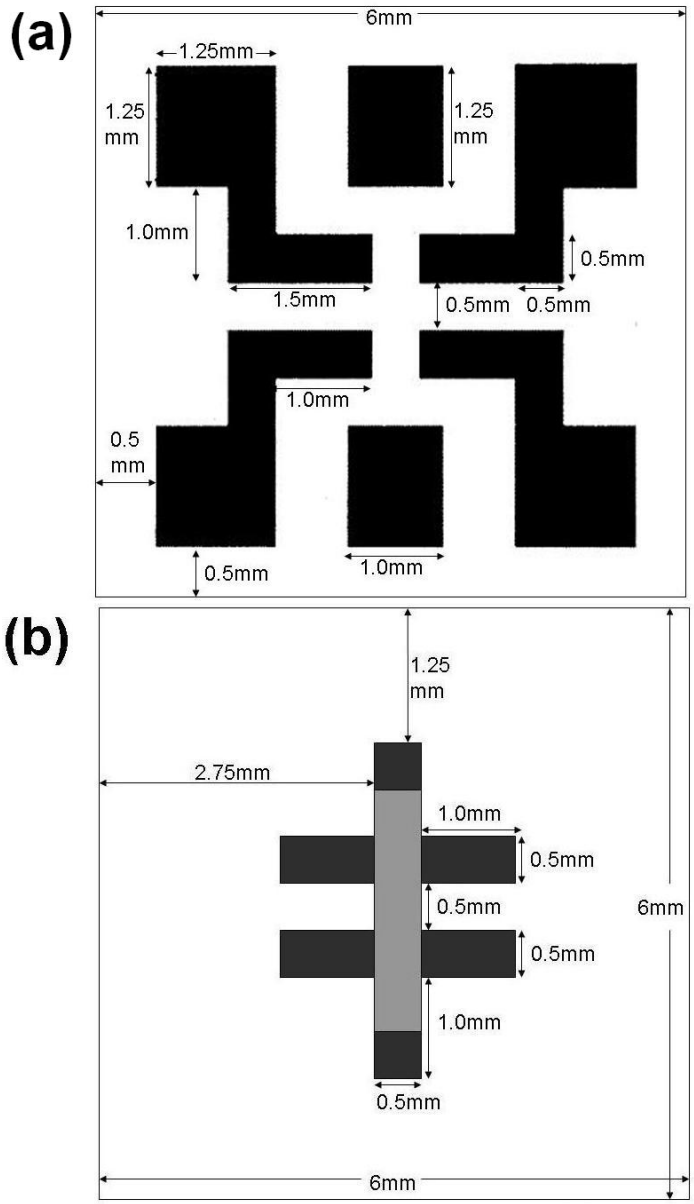

Figure 2.4: Schematic of the metal shadow mask used to deposit (a) 100Å thick Pt electrodes onto substrate. (b) a-Sb and a-Bi films. The black and dark regions in (a) and (b) denote holes in the mask through which material is deposited. The darker region denotes overlap of the film and the Pt electrodes. (Adopted from Ref.[16]).

Chapter 3

Magnetic Field Tuning of Insulating Homogeneous Amorphous Bi Films

3.1 Introduction

The perpendicular magnetic field tuned SI transitions of strongly disordered films has received lots of attention in recent years. The dirty-boson picture was proposed to describe the magnetic field tuned transition from superconductivity. In this picture the insulator consists of Bose-condensed, field-induced vortices and localized Cooper pairs [25]. In mentioned early experiment by Paalanen, Hebard and Ruel reported a *peak* in the magnetoresistance of InO_x films on the insulating side of the SI transition [26]. The behavior of the Hall resistance at fields close to the peak field led these authors to suggest that there was a crossover from the state proposed by Fisher in which there are localized Cooper pairs, to one in which transport is dominated by single-particle excitations. They referred to this as a crossover between Bose and Fermi insulators [26]. This peak in $R(B)$ in

the insulating regime of the field-tuned SI transition has been the subject of numerous investigations in recent years. With improvements in sample fabrication procedures and the introduction of new materials, changes of resistance of several orders of magnitude have been reported [27, 28, 7, 9, 30]. Also of interest in the present context are observations of Arrhenius activated behavior, *i.e.*, a hard gap in InO_x and TiN films both in zero field in insulating films, and in magnetic fields on the insulating side of the SI transition [31, 32, 9].

In this chapter, we report an apparent perpendicular magnetic field tuned quantum phase transition between two separate insulating ground states in thin films on the insulating side of the disorder or thickness-tuned superconductor-insulator transition. A central piece of evidence for this assertion is that isotherms of magnetoresistance (MR), which defined as

$$MR \equiv \frac{[R(B,T) - R(0,T)]}{R(0,T)} \times 100\% \tag{3.1}$$

cross at a well-defined magnetic field higher than that corresponding to the peak in $R(B)$.

3.2 Perpendicular Field Tuning and Magnetoresistance Peak

The data employed in the present work were obtained from studies of homogeneous amorphous Bi (a-Bi) films that were grown by quench-condensation *in situ* at liquid helium temperatures on (100) $SrTiO_3$(STO) single-crystal substrates precoated *in situ* with a 14.67Å underlayer of amorphous Sb (a-Sb). Films grown by deposition onto substrates held at liquid helium temperatures and precoated *in situ* with thin underlayers of either a-Ge or a-Sb are known to be homogeneous [1]. The underlayers have zero conductance within instrumental resolution. All

the measurements were carried out using a four-terminal configuration employing a DC current source with currents in the linear regime of the current-voltage (I-V) characteristic.

Representative examples of the evolution of $R(T)$ with thickness of several insulating films of a-Bi films are shown in Fig. 3.1. Representative data of $R(B)$ and the field dependence of the MR at 600mK in films ranging in nominal thickness from 19.74Å to 21.12Å are presented in Fig. 3.2 and Fig. 3.3. Peaks in R(B) are observed in films thicker than 20.53Å. The values of the magnitudes of the peaks in $R(B)$ and the fields at the peaks both increase with film thickness. It is important to note that large peaks in $R(B)$, at fields above the critical field of the SI transition have not been previously reported for superconducting films grown on substrates with a-Ge or a-Sb underlayers. On the other hand in the case of nominally granular quench-condensed films, grown on substrates that are not precoated, $R(B)$ increases dramatically with increasing field, rising to values several orders of magnitude higher than the normal resistance[33]. Such films are also exhibit nonmonotonic variations of $R(T)$ which are not found in precoated films. Giant magnetoresistance peaks have been found in studies of films quench-condensed onto substrates perforated with nanometer scale arrays of holes [34].

We now turn to the temperature dependence of $R(B)$ and the MR for films of specific thicknesses. Representative data of $R(B,T)$ for films, 20.91Å and 21.12Å thick, are presented in Figs. 3.4 and 3.5. The peak height increases with decreasing temperature, which is consistent with results reported for InO_x and TiN_x films. The peak field, B_{peak}, is a function of temperature and can be fit with the form:

$$B_{peak} = B_0 + \alpha T^{\beta} \tag{3.2}$$

over the range of temperatures studied, as shown in Fig. 3.6. From the measurements, $B_0 = 1.92 \pm 0.04$, $\alpha = 2.63 \pm 0.06$, and $\beta = 2.78 \pm 0.10$ for the 20.91Å thick film, and $B_0 = 2.37 \pm 0.07$, $\alpha = 3.791 \pm 0.09$, and $\beta = 2.41 \pm 0.13$ for the 21.12Å thick film. It is unclear as to whether any of the theoretical models for the peak, which will be considered later, are consistent with these observations.

3.3 Arrhenius Conduction

The temperature dependencies of the resistances of the 20.91Å and 21.12Å thick films at temperatures below 1K can be fit by an Arrhenius form:

$$R = R_0 exp(T_0/T) \tag{3.3}$$

in fields ranging from 0 to 10 T. This is shown in Figs. 3.7(a) and 3.7(b). The field dependencies of the activation energy $T_0(B)$, and the prefactor $R_0(B)$, are plotted in the lower halves of Figs. 3.8 and 3.9. The activation energy exhibits a peak at a magnetic field close to B_0 described in the previous paragraph.

The measurement of resistance at temperatures below 300mK is difficult for several reasons. The I-V characteristics become non-linear at currents larger than 1pA. The resistance itself becomes so large that combined with the capacitances in the measuring circuit, with its heavy filtering, results in an extraordinarily long time constant. Also, $R(T)$ can exceed the input impedance of the voltage amplifier, which can lead to erroneous results. Therefore, data below 300mK were questionable and were excluded.

The fact that these films exhibit an Arrhenius type conduction form is different from the results of previous studies of homogeneous *a*-Bi films by Markovic and Parendo[14, 20]. They found the conduction behavior on the insulating side of

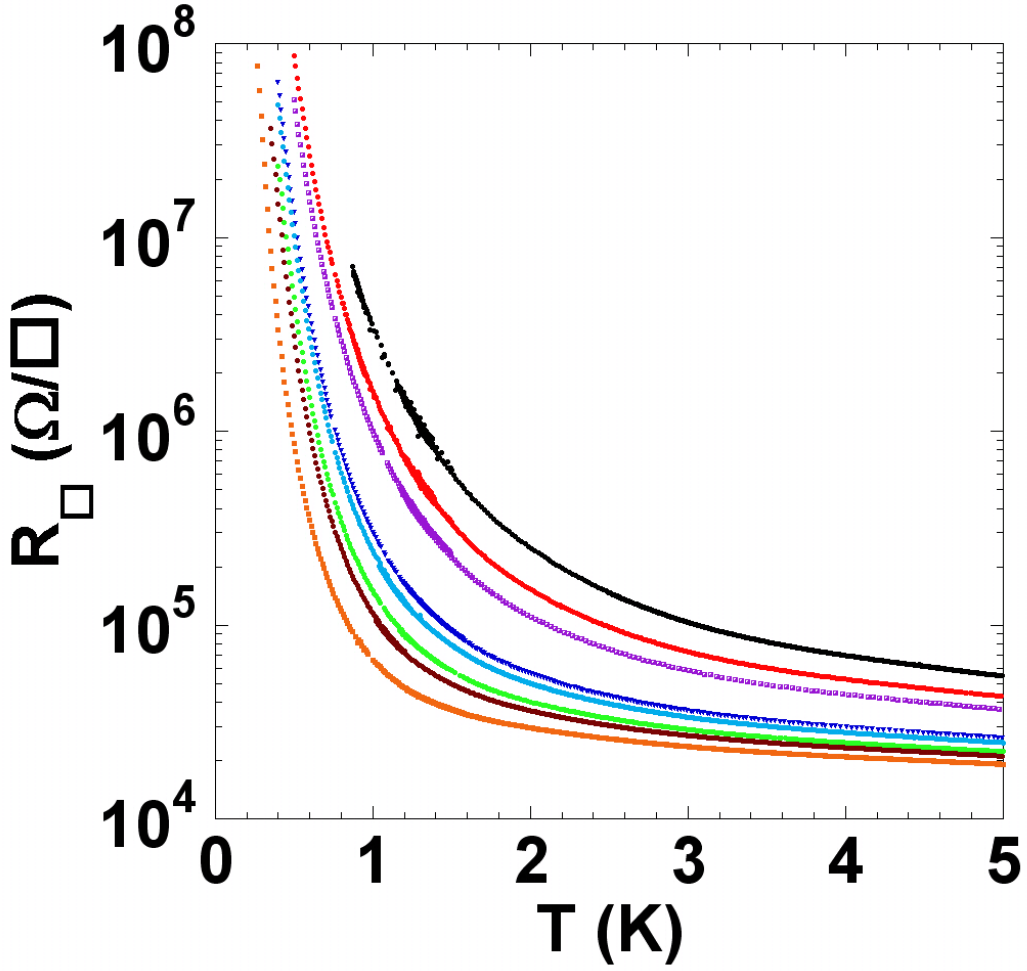

Figure 3.1: Zero field resistance vs. temperature of a sequence of nominally homogeneous *a*-Bi films with thicknesses of 19.74Å (top), 19.94Å, 20.16Å, 20.36Å, 20.53Å, 20.71Å, 20.91Å, 21.12Å (bottom). Notice that the resistances of these films monotonically increase with decreasing temperature and do not exhibit the local minima found in nominally granular films.

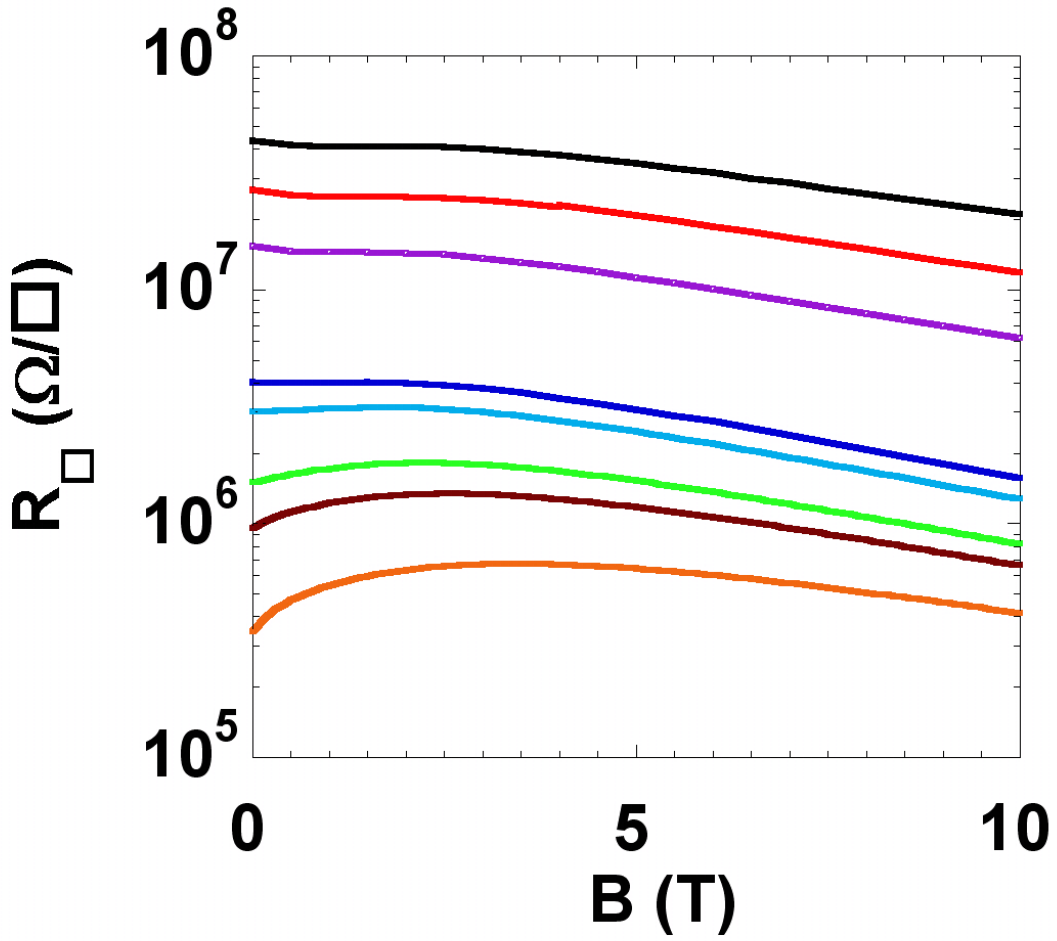

Figure 3.2: Resistance as a function of field at 600mK in films of thicknesses of 19.74Å (top), 19.94Å, 20.16Å, 20.36Å, 20.53Å, 20.71Å, 20.91Å, 21.12Å (bottom). The labels are thicknesses in units of Angstroms.

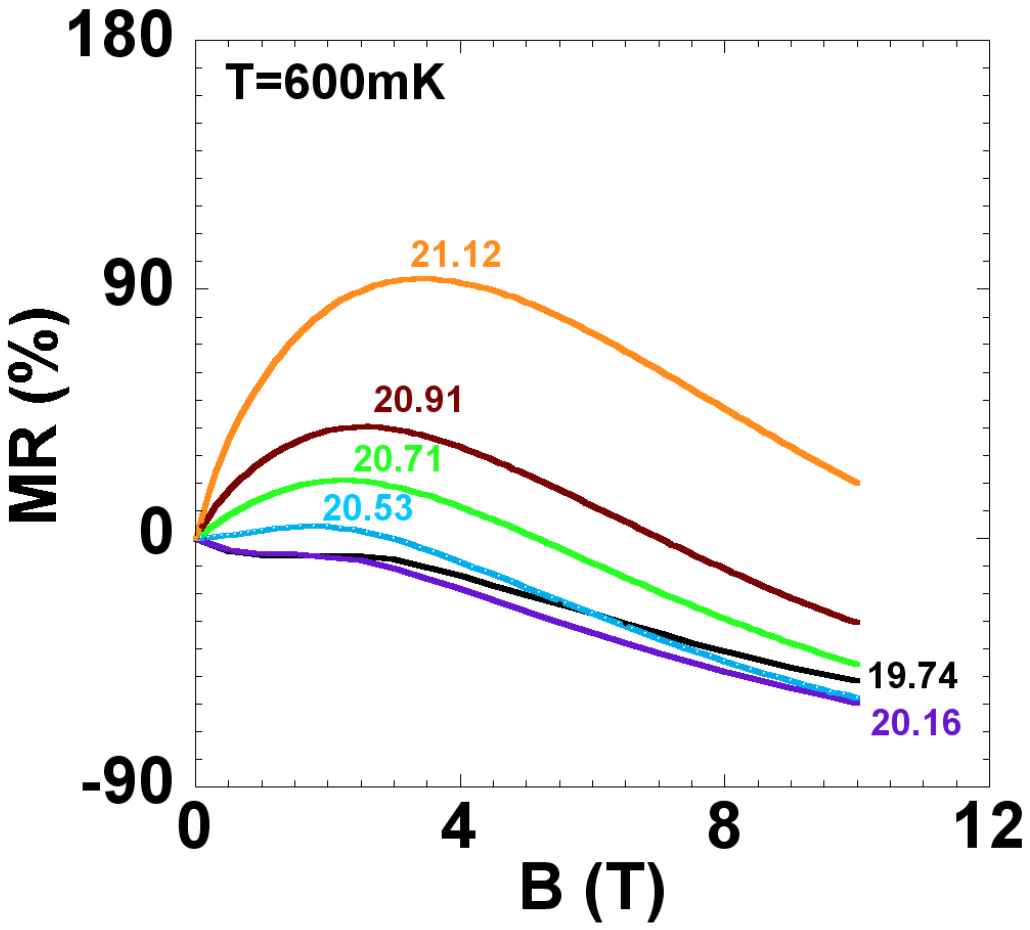

Figure 3.3: MR as a function of field at 600mK in films of different thicknesses. MR is defined inn the text. The labels are thicknesses in units of Angstroms. The data of the 19.94Å thick film was skipped for clarity.

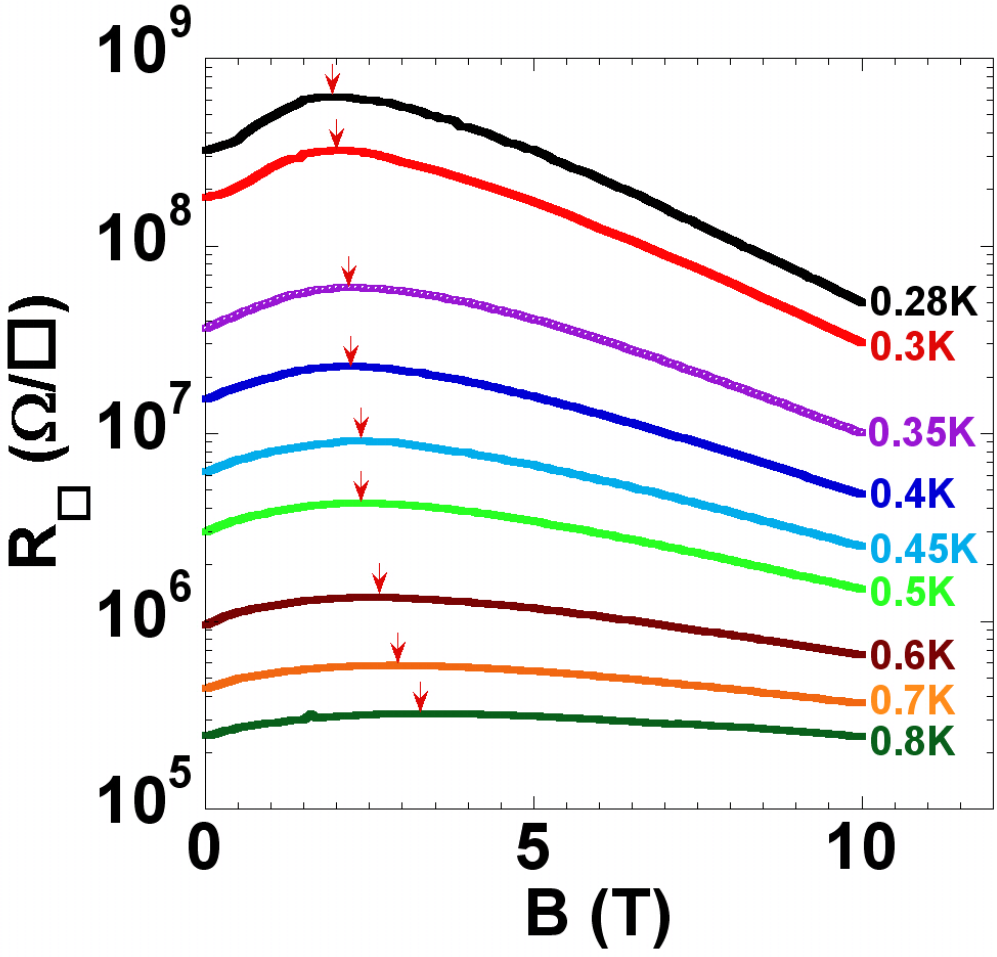

Figure 3.4: Sheet resistance vs. perpendicular magnetic field at different temperatures for the 20.91Å thick film. The arrows indicate the resistance peaks.

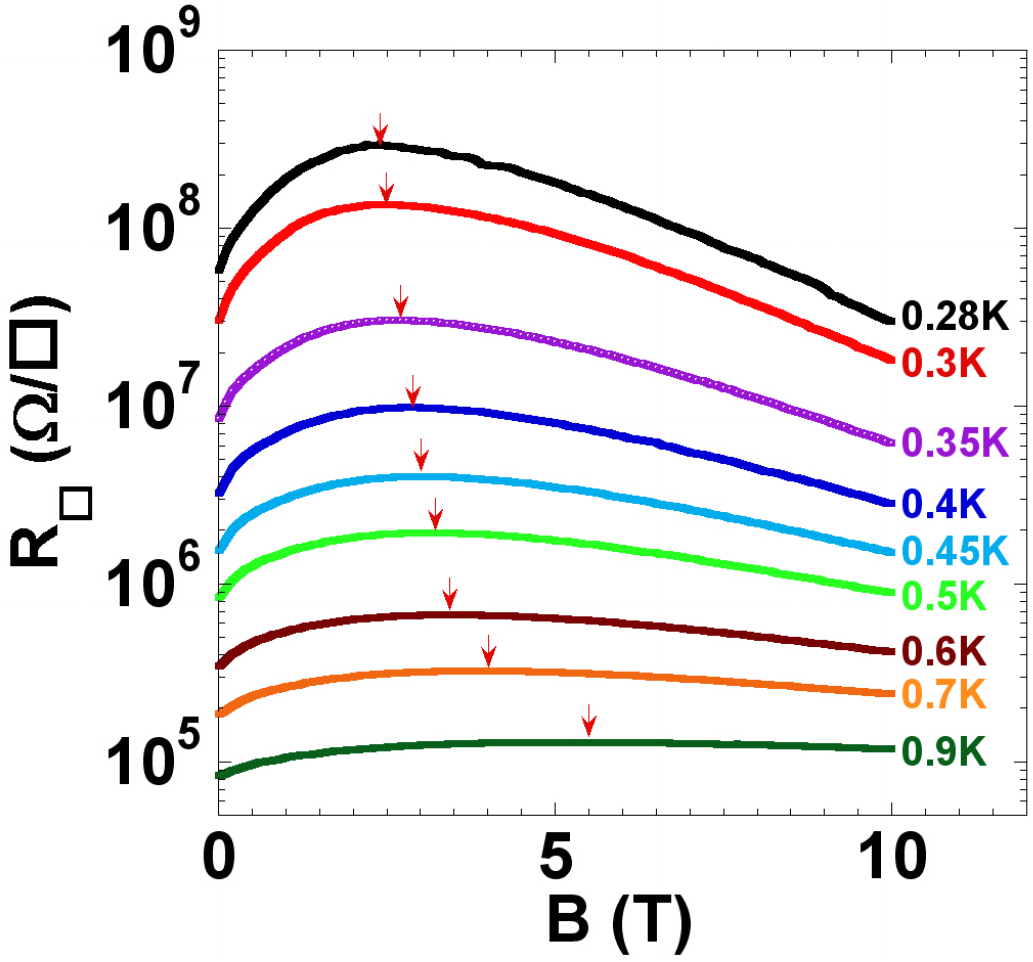

Figure 3.5: Sheet resistance vs. perpendicular magnetic field at different temperatures for the 21.12Å thick film. The arrows indicate the resistance peaks.

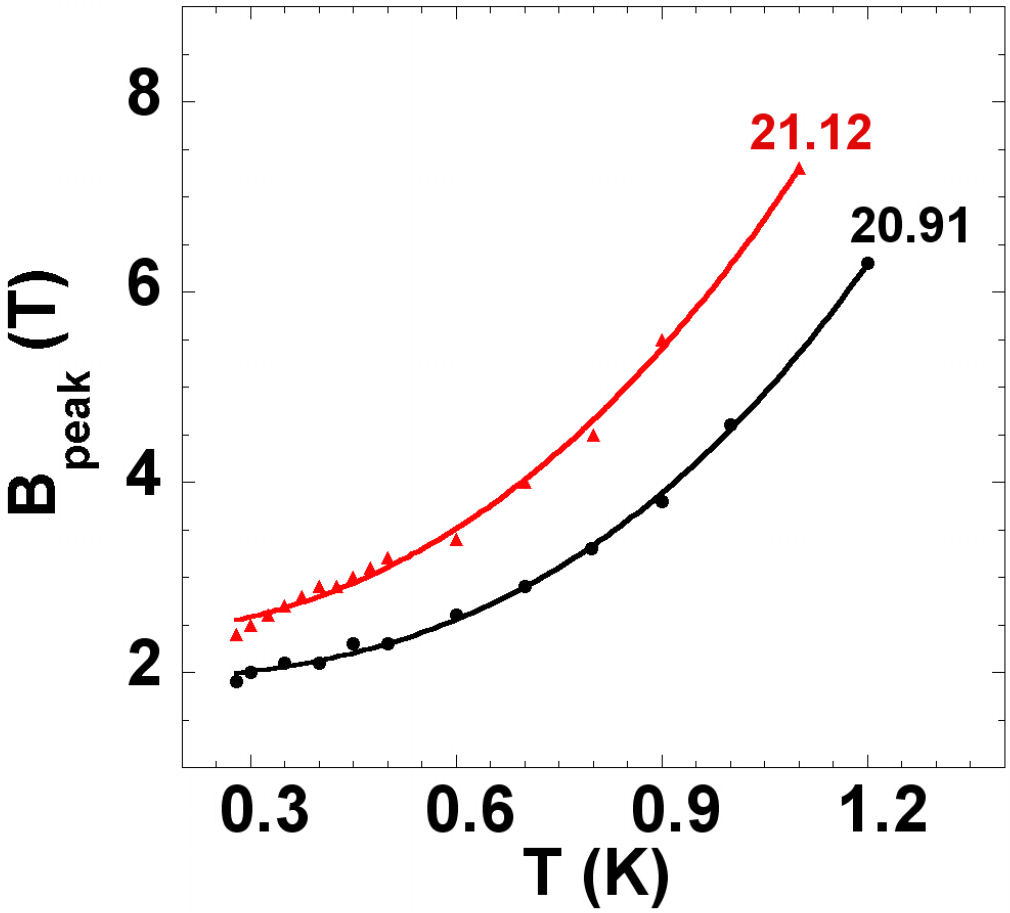

Figure 3.6: The magnetic field at the MR peak vs. temperature. The two thicknesses are labeled with numbers whose units are Angstroms.

the SI transition was governed by 2D Mott variable range hopping. With all the growth conditions controlled in the same manner as in those studies, the only difference is the thickness of the a-Sb underlayer, which is around 5Å thicker in the present work. After the whole series of films were studied, the surface of the thickest film was characterization by atomic force microspectroscopy(AFM). A 3Å thickness variation was found, which will be discussed in chapter 5. We suspect that the thicker underlayer lead to this thickness variation. Therefore, the difference in behavior may be due to the greater thickness of the a-Sb underlayer.

3.4 Perpendicular Field Tuned Quantum Phase Transition in the Insulating Regime

The most striking result is the occurrence of a crossover in the plot of the MR vs. B, as shown in Figs. 3(c) and 3(d). The magnetic field at the crossing point, B_c, corresponds to two features of the Arrhenius fit. First, the activation energy at this crossing field returns to the value it exhibited at zero field. Therefore, $T_0(B) - T_0(0)$ is always positive when $B < B_c$ and negative when $B > B_c$. Second, the prefactors, R_0, in these two films, are equal in value to $h/4e^2$, which is the quantum resistance for electron pairs. Parenthetically the first appearance of positive magnetoresistance at 600mK for the film thicker than 20.53Å also coincides with the zero field prefactor falling below $h/4e^2$. These three features lead us to suggest the existence of a quantum critical point at $B = B_c$ with the MR rather than R as the observable. Indeed, if the Arrhenius conduction were to extend to zero temperature, in zero temperature limit, we would expect

$$MR(B,T)|_{T\to 0} = \left[\frac{R_0(B)}{R_0(0)} exp(\frac{T_0(B)-T_0(0)}{T}) - 1\right]_{T\to 0}$$

$$= \begin{cases} \infty, & B < B_c \\ \frac{h/4e^2}{R_0(0)} - 1, & B = B_c \\ -1, & B > B_c \end{cases} \tag{3.4}$$

even though all resistances would diverge.

Further support for the idea of a quantum phase transition comes from the success of finite size scaling. Here we use the scaling form first introduced by Fisher[25]:

$$R = R_c \mathcal{F}(\frac{|B-B_c|}{T^{1/\nu z}}) \tag{3.5}$$

However, we use the MR as the observable in place of the resistance. Both films' data, within a certain range of fields and at sufficiently low temperatures can be scaled with critical exponent product $\nu z = 0.65 \pm 0.08$. This is shown in Fig. 3.10. With the assumption $z = 1$, this product would correspond to the universality class of a 2+1 dimensional XY model. Similar values have been found for magnetic field and electrostatically tuned SI transitions [14, 20]. The data points close to the peak in $R(B)$ and at high temperatures fail to scale, which may due to the limits on the size of the quantum critical regime.

It is interesting that the MR rather than the R isotherms as a function of B cross as a function of magnetic field. The low temperature zero field resistance must result from a combination of effects including the motion of strongly localized electrons as well as participation of presumably localized Cooper pairs. The application of a magnetic field to the film adds vortices and the behavior of these

added vortices results in a highly resistive phase that appears to disappear at a field-tuned quantum phase transition. That this high resistance phase and the observed crossover are associated with Cooper pairing is supported by the robust observation that at the crossover magnetic field the prefactor of the Arrhenius fit to the data is the quantum resistance for electron pairs.

Additional evidence for the presence of vortices in the film near the magnetoresistance peak is the anisotropy of magnetoresistance. At 400 mK for the 21.12Å thick film, our preliminary results of the MR in a 2.5T parallel field is 20.95%, while it is 198.7% in a 2.5T perpendicular field. This result is consistent with previous observations by Markovic *et al.*[35], which were also interpreted as the evidence of vortices in the insulating Bi films at low magnetic fields. With the ability to apply higher fields,than Markovic, we found the anisotropy diminishes when the field is larger than the peak field and vanishes near B_c. For instance, at 400mK the MRs in parallel and perpendicular fields of 7.3T are 56.2% and 60.6% respectively. This result is consistent with the idea that local superconductivity and vortices disappear close to to the field-tuned quantum phase transition.

To the best of our knowledge none of the models of the SI transition predict a quantum phase transition such as the one reported here, although it is quite possible that they may be extended to include one [25, 36, 17, 37, 38, 39, 40, 12].The condition of R_0 equal to $h/4e^2$ delineates a phase boundary in these thickness and field tuned insulating films as evidenced by two observations: the magnetoresistance peak is found only in the thicker films when the zero-field prefactor falls below $h/4e^2$ and the prefactor at the crossover field B_c is $h/4e^2$. This suggests that quantum fluctuations of vortices play a role in the present observations, that B_c is the critical field for the vanishing of local superconductivity, and that the

transition is from a Bose insulator with localized Cooper pairs to a Fermi insulator.

One might ask why these effects have not been observed previously, given the significant number of studies of the field-tuned superconductor-insulator transition. Most studies have focused on films that are superconducting in the absence of a magnetic field. Thus there is no zero-field reference resistance as would be needed to evaluate the magnetoresistance. Secondly the crossover field is at 3.9T and 7.3T for the two films reported here, with the 7.3T crossover a property of the less disordered film. With further reduction of disorder with an increase of thickness, the crossover did move to unattainably high values of magnetic field and be unobservable.

In summary, isotherms of the MR have been observed to cross at a well-defined magnetic field higher than that of the peak in $R(B)$ of quench-condensed insulating films of a-Bi. Curves of $R(T)$ at all magnetic fields follow an Arrhenius form for temperatures below 1K. The prefactor of this form becomes equal to the quantum resistance for pairs and the activation energy returns to its zero-field value at the crossover field. Data near the crossover are consistent with finite size scaling and the universality class of the $(2+1)D$ XY Model. We suggest that these observations are evidence of a quantum phase transition between two distinct insulating phases, which might be a Bose insulator to a Fermi insulator.

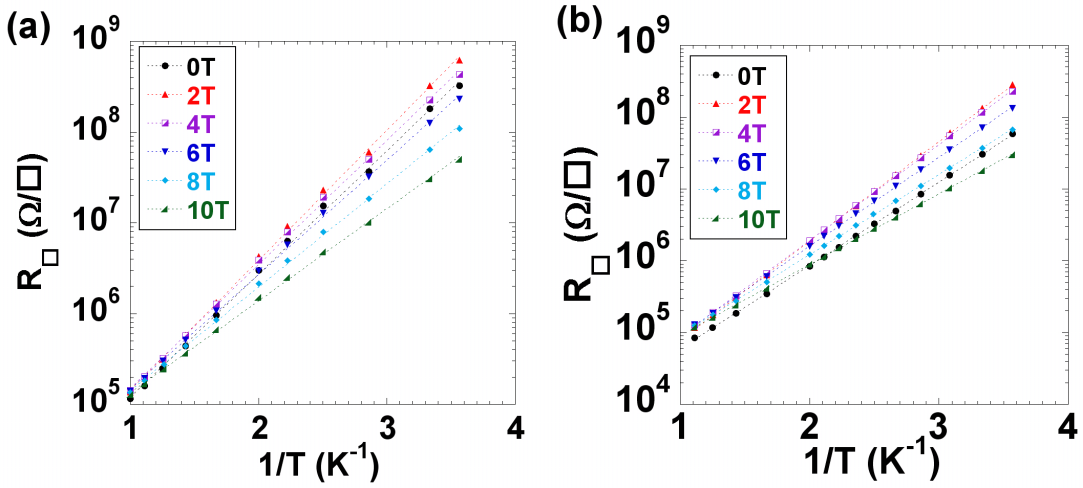

Figure 3.7: Arrhenius plots of the (a) 20.91Å and (b) 21.12Å thick films in six representative magnetic fields. The resistances increase by more than three decades in these two films within the temperature range from 1K to 0.28K.

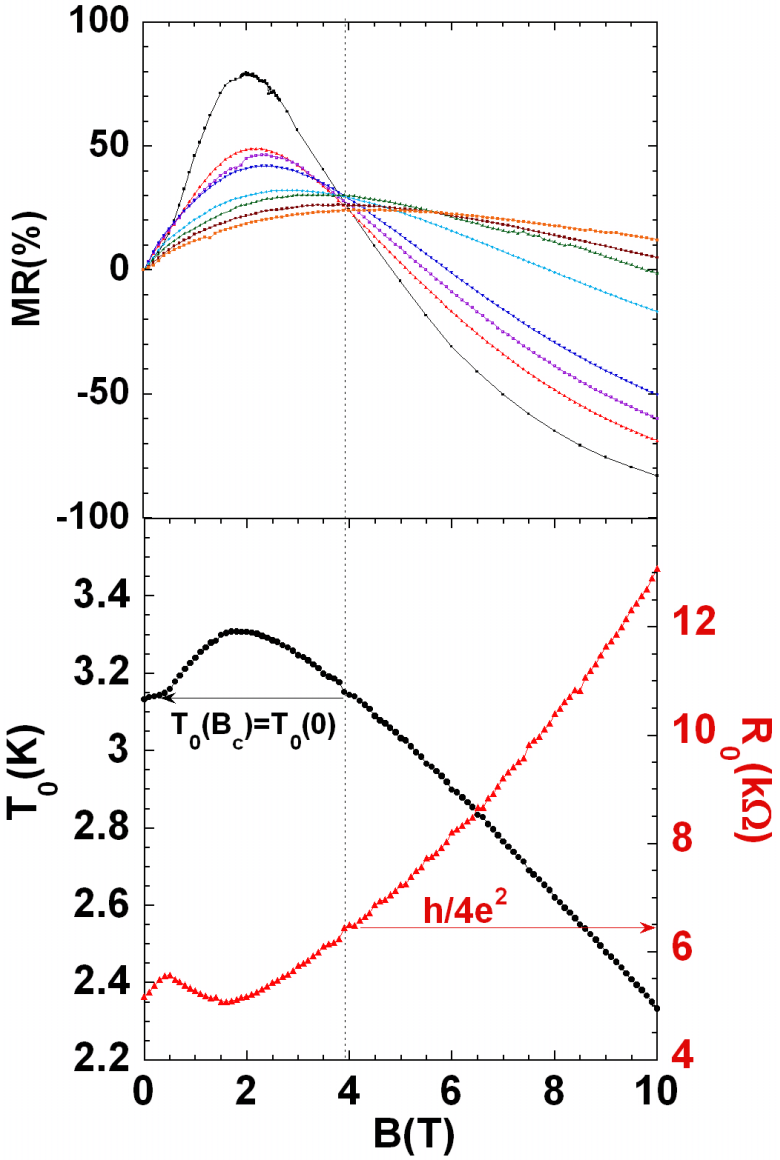

Figure 3.8: The MR, the activation energy T_0,and the prefactor R_0 vs. magnetic field of the 20.91Å thick film are plotted in the upper and lower panels. The MR is measured at 300mK, 400mK, 450mK, 500mK, 700mK, 800mK, 900mK, and 1K.

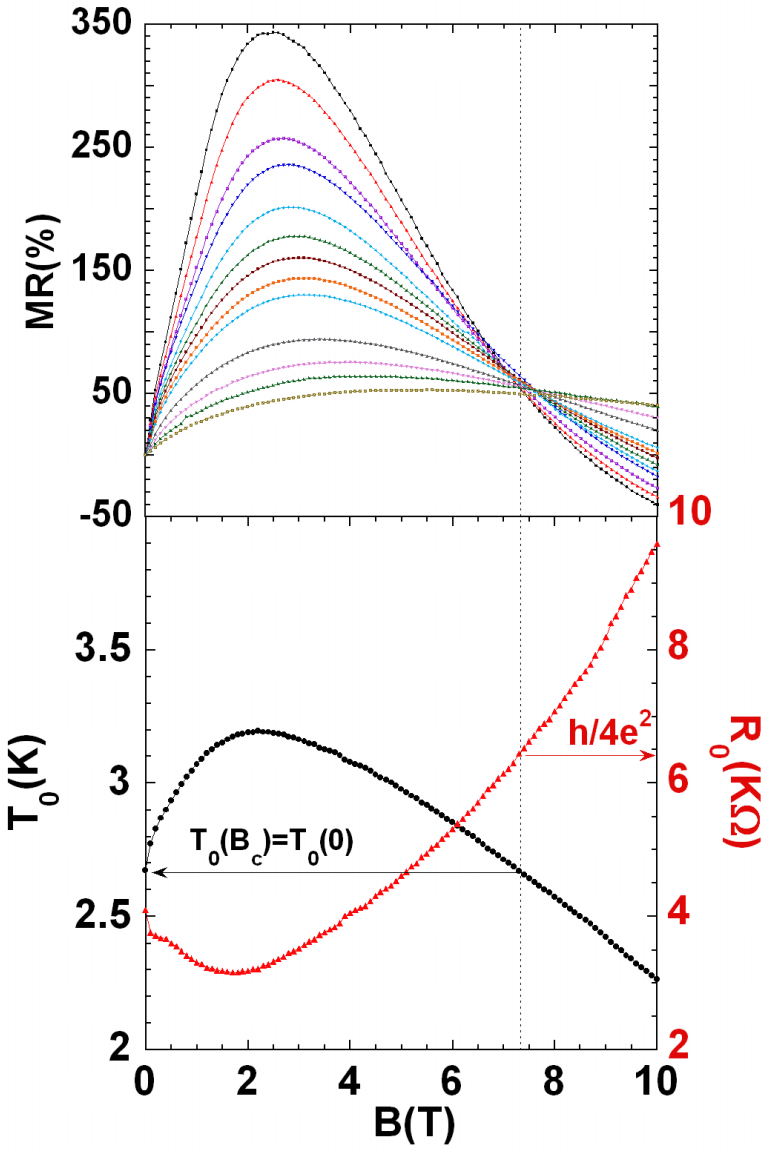

Figure 3.9: The MR, the activation energy T_0,and the prefactor R_0 vs. magnetic field of the 21.12Å thick film are plotted in the upper and lower panels. TheMR is measured at 300mK to 500mK with 25mK as the common increment and 500mK to 900mK with 100mK as the increment.

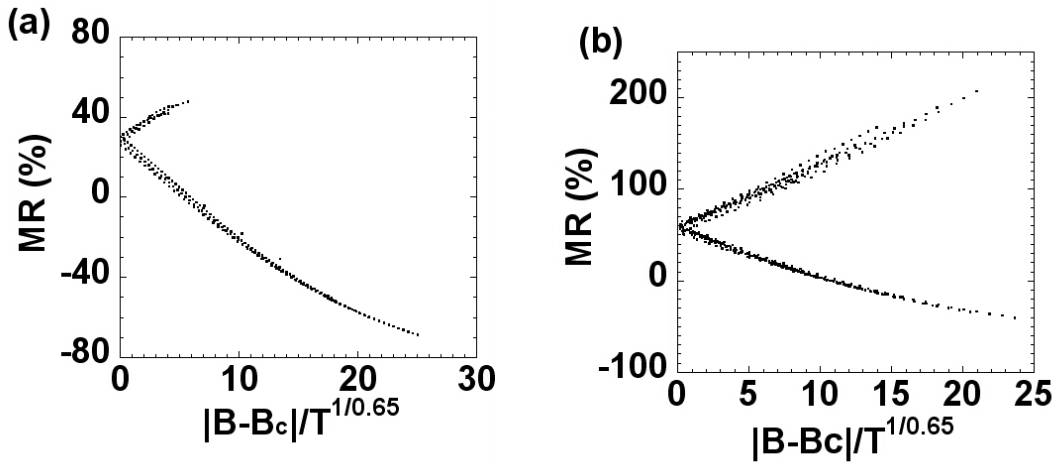

Figure 3.10: Scaling of the MR of (a) the 20.91Å and (b) the 21.12Å thick films. Both plots employ data from below and including 500mK. The magnetic field range of 20.91Å film is from 2.5 to 10 Tesla, while it is 5 to 10 Tesla for the 21.12Å film. In the case of the 20.91Å thick film, there is a shorter upper branch due to the closeness of $B_c = 3.9T$ and the peak in $R(B)$, while $B_c = 7.3T$ in the case of the 21.12Å thick film.

Chapter 4

Current-Voltage Characteristics and Hot Electron Effects in Insulating Bi Films

4.1 Introduction

One of the most interesting questions is whether localized Cooper pairs or vortices still exist on the insulating side of the SI transition. Some experimental evidence suggests that this might be the case. An example of this is the existence of the magnetoresistance peak on the insulating side of magnetic field tuned SI transition in amorphous InO_x, polycrystalline TiN, and nano-honeycone patterned amorphous Bi (a-Bi) films. The current-voltage (I-V) characteristics are also found to be non-linear in the insulating regime of various materials, *e.g*, Al, Be, Ga, InO_x and TiN [41, 42, 43, 11, 44, 12]. Vinokur *et al.* interpreted the non-linearity of the I-V characteristics of TiN films as being due to a charge Berezinsky-Kosterlitz-Thouless(BKT) transition leading to a superinsulating state, while others have

interpreted it as being due to heating of electrons[45]. However, it is still unclear whether the non-linearity of I-V curves is related to the presence of localized Cooper pairs.

On the other hand, it has been reported that the hot electron effects are found on both sides of the SI transition of a-Bi films[46]. They bring about a decoupling of the electron temperature from the environmental temperature at low temperatures around the transition regime. This directly indicates that the non-linearity of I-V curve on the insulating side of a-Bi may be also due to heating.

In this chapter, the I-V characteristics of insulating a-Bi films will be presented. The results are consistent with the heating model proposed by Altshuler *et al.* and used successfully to describe the I-V curves of InO_x[53, 45]. This agreement suggests the heating mechanism is due to weakness of the electron-phonon coupling in a-Bi. The model can be used to quantitatively estimate the heating effect.

The data employed in this chapter were taken on 20.91Å and 21.12Å thick homogeneous a-Bi films sequentially grown by quench-condensation on (100) $SrTiO_3$(STO) single-crystal substrates precoated *in situ* with a 14.67Å underlayer of amorphous Sb (a-Sb). The Arrhenius plot of resistance measured in the linear I-V characteristic regime, vs. temperature is shown in Fig. 4.1. These films exhibit activated conduction behaviors below 1K, which were discussed in the previous chapter. As mentioned there, the I-V characteristics become very non-linear below 300mK. Therefore, the linear resistance cannot be well determined at very low temperature. The solid lines in the plot are fits to Arrhenius conduction, from which the activation energy and prefactor are obtained. All the I-V characteristics are obtained by applied a DC bias current to the current leads of sample and the voltage is measured in steady state.

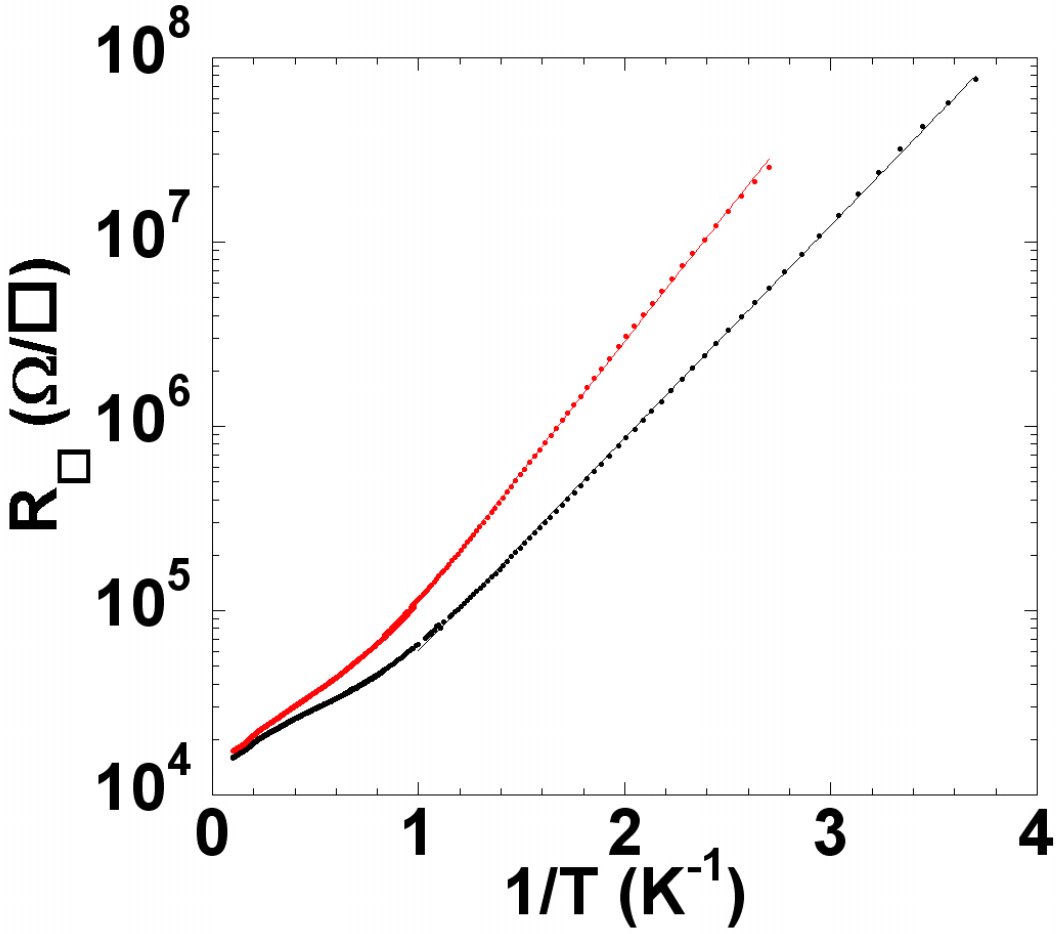

Figure 4.1: Arrhenius plot of resistances of the 20.91Å (top) and the 21.12Å (bottom) thick homogeneous a-Bi films. The solid lines are the fits of Arrhenius conduction to the data points below 1K.

4.2 Non-linear I-V Characteristics of insulating *a*-Bi Films

The I-V characteristics of the 21.12Å thick film in zero field at various temperatures are shown in Fig. 4.2. A voltage value is measured when the bias current is in the range of 100pA to 10nA for both bias directions. During the measurements, the 2182A nanovoltmeter sent out an input DC bias test current of 50pA or 220pA depending up the measurement range[47]. This has been corrected by subtracting from the applied current this test current. As shown in the Fig. 4.2, the non-linearity starts to develop below 500mK when the bias current is higher than 1nA. It becomes non-linear over the whole measured current range below 300mK. The I-V characteristic is symmetric respect to the origin. Thus, the behavior in one bias direction is representative of both signs.

The differential resistance R_D, which is plotted in Fig. 4.3, is obtained by taking the slope at consecutively measured values of current and voltage. Above 500mK, R_D is nearly a constant at the same temperature. Below 500mK, it decreases significantly with increasing current, except it saturates at low bias currents at 400mK. The values of R_D at lowest current level above 300mK are identical to the linear resistance values shown in Fig. 4.1, where Arrhenius behavior is exhibited.

The observation that R_D decreases with increasing bias current at low temperatures suggests that the electrons are heated by the bias current while the environment may still remain at low temperature. With this hypothesis, we then assume that an effective electron temperature T_{el} is higher than that of the environment due to the input bias power $P = IV$. Then, R_D is a measure of the resistance when the electrons are at this effective temperature T_{el}. The values of $R(T)$, which follow the Arrhenius form can then be used as a thermometer.

By inserting the R_D into $R(T)$, the effective electron temperature can thus be obtained. Using this method, the effective temperature T_{el} vs. bias current I is plotted in Fig. 4.4 at different dilution refrigerator temperatures. It is clear to see that the effective electron temperature is in equilibrium with the dilution refrigerator above 500mK. However, the electron temperature can deviate by as much as 400mK at temperatures lower than 300mK.

4.3 The Electron-Phonon Coupling and the Hot Electron Effect

In order to quantitatively understand this hot electron effect, we use the model which gave a successful description of the behavior of InO_x[45, 53]. In this model, the power $P = IV$ dissipated in the electron gas is carried out by phonons through the electron-phonon coupling. The heat balance equation is given by:

$$P = \Gamma\Omega\left(T_{el}^{\beta} - T_{ph}^{\beta}\right) \tag{4.1}$$

where Γ is the electron-phonon coupling constant, Ω is the volume of the sample, and β depends on the electron-phonon relaxation rate. β has been found to be ~ 5 for most metals[48, 49, 50, 51]. Altshuler *et al.* and others found β to be ~ 6 for very dirty conductors and for InO_x[45, 52, 53, 54]. Assuming the phonons are in a equilibrium with the dilution refrigerator and $\beta \approx 6$, a comparison of P and $T_{el}^6 - T_{ph}^6$ of data below 400mK is plotted in Fig. 4.5. Although for this particular film the applied bias currents and bath temperature are limited, the data points with bias currents higher than $1nA$ show a linear relation. This suggests that this heating model can also explain the I-V curves of insulating

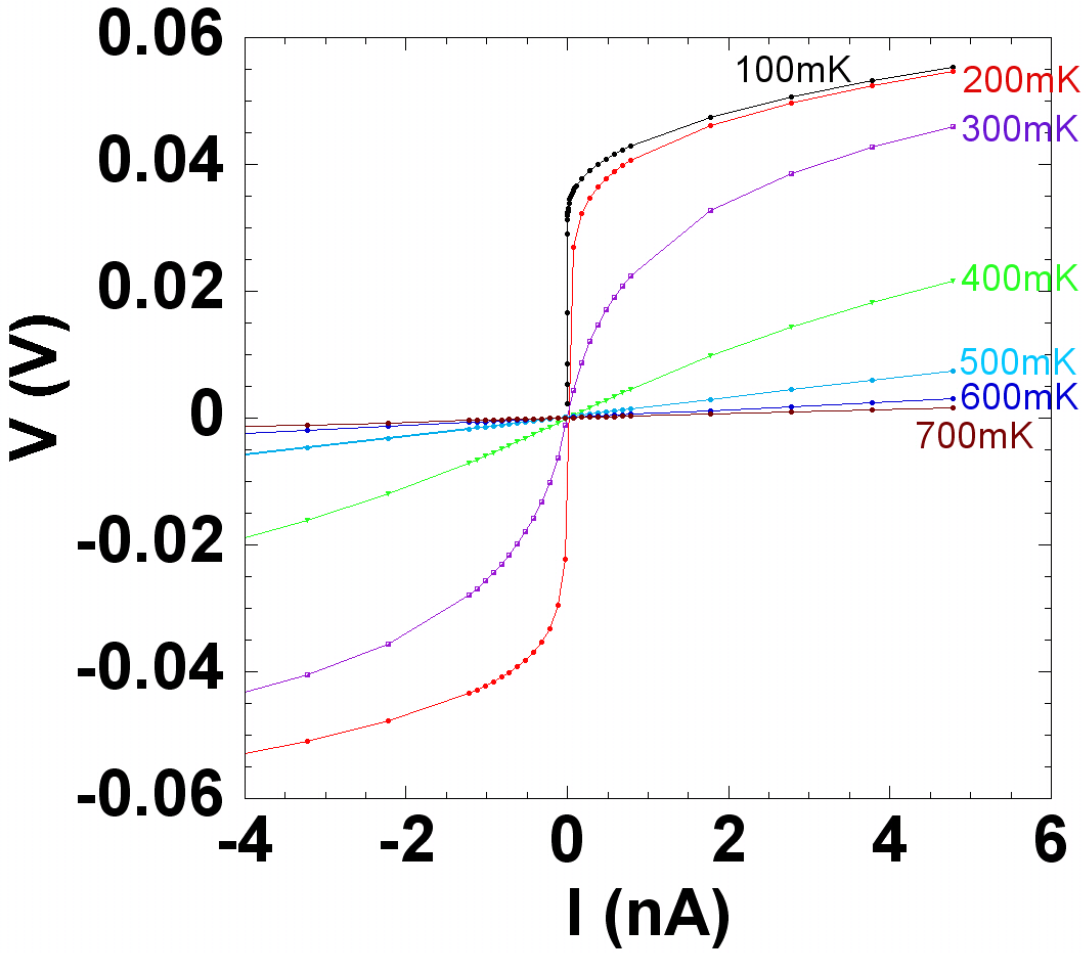

Figure 4.2: I-V characteristics of the 21.12Å thick homogeneous *a*-Bi film in zero magnetic field at different temperatures. The numbers marked on the right indicate the corresponding dilution refrigerator temperature when the measurements were performed. The connecting lines are guides to the eye.

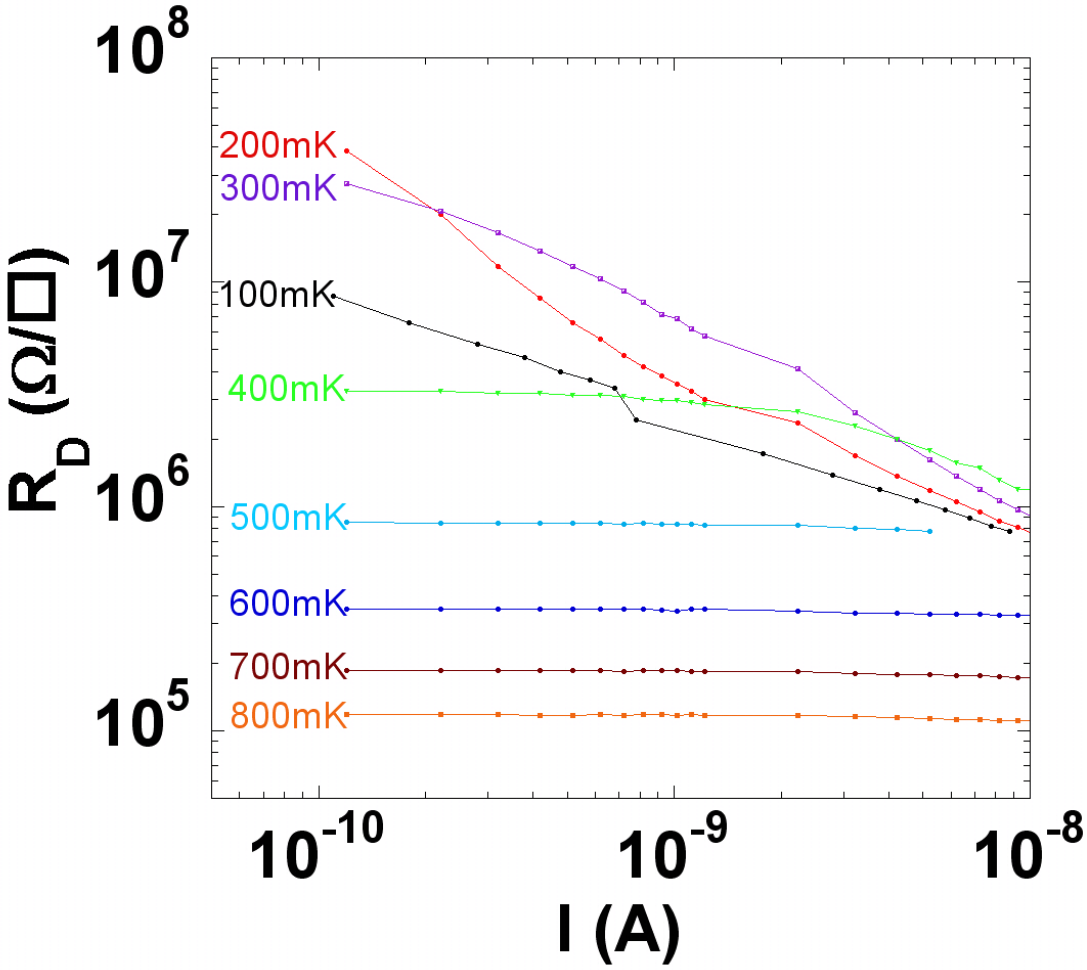

Figure 4.3: The differential resistance R_D vs. bias current of the 21.12Å thick homogeneous a-Bi film in zero magnetic field. The labeled temperatures are those of the dilution refrigerator when the measurements were performed.

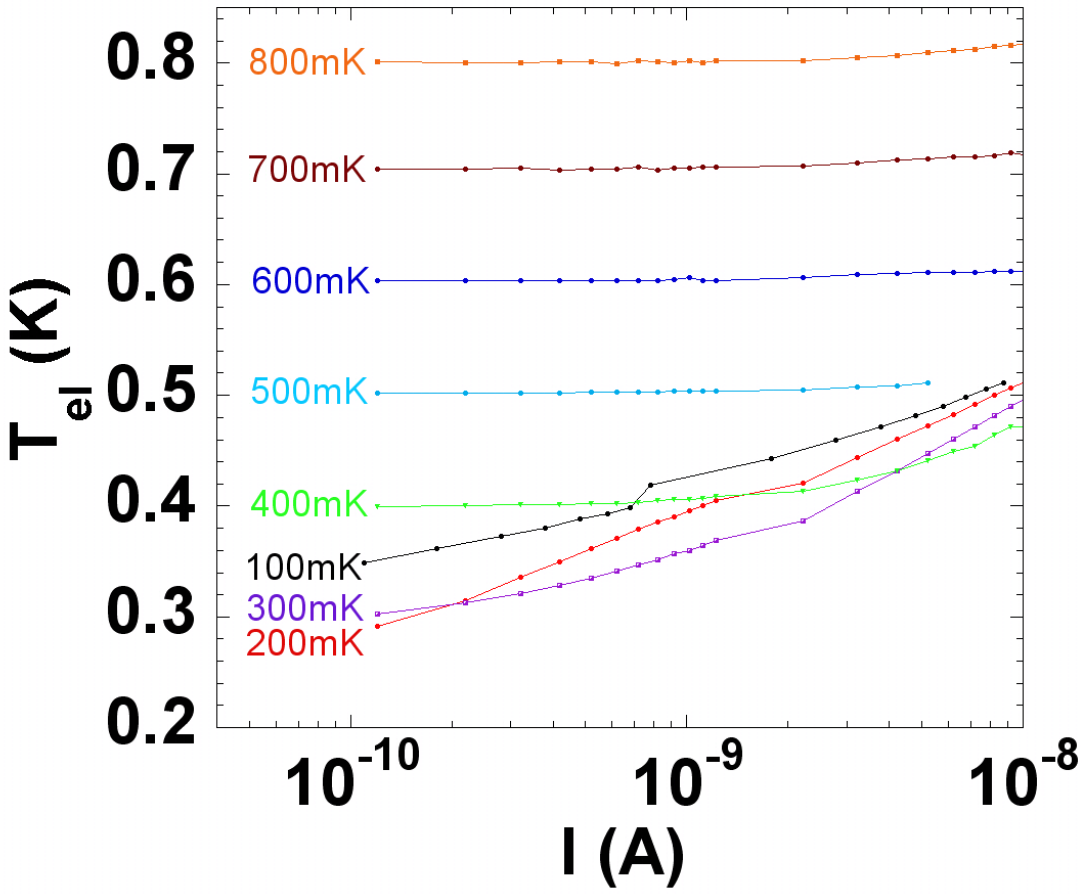

Figure 4.4: The effective electron temperature vs. bias current of the 21.12Å thick homogeneous *a*-Bi film in zero magnetic field. The labeled temperatures are those of the dilution refrigerator when the measurements were performed.

a-Bi films. With the sample volume taken to be $5.23 \times 10^{-7} mm^3$, the electron-phonon coupling constant can be obtained by a linear fit to the data points with the current lower than $1nA$. The values are 4.25, 4.21, 4.30, 4.78 in units of $10^7 Wm^{-3}K^{-6}$at dilution refrigerator temperatures of 100, 200, 300, and 400mK, respectively. The uncertainty of these values are about 10%. It has been found that $\Gamma = 1.85 \times 10^9 Wm^{-3}K^{-6}$ for InO_x[45], and $\Gamma = 8.4 \times 10^7 Wm^{-3}K^{-6}$ for TiN[55]. The result for this a-Bi film is smaller than all the other results, but is of the same order as that of TiN films. The values decrease with decreasing temperature, which indicates that the electron-phonon interaction becomes weaker at lower temperature. This also explains to the fact that the non-linearity is developed at low temperatures because the electron temperature is more easily decouples.

The same analysis can be applied to the non-linear I-V characteristics of a thinner 20.91Å film at low temperatures, which shown in Fig. 4.6. The electron-phonon coupling constants Γ are found to be 2.14, 2.09, 2.07, 2.38, 3.30, 3.38, and 3.10 in units of $10^7 Wm^{-3}K^{-6}$at dilution refrigerator temperatures ranging from 100mK to 400mK with 50mK increments, again with a 10% of uncertainty. The coupling constant still decreases with decreasing temperature. Also, these values are smaller than those found for thicker and presumably more ordered films. This reveals that the coupling becomes stronger in more ordered films.

Parendo *et al.* reported this electron temperature decoupling from the temperature of the environment in a-Bi films near the SI transition [46]. They further reported the dependence of the effective electron temperature on the power to be $T_{el} \sim P^{0.18 \pm 0.05}$, which is consist with the limiting case of Eq 4.1 when $T_{ph} \to 0$, with $\beta = 5.56 \pm 2.1$. In the study of TiN, $\beta = 5.5$ in parallel magnetic fields.

However, $\beta = 6$ provides the best description in the present study. Moreover, Eq 4.1 is more general than the limiting case found by Parendo and can also explain the situation when T_{ph} is non-zero.

One may notice that the data points in Fig. 4.5 and Fig. 4.6 deviate from linearity in the low power regime. This deviation becomes more significant at lower dilution refrigerator temperatures. This may be due to the assumption that the phonon temperature of the film is the same as that of the refrigerator thermometer being no longer valid at low temperatures. At lower temperatures, the Kapitza boundary resistance becomes significantly large. Thus, the phonons in the films may also decouple from the environment. This results in the phonon temperature being different from the dilution refrigerator thermometer temperature. Therefore, deviations are not unreasonable.

Nevertheless, the fact that Eq 4.1 can well describe the high current part of the data suggests that the electron-phonon coupling is the main thermal restriction on the thermal equilibrium between electrons and the environment. The effective electron temperature decouples from the environment when a high bias current is applied to the sample.

This model provides a quantitative way to estimate the effect due to the weak coupling between the electrons and phonons. If the bias power P is larger than the value of $\Gamma\Omega$ in Eq 4.1, a strong heating effect of the electrons is expected. This can be used to determine the bias current for measurements. For example, if the same Arrhenius type form is still valid in the 21.12Å film down to 200mK, the expected resistance will be around $2.5G\Omega$. With the coupling constant we obtained, if one want to observe this expected resistance without heating the electrons higher than 205mK, then a current smaller than 9.5pA needs to be applied. This method

was used to estimate the heating effects for all of the results, especially those in Chapter 5, where a flattening out of the resistance was found at low temperatures but was not be due to this heating effect.

4.4 I-V Characteristics in Perpendicular Magnetic Fields

As shown in the previous chapter, these two films exhibited a magnetoresistance peak when a perpendicular field was applied. In the range of applied fields up to 10 Tesla, all the resistances follow an Arrhenius conduction form below 1K. It is also found that the I-V characteristic are non-linear around the peak regime, which is similar to what was observed for InO_x and TiN. A comparison between the non-linearities in zero and non-zero field may help us to understand the nature of these magnetoresistance peaks.

The I-V characteristics of the 20.91Å film in a two Tesla perpendicular magnetic field have been measured at different temperatures, as shown in Fig. 4.7. They are similar to the zero external magnetic field case in that the I-V curves are very non-linear at low temperatures. The differential resistance R_D, shown in the Fig. 4.8, is obtained by the method employed for zero field, which is described in Section 4.2. R_D saturates at low bias and is equal to the linear resistance that is measured, while it decreases with increasing bias current. These features are exactly the same as was found in zero field, which suggests that the non-linearity may also be due to hot electron effects.

Since $R(T)$ was also measured in this two Tesla magnetic field and shows Arrhenius type conduction, we can use it as a thermometer to performed the analysis using the heating model. In Fig. 4.9, the bias power $P = IV$ vs. $T_{el}^6 - T_{ph}^6$ is plotted at temperatures ranging from 100mK to 400mK with 50mK increments. Here

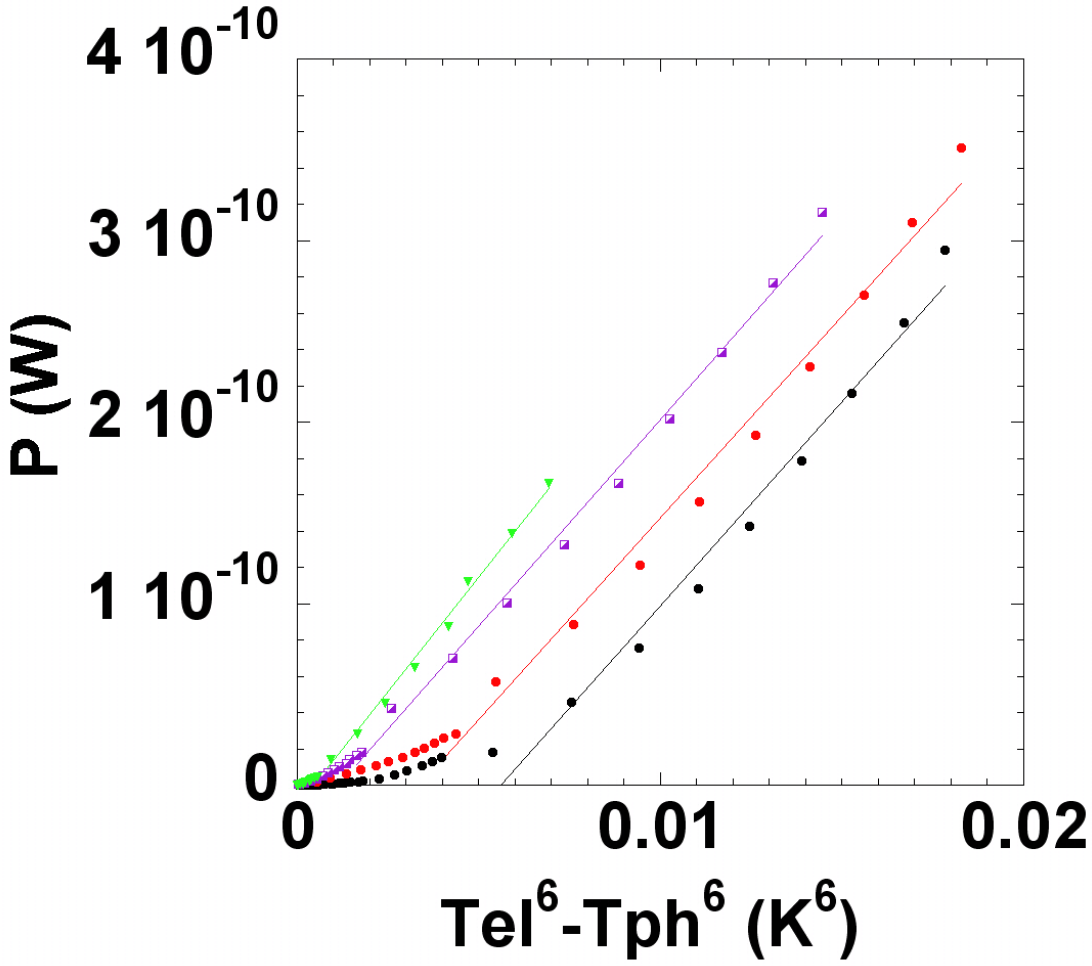

Figure 4.5: The input bias power vs. non-linear temperature difference between the effective electron temperature and phonon temperature of the 21.12Å thick homogeneous a-Bi film in zero magnetic field at 400mK(left), 300mK, 200mK, 100mK(right). The solid lines are linear fits used to obtain the electron-phonon coupling constant.

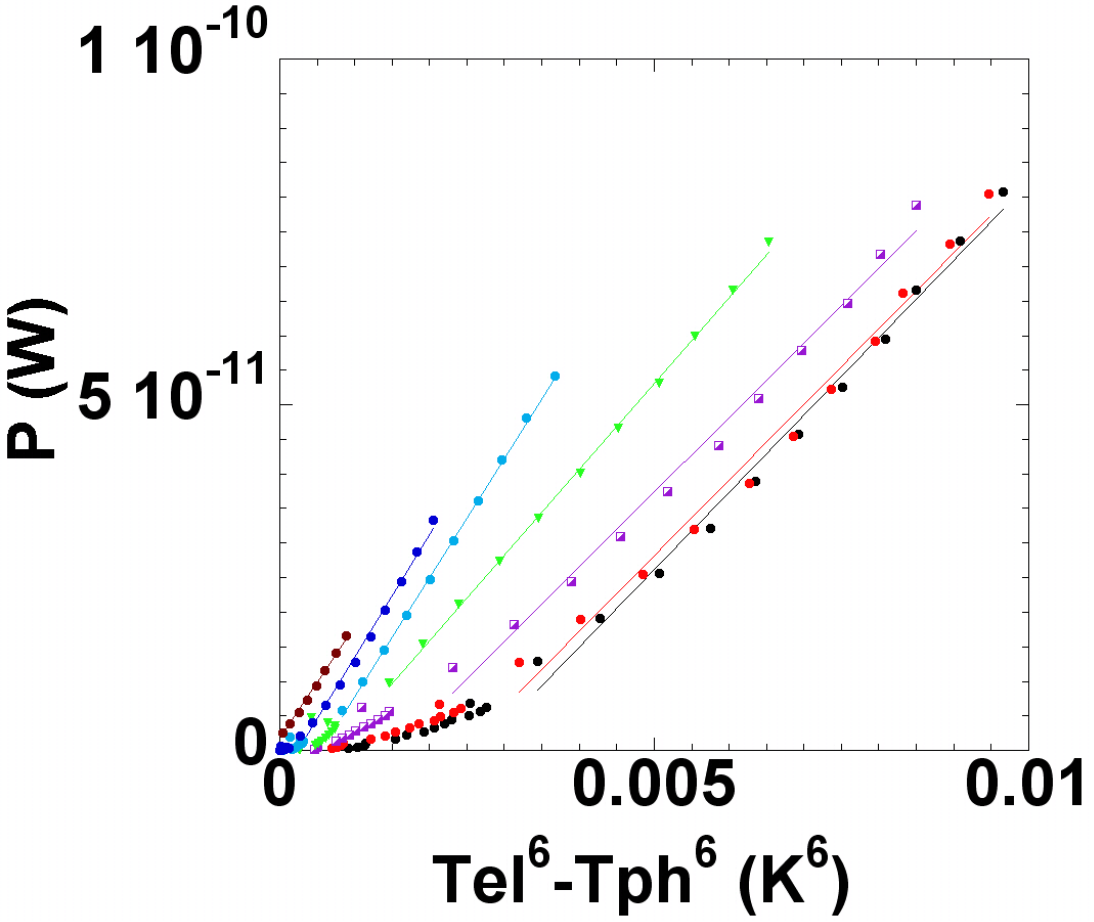

Figure 4.6: The input bias power vs. non-linear temperature difference between the effective electron temperature and the phonon temperature of the 20.91Å thick homogeneous a-Bi film in zero magnetic field at 400mK(left) to 100mK(right) with 50mK increments. The solid lines are linear fits to obtain the electron-phonon coupling constant.

T_{el} is obtained using the same method employed for zero field and T_{ph} is assumed to be equal to the temperature of the dilution refrigerator. One can clearly see the main features are the same as in Fig. 4.6, which suggests that the non-linear I-V curves around the peak are due to hot electron effects. From the slope of the lines in the Fig. 4.6, the electron-phonon coupling constant Γ can be obtained as 3.86, 4.00, 3.68, 4.88, 7.05, 7.12, and 6.46 in units of $10^7 W m^{-3} K^{-6}$at dilution refrigerator temperatures of 100mK to 400mK in 50mK increments, respectively. The uncertainty in Γ is also around 10%. These values are consistently about a factor of two larger than those at the same temperatures in zero field. It is unclear why the magnetic field improves the electron-phonon coupling. However, these numbers are closer to the electron-phonon coupling constant found for TiN, which was also obtained in the presence of a perpendicular magnetic field[55].

To summarize, we have explored the I-V characteristics of insulating a-Bi films at different temperatures in zero and non-zero perpendicular magnetic fields. The I-V curves reveal strong non-linearities at low temperatures. The main features can be explained by the hot electron model in the dirty limit. When a high bias current is applied, the effective electron temperature is driven out of thermal equilibrium from the environment mainly due to the weakness of electron-phonon coupling. The electron-phonon coupling of a-Bi is obtained, which can be used for a quantitative estimate of the heating effect.

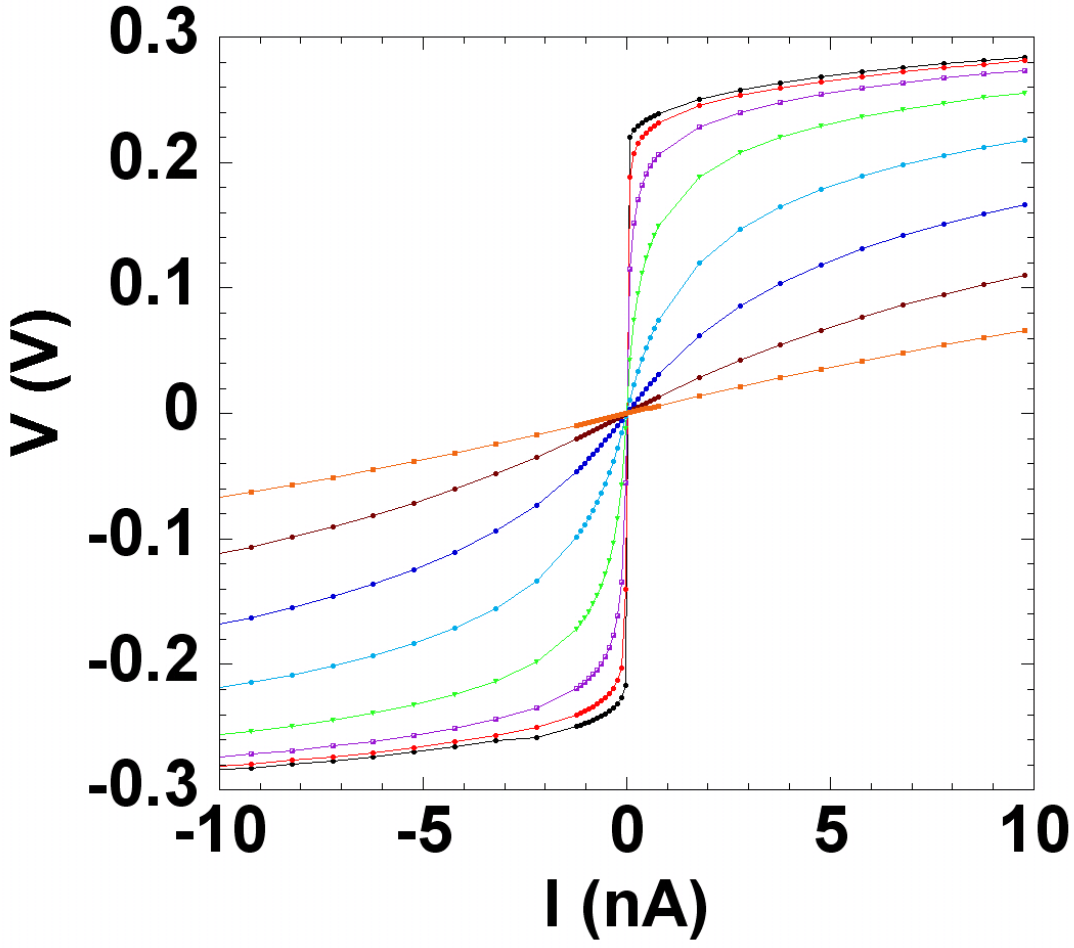

Figure 4.7: I-V characteristics of the 20.91Å thick homogeneous a-Bi film in a 2 Tesla perpendicular magnetic field at temperatures from 100mK(outer), 200mK to 500mK(inner) with 50mK increment.s The I-V curve at 150mK is skipped for clarity. The connecting lines are guides to the eye.

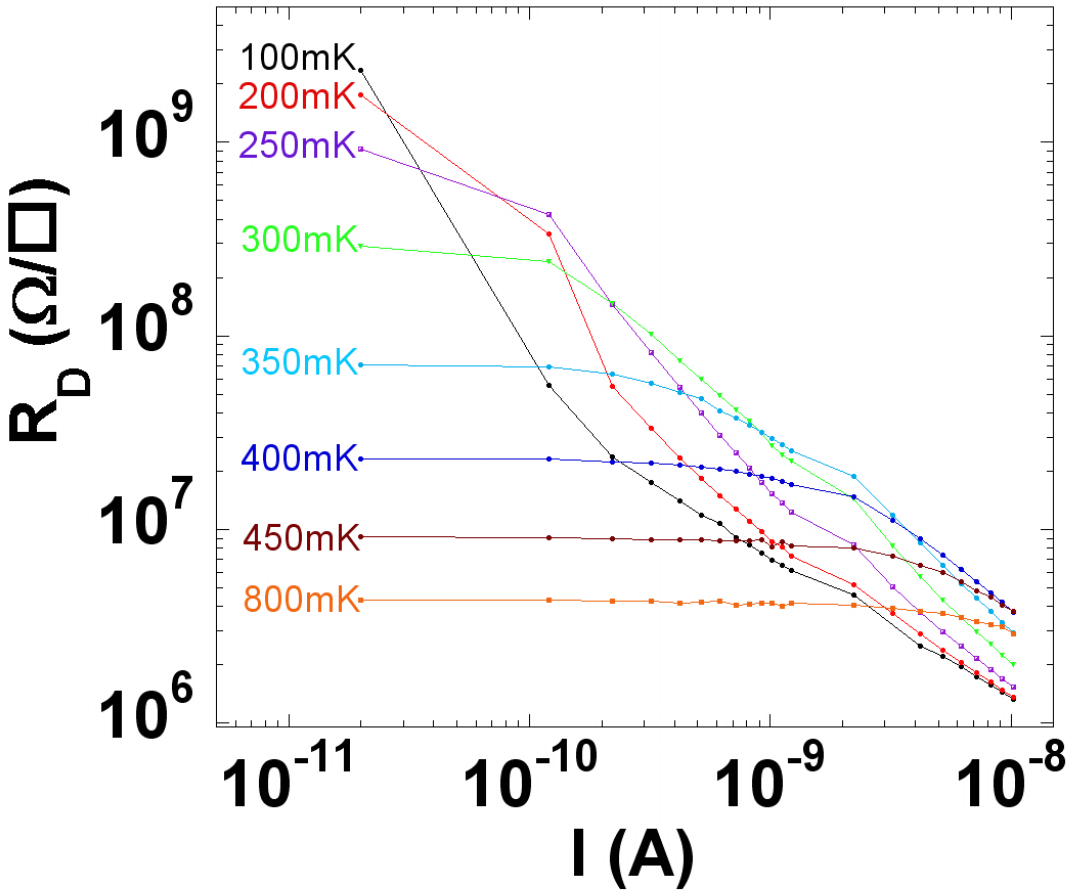

Figure 4.8: Differential resistance R_D vs. applied bias current of the 20.91Å thick homogeneous a-Bi film in a 2 Tesla perpendicular magnetic field at different temperatures. The labeled temperatures are those of the dilution refrigerator when the measurements were performed.

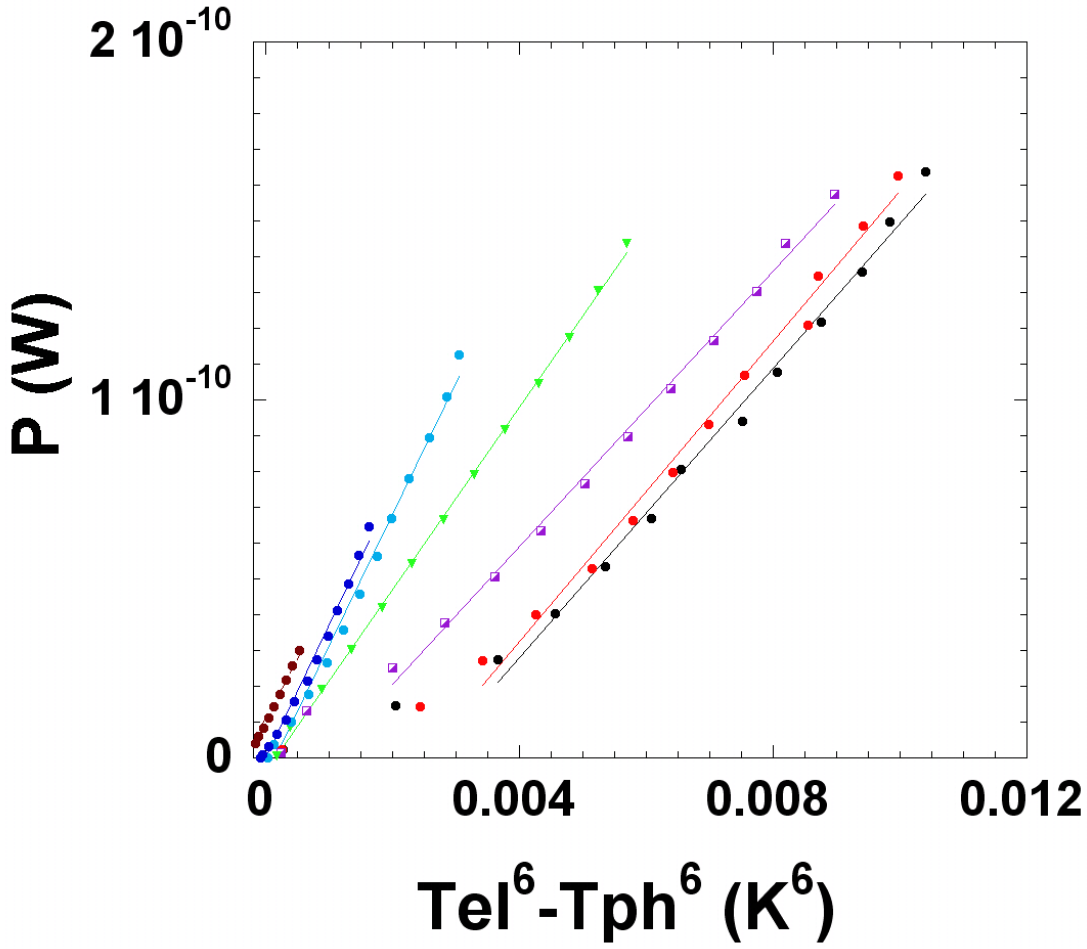

Figure 4.9: The input bias power vs. temperature difference between the effective electron temperature and the phonon temperature of a 20.91Å thick homogeneous a-Bi film in a 2T perpendicular magnetic field from 400mK(left) to 100mK(right) with 50mK intervals. The solid lines are linear fits used to obtain the electron-phonon coupling constant.

Chapter 5

Electrical Transport near the Onset of Superconductivity

5.1 Introduction

For film thicknesses greater than a certain critical thickness, the conduction at low temperatures favors superconductivity. Over the last two decades, the transport properties of many disordered thin films in this regime have been explained by vortex dynamics, especially in the presence of magnetic fields.[56, 57, 3, 58] However, detailed theoretical mechanisms haven't been clearly worked out.

Of particular interest are the many experimental reports that the resistance at the lowest temperatures becomes independent of temperatures near the SI transition of homogeneous or granular films. This has been found with many different tuning parameters[56, 59, 19, 60]. These results have been interpreted in many different ways, which include the formation a metallic state, the occurrence of macroscopic quantum tunneling, or just the failure to cool the carriers. The physics in this regime is still unclear.

In the presence of high levels of disorder, Ghosal, Randeria, and Trivedi predicted that a two-dimensional s-wave superconductor breaks into superconducting islands separated by an insulating sea[36]. Dubi, Meir, and Avishai also predicted that for the system with low electron densities or high disorder, increasing the magnetic field suppresses the correlations between the phases of the superconducting order parameter on the different islands[38]. These theoretical works demonstrate the possibility that superconducting thin films may break into superconducting islands in the presence of strong disorder or in a magnetic field. Experimentally, scanning tunneling microscope investigation on amorphous InO_x and polycrystalline TiN films near the transition temperature have revealed that the system breaks into small superconducting patches embedded in an insulating background[61]. It is still unclear whether this is due to spacial chemical composition variations in these binary compound films or is an intrinsic property of highly disordered films which are strongly localized. However, as a consequence, it is reasonable to treat such systems in a manner analogous to random Josephson junction arrays (JJAs). The two-dimensional JJA has been well studied and has a fully developed theoretical description. The similarity between quasi-2D thin films and JJAs has been noticed recently and been used to explain the conductivity on the insulating side of the SI transition[12]. There are also some theoretical works on the SI transition that are based on the JJA framework[62]. However, there is still a lack of experimental work establishing the relation between the 2D SI transition and JJA physics.

In this chapter, the theory of the transport properties in a regular JJA will be described first. Then we will present the results of surface characterization of an amorphous bismuth (a-Bi) film by atomic force microspectroscopy (AFM).

We then will compare our experimental data with this theoretical framework. We find that the Josephson junction array model can consistently explain the data.

5.2 Electrical Transport in an Ordered Josephson Junction Array

In this section, we first consider the transport properties of a single Josephson junction, and then derive the behavior of the resistance for vortices moving in a Josephson junction array(JJA). In 1962, Josephson[63] predicted that a zero-voltage supercurrent should flow between two superconductors separated by a thin insulating barrier:

$$I_s = I_{c0} sin\gamma \tag{5.1}$$

where γ is the gauge-invariant phase difference, which is defined as $\gamma \equiv \triangle\varphi - (2\pi/\phi_0)\int \mathbf{A}\cdot \mathrm{d}\mathbf{s}$. Here $\triangle\varphi$ is the difference in the phases of the order parameters in the two electrodes, and ϕ_0 is the flux quantum. The critical current I_{c0} is the maximum supercurrent that the junction can support. Josephson further predicted that if a voltage difference V were maintained across a junction, the phase difference γ would evolve according to:

$$d\gamma/dt = 2eV/\hbar \tag{5.2}$$

Without an external magnetic field, the vector potential $\mathbf{A}$ can be taken to be zero and γ and $\triangle\varphi$ can be used interchangeably.

Typically, a single Josephson junction can be described by the resistively and capacitively shunted junction (RCSJ) model. The equivalent circuit is shown Fig.

5.1(a). Within this model, the time dependence of the phase γ in the presence of an externally supplied bias current can be derived by equating the bias current I to the total junction current from the three parallel conductance channels[64]:

$$I = I_{c0} sin\gamma + V/R + CdV/dt \tag{5.3}$$

Here R and C are the shunt resistance and the shunt capacitance, respectively. We define $E_J = (\hbar/2e)I_{c0}$ as the Josephson coupling energy and $E_c = e^2/2C$ as the charging energy. Substituting Eq. (5.2) into (5.3), we obtain the second order differential equation:

$$d^2\gamma/d\tau^2 + (\omega_0 RC)^{-1} d\gamma/d\tau + sin\gamma = I/I_{c0} \tag{5.4}$$

Here, we have introduced a dimensionless time variable $\tau = \omega_0 t$, and the plasma frequency of the junction $\omega_0 = (2eI_{c0}/\hbar C)^{1/2} = (8E_J E_c)^{1/2}/\hbar$. The junction dynamics can be described by the solution of Eq. (5.4), which is the equation of a particle of mass $(\hbar/2e)^2 C$ moving along the γ axis in an effective potential

$$U(\gamma) = -E_J cos\gamma - (\hbar I/2e)\gamma \tag{5.5}$$

subjected a viscous drag force, which is described by the second term of Eq. (5.4). We define a dimensionless damping parameter $\alpha = (2RC\omega_p)^{-1}$ to describe the damping of the system, in which $\alpha > 1$ is overdamped and $\alpha < 1$ is underdamped. The potential with the form of Eq. (5.5) is often referred to as a "tilted washboard" potential, as shown in Fig.. 5.1(b).

Now, we start to consider the case of an ordered square JJA with a lattice constant a. Let us consider zero external magnetic field, which has the frustration number $f \equiv Ha^2/\phi_0 = 0$. At very low temperature, pairs of vortices of

opposite helicity will be thermally generated and they will form tightly bound vortex-antivortex pairs. Kosterlitz and Thouless have shown that for the superfluid ^4He film case, there is a sharply defined temperature, T_{BKT}, at which vortex pairs start to unbind[65]. Beasley, Mooij, and Orlando shown that this Kosterlitz-Thouless or Berezinsky-Kosterlitz-Thouless(BKT) transition was also applicable to sufficiently thin superconducting films[66]. It has also been shown to be applicable to Josephson junction arrays[64]. The transition temperature of an array can be expressed as:

$$k_B T_{BKT} = (\pi/2) E_J \tag{5.6}$$

In this picture, there exist unbound free vortices above T_{BKT} even in zero magnetic field. These unbound vortices will give rise to a linear resistance with a temperature dependence as predicted by Halperin and Nelson[67]:

$$R(T) = R_0 exp\left[-b/\left(T - T_{BKT}\right)^{1/2}\right] \tag{5.7}$$

where R_0 and b are constants.

Now, let us consider a single vortex moving along a row of cells in an infinite square array. Its equation of motion can be written as[68]:

$$M_v \ddot{x} + \eta \dot{x} = E_J[(\alpha_0/2) sinx + i/i_{c0}] \tag{5.8}$$

where $M_v = (\phi_0/2\pi)^2 C/2$ is the vortex effective mass, C is the junction capacitance, x is the position normalized by $a/2\pi$, i is the applied transport junction current in the direction perpendicular to x, and η is the viscosity given by $\eta = (\phi_0/2\pi)^2/2r_e$, where the r_e is the effective damping resistance. The number $\alpha_0 E_J$ represents the potential barrier height for the center of a vortex to move

across a single junction. $\alpha_0/2$ has been estimated to be equal to 0.2 in a square lattice and 0.043 in a triangular lattice[69]. In the presence of a magnetic field and a current, a vortex can also be forced over a barrier by the $\mathbf{j}\times\mathbf{B}$ force and will move perpendicular to the current direction. One can see that there is a direct analogy between the motion of a vortex in an array and the dynamics of a single Josephson junction. Therefore, a single vortex moving in a JJA in real space is just like the motion of the phase in a tilted washboard potential which is described by the right hand side of Eq. (5.5).

Assuming sufficient damping to be present, the vortex will settle down in the lowest energy state after crossing through one barrier. Then, each tunneling event through successive barriers will be independent. With Eq. (5.2), one can derive the sheet resistance due to vortex motion in a square lattice of junctions[69]:

$$R_{\square} = \frac{h}{2e}(a^2 n_f)\frac{1}{i\tau_0} \tag{5.9}$$

where a is the lattice spacing, n_f is the areal density of free vortices, i is the current through one junction, and τ_0 is the average time for a vortex to cross one junction, which need to considering vortex motion which been describe by Eq (5.8).

One may then realize that vortices can escape from the well of the tilted washboard potential either by thermal excitation or by macroscopic quantum tunneling (MQT), as shown in Fig.. 5.3(b). Therefore, resistance is contributed by both the thermal and quantum parts[70]:

$$R(T) = R_{Quantum} + R_{Thermal} \tag{5.10}$$

From Eq. (5.8), one Josephson junction would be one "potential hill" for a vortex in real space. Then, $1/\tau_0$ would be equal to the difference between the uphill and downhill rates, i. e., $1/\tau_0 = \Gamma^+ - \Gamma^-$, where $\Gamma^\pm$ is the escape rate for the downhill(+) and uphill(-) directions.

If the escape process is driven by thermal excitation, the escape rate is given by[71]:

$$\Gamma^\pm = \frac{\omega_R}{2\pi} f_q exp\left(-U_0^\pm / k_B T\right) \tag{5.11}$$

where $U_0^\pm$ is the barrier height for the downhill(+) and downhill(-) directions, which is equal to $2\alpha_0 E_J \mp hi/4e$ respectively, ω_R is the damping related frequency and barrier frequency, which is defined as $\omega_R = \omega_0 \left[(1+\alpha^2)^{1/2} - \alpha\right]$, and f_q is the quantum correction term. The latter approaches unity at high temperature. By combining Eqs. (5.9) and (5.11) and taking the small current limit, Iansiti *et al.* showed that the resistance vs temperature is[72]:

$$R_{Thermal} \approx \frac{h}{4e^2} \frac{\hbar\omega_0}{k_B T} \left(a^2 n_f\right) a_t f_q exp(-2\alpha_0 E_J / k_B T) \tag{5.12}$$

where q is includes the effect of quantum fluctuations on the escape rate, and a_t is a prefactor estimated by Buttiker, Harris , and Landauer to be[73]:

$$a_t \approx \frac{4}{\left[(1 + k_B T/3.6\alpha U_0)^{1/2} + 1\right]^2} \tag{5.13}$$

One can see that the resistance should exponentially decay in the high temperature limit and this has been reported for single junctions and for a regular JJAs in low magnetic fields. In experiments on JJAs, there are reports that in the presence of magnetic field the resistance exhibits an Arrhenius type form within in a certain temperature range and the activation energy has been used to infer the barrier

height[74, 75].

On the other hand, if the escape process is due to quantum tunneling, the escape rate Γ can be estimated by the Wentzel-Kramers-Brillouin(WKB) approximation in the small current limit as[71]:

$$\Gamma^{\pm} = \frac{\omega_0}{2\pi}\chi\sqrt{v^{\pm}}exp(-v^{\pm}s) \tag{5.14}$$

where $v^{\pm} = U_0^{\pm}/\hbar\omega_0$, $U_0^{\pm}$ is the barrier height of downhill(+) or uphill(-) motion, equal to $2\alpha_0 E_J \mp hi/4e$, ω_0 is the plasma frequency and χ and s are numerical constants, which are functions of the shape of the potential and of the magnitude of the damping. Again, as in the thermal treatment, one can obtain the sheet resistance for quantum tunneling by combining Eq (5.14) and Eq (5.9).

In zero field and for $T > T_{BKT}$, n_f and τ_0 come from thermal excitation and it has been shown that Eq. (5.9) is reduced to Eq. (5.7)[69]. Below the transition temperature, n_f becomes zero because of the formation of vortex-antivortex pairs. However, in a nonzero magnetic field, the vortex density will be directly proportional to the external field, $n_f = B/\phi_0$, and will persist even when the temperature is below T_{BKT}.

In both the thermal or quantum excited case, the average time for a vortex to cross one junction, $1/\tau_0$, will proportional to the current i in the small current limit[72]. One can easily realize that this current i will cancel out when this average time is substituted into Eq (5.9). This reveals that there should be a linear regime in the I-V characteristic in the small current limit.

From the above discussion, one finds that the system will be dominated by different mechanisms in different ranges of temperature. There should be a crossing temperature, T_{cr}, demarcating the boundary between the thermal and quantum

regimes. In the small current limit, this crossing temperature between quantum and thermal regimes has been estimated to be[64]:

$$k_B T_{cr} = \hbar\omega_R/2\pi \approx \begin{cases} \hbar\omega_0/2\pi = \sqrt{2E_c E_J}/\pi, & \alpha \ll 1 \\ \hbar\omega_0^2 RC/2\pi = (R/R_Q)E_J, & \alpha \gg 1 \end{cases} \tag{5.15}$$

where $R_Q = h/4e^2 \approx 6450\Omega$ is the quantum resistance of electron pairs. Here, $\alpha \gg 1$ corresponds to the underdamped case and $\alpha \ll 1$ to the overdamped. Therefore, $R \approx R_{thermal}$ when $T > T_{cr}$ and $R \approx R_{Quantum}$ for $T < T_{cr}$. One important feature of $R_{Quantum}$ is that it is nearly temperature independent at very low temperatures when E_J is nearly a constant.

5.3 Characterization of the Surfaces of Amorphous Bismuth Films

In the introductory section to this chapter, we have stated that there are theories predicting that in the presence of strong disorder and magnetic field, 2D superconducting thin films may break into small superconducting islands. In this case, the SI transition is driven by phase fluctuation between the superconducting islands which have non-zero order-parameter amplitudes[36, 38]. In this scenario it is reasonable to consider the system as a random JJA near the SI transition, tuned either by disorder or magnetic field. However, the superconducting islands can be generated directly by the morphology of the thin film, such as by variations of the chemical composition in binary compound systems or by the presence of isolated grains in a monatomic thin films. Therefore, it is critical to identify the source for the formation of superconducting islands.

For quench-deposited *a*-Bi, the most important parameter determining the morphology is the thickness variation. Once the thickness variation is at the same order as the film thickness, isolated grains may be formed. The most powerful tool to carry out surface characterization is atomic force microscopy (AFM). It allows us to verify the thickness variation down to the Angstrom level. Unfortunately, we are not able to carry out the AFM studies *in situ*. Thus, it is not possible to characterize every film during the process of sequential deposition. However, we can characterize the thickest film, which is 23.42Å in this study, after the transport measurements are completed. In fact, the thickness of the first film which has measurable resistance below 1K. was 19.74Å. The film thickness at the onset of superconductivity was 22.24Å, and the one on which we carried out a magnetic field tuned SI transition was 23.42Å thick. The total thickness increment was 3.68Å over the entire thickness-tuned SI transition and was 1.18Å over the conductive branch of the SI transition. Therefore, the characterization of the surface of the last film should represent the thickness variation of the films on the conductive branch of the SI transition. We suspect that the thickness variation is set at the very earliest stages of the film growth process and that subsequent depositions do not change it very much.

The 23.42Å film was warmed slowly back up to room temperature. Figure 5.2 shows a $300nm \times 300nm$ scan of the film. The average root mean square roughness,R_{rms} is 3Å relative to a total thickness of 38.09Å, with 23.42Å of amorphous bismuth on top of a 14.67Å thick layer of amorphous antimony. The cross-sectional analysis is shown in Fig. 5.3a. This indicates that the surface is bumpy. However, the maximum thickness variation is around 15Å, which is smaller than the total film thickness. This suggests that the film is well connected but with a

thickness variation around 13% of the bismuth thickness. The most striking result is that the radial Fourier power density spectrum of the thickness variations, as shown in Fig. 5.3b, has a broad peak around $k = 10^8 m^{-1}$, which indicates that the periodicity of the roughness is $2\pi/k = 63nm$. The AFM scan reveals that this film does not consist of isolated grains but is a continuous material with a thickness variation.

5.4 Transport in the Superconductive Branch in Zero Magnetic Field

In this section, we report the electrical transport properties of thickness-tuned, nearly superconducting, amorphous bismuth films in zero magnetic field. The measurements were performed with a DC technique in a regime of linear current-voltage (I-V) characteristics. The I-V characteristics of the films were typically non-hysteretic. A representative I-V curve of a conductive film is shown in Fig. 5.4a. The voltage changes rapidly near $21\mu A$. However, the corresponding Joule heating is very large, leading us to indicate that this non-linearity is due to heating rather than to exceeding the critical current of the film. The current flow through a single junction is not known. Therefore, the I-V characteristic cannot provide information on the coupling energy. However, the non-hysteretic I-V characteristic reveals that the system is overdamped if the film behaves as a random JJA. Consequently we will consider overdamped limit and take $\alpha \gg 1$ in the comparison of our results with the JJA model. In Fig. 5.4b, the I-V characteristics in zero field at two different temperatures all show linear behavior in the small current limit. This feature is consistent with the previous discussion for either thermal excitation or quantum tunneling in a JJA.

In films with thicknesses ranging from 22.24Å to 23.42Å, the resistance decreased with decreasing temperature as shown in Fig. 5.5. However, instead of developing global superconductivity, the resistances of these films flatten out at the lowest temperatures. This suggests that the conduction mechanism may change in going from high to low temperatures. First, we will focus on the high-temperature part. We define the resistance at 9K as the normal resistance R_N . Then we find that the resistance regime between $90\%R_N \sim 10\%R_N$ can be well described by Eq (5.7). The solid line in Fig. 5.5 represents this Halperin-Nelson form for the resistance above the BKT transition. From the fit, the transition temperature, T_{BKT}, can be obtained for films of different thicknesses, as shown in Fig. 5.6. From Eq (5.6), one can calculate the Josephson coupling energy E_J at each thickness. E_J is expected to increase with increasing thickness because the links should become more robust, which is consistent with our result.

The experimental data start to deviate from the theory, and eventually flatten out at the lowest temperatures. This deviation happens at higher temperatures in thicker films, whose resistances are smaller and therefore should exhibit less Joule heating at the same applied current. This indicates that the flattening out is not due to heating or failure to cool the carriers. Furthermore, we can use the heating model proposed by Altshuler *et al.*[53], which quantitatively describes the heating of highly disordered films due to a weak electron-phonon coupling at low temperatures. We find that the electron-phonon couplings are strong enough to carry away the Joule heat due to the applied current. This rules out the flattening of the resistance as coming from failure to cool the carriers.

This deviation from the Halperin-Nelson form and the flattening out of $R(T)$ at the lowest temperatures may be a consequence of macroscopic quantum tunneling(MQT). In a regular JJA, the crossover temperature from the thermal to the quantum regimes should increase with the plasma frequency, as expressed by Eq. (5.15). If we treat the films as random JJAs, the Josephson coupling energy E_J should increase with increasing thickness because the links become more robust. Here we use the value of resistance at 50mK as the flattening out resistance and substitute it into the Halperin-Nelson form, i.e, Eq. (5.7) to obtain the crossover temperature T_{cr}. In Fig. 5.7, we plot T_{cr} versus T_{BKT} and find that the two temperatures are linearly proportional to each other. Substituting Eq. (5.6) into Eq. (5.15), we obtain $T_{cr} = (2R/\pi R_Q)T_{BKT}$, assuming that system is overdamped and that the shunt resistance remains nearly constant for films of different thicknesses. This is also consistent with our observation of a non-hysteretic I-V characteristic, which is a feature of overdamped regime in the RCSJ model. One peculiar feature is the non-zero value of T_{cr} as $T_{BKT} \to 0$. This indicates that this crossover between the thermal and quantum regimes still happens even when the $T_{BKT} \to 0$. Therefore, the resistance crossover to the flattened out regime persists when the system is close to the SI transition. This is not included in the JJA model.

Another uncertain quantity is the free vortex density n_f. Below T_{BKT}, vortices and antivortices are bound and there are no free vortices, i.e., $n_f = 0$. From Eq. (5.9), the resistance should then be zero. The fact a nonzero resistance is still measured at the lowest temperatures means there are free vortices. These may due to trapped flux from the superconducting magnet, such that the background is a nonzero magnetic field. An alternative explanation is that the quantum fluctuations generate a non-zero density of vortices. Petkovic, Vinokur and Nattermann

investigated this possibility[76]. However, we cannot draw a definitive connection to their theory from our results.

5.5 Tuning by a Perpendicular Magnetic Field

In this section, we will present the results of tuning the SI transition with a perpendicular magnetic field for the 23.42Å thick film. This film, after being deposited, was rotated so that it was oriented perpendicular to the direction of the external field. All the measurements were performed with a DC technique in the linear regime of the I-V characteristic.

In Fig. 5.8, we show an Arrhenius plot of resistance vs. inverse temperature at fields from 0.005 to 3 Tesla. Over a significant temperature range, the resistance at all fields can be fit by an Arrhenius type form. We use the data from 200 to 500mK to extract the activation energy at different magnetic fields, which is shown in Fig. 5.9. The activation energy smoothly changes from negative to positive, suggesting the sample is undergoing a magnetic field-tuned SI transition. Furthermore, the activation energy can be well described by a power law with a non zero constant term T_0:

$$T_{act} = T_0 + a_0 B^b \tag{5.16}$$

where T_0, a_0, and b are the constants and the values are given in the caption of Fig. 5.9. According to the discussion in the previous sections, the resistance of a JJA should drop exponentially in the regime of thermally excited vortex motion, as given by Eq. (5.12), and the activation energy should be the barrier height of the tilted washboard potential. Therefore, Eq. (5.16) describes how the barrier height varies with magnetic field, assuming the film corresponds to a random

JJA. From Eq. (5.16), the magnitude of the barrier height in the zero field limit should be $|T_0|$, which has a value of $0.43K$. On the other hand, we know the BKT temperature of this film in zero field is $T_{BKT} = 0.68K$. From Eq (5.6), we found that the $E_J/k = 2T_{BKT}/\pi = 0.43K$, which is exactly equal to $|T_0|$. This implies that the tunneling barrier height in this film is directly equal to E_J, with the correction factor $\alpha_0 = 0.5$ in Eq (5.8). The difference between the value of α_0 found here and the predictions for ordered square or triangular arrays may be due to the fact that the film is not a regular array but is a random array. In the following, we consider the barrier height to be equal to E_J.

In Eq. (5.16), the regime in which $T_{act} < 0$ also reveals how the barrier height or E_J varies with external magnetic field. The value is consistent with the idea that the external magnetic field should lower the coupling energy. It is still unclear why this activation energy smoothly changes sign from negative to positive. The negative sign of the active energy can be explained by vortex motion, which was extensively discussed here. The positive sign could correspond to the charge mode of the JJA. One natural conjecture regarding the transport behavior is that it is due to quasi-particle tunneling due to thermal excitation with the T_{act} as the barrier height. However, it still not clear why the barrier height systematically varies with magnetic field. Also, the physical meaning of the prefactor in the insulating regime is unclear.

Now, we focus on the conductive branch of the data. Apparently, the resistance also deviates from the Arrhenius form at low temperatures, especially for films in low magnetic fields. This observation rules out heating effects or failures of cooling the carriers, because the films have a lower resistance and therefore lower dissipation in low magnetic field. We also can compare the Joule heating

with the electron-phonon coupling in these samples. We find that the coupling is strong enough to cool the carriers. As in the zero field case, these temperature-independent resistances at low temperature can also be due to quantum tunneling.

Imitating the analysis carried out for the zero field case, we use the flattening resistance in different fields to substitute into the Arrhenius type fit at higher temperatures to obtain a crossing temperature T_{cr}. In Fig. 5.10, we plot T_{cr} versus T_{act} from 0.01 Tesla to 1 Tesla. The part with a negative T_{act} represents how T_{cr} varies with the coupling energy E_J, since we know that $|T_{act}| = E_J$ on the conductive branch from the previous discussion. Generally, the crossing temperature decreases with decreasing of $|T_{act}|$, which qualitatively agrees with Eq. (5.15). Nevertheless, T_{cr} is not linearly proportional to T_{act} as in the case of thickness tuning, especially close to the critical regime of SI transition. It is possible that when the exponent in Eq. (5.12) is small, the prefactor will start to affect the resistance significantly. Equation (5.15), which only compares the exponent term of thermal and quantum regimes, is no longer valid.

At the lowest temperatures, thermal excitations become weak compared to quantum tunneling. Then the resistance is expected to be driven by quantum tunneling. In the presence of an external magnetic field at low temperatures, we assume the free vortices are generated by external field rather than by thermal excitation, and the vortex density simply is $n_f = B/\phi_0$. The vortices in the sample move in a tilted washboard potential which has a barrier height T_{act}. We consider the sample to be in the overdamped regime, such that α is large enough to modify the plasma frequency with a damping-related frequency ω_R [64, 71]:

$$\omega_R \approx \omega_0/2\alpha = \omega_0^2 RC = 4e^2 RE_J/\hbar^2 \tag{5.17}$$

Here R is the shunt resistance. Combining combining Eq (5.9), (5.17) and (5.13), in the large damping and the small current limits, we obtain:

$$R_{\square} = \frac{h}{4e^2}\chi(\frac{a^2}{\phi_0}B)(\sqrt{\frac{4Re^2}{\hbar}})(\frac{s\hbar}{4Re^2} - \frac{1}{2})exp(-\frac{s\hbar}{4Re^2}) \tag{5.18}$$

In order to calculate this sheet resistance, we need to estimate the shunt resistance R, the average lattice spacing of junctions, a, and the damping parameter α, which determines values of the damping related constants χ and s[77]. We assume the shunt resistance does not change in the presence of an external magnetic field. From the slope of T_{cr} vs. T_{BKT} in the thickness tuning experiment, we find the value of the shunt resistance to be $1.1R_Q$. For the average lattice spacing of junctions a, we use the periodicity found by the AFM scan in the previous section, namely, $a = 63nm$.

Now, the only uncertain parameter is the damping parameter α. Unfortunately, we cannot determine α from our data. Furthermore, α itself is a function of E_J and E_C. However, in order to get a feeling for Eq (5.18), we assume α does not change with magnetic field. As a consequence, s and χ are also independent of magnetic field. With these assumptions, from Eq. 5.18, the sheet resistance will become linear in the magnetic field. In Fig. 5.11, we show the sheet resistance below the crossing temperature, at 50mK, versus magnetic field on the conductive branch of the field-tuned transition. The solid lines are the theoretical resistances with the corresponding values of α, with no other free parameters. The experimental result is in good agreement with the theory with $\alpha = 4.7$. With $\alpha = 4.7$, $[(1+\alpha^2)^{1/2} - \alpha] = 0.1052$ and $1/2\alpha = 0.1064$, which also verifies that the approximation in Eq. (5.16) is reasonable and consistent with the assumption that the film is in the overdamped regime. Nevertheless, one must note that this rough estimation

is based on α being a constant as the external magnetic field is varied. In fact, the external magnetic field will decrease E_J and may alter E_C. Therefore, further consideration is needed for precise predictions of resistance.

5.6 Magnetoresistance in the Superconducting Branch

This series of films exhibited a magnetoresistance peak in perpendicular filed and a possible quantum phase transition on the insulating side of the SI transition, which was discussed in Chapter 3. The resistances at 300 mK, of films of thicknesses ranging from 21.12Å to 23.42Å are plotted as a function of magnetic field in Fig. 5.12. The magnetoresistance peak shifts to a higher magnetic field with increasing thickness. For the 22.24Å thick film, the magnetoresistance peak appears at 9.3 Tesla, while the peak shifts to a field higher than 10 Tesla at a thickness of 23.42Å.

Although the magnetoresistance peak shifts to very high magnetic fields in this series of films, the magnetoresistance is still different from previous work on homogeneous a-Bi films with thinner a-Sb underlayers. This difference can be seen in Fig. 5.13. The resistance of the 22.24Å thick film at different temperatures as a function of magnetic field is plotted in Fig. 5.13a. In Fig. 5.5, the plot of $R(T)$ of this film in zero field showed a tendency towards superconductivity. The resistance at various temperatures of a 11.20Å thick a-Bi film from an entirely different sequence of films is plotted as a function of magnetic field[78] in Fig. 5.13b. This film was grown over a 10Å a-Sb underlayer. This film is thinner than those not exhibiting superconductivity grown with a thicker underlayer but it is globally superconducting at 0.8K in zero field. It is clear to see that there is no magnetoresistance peak in this film.

There are two possible reasons for films with thinner underlayers having no magnetoresistance peak. They may be so far away from criticality that the peak is shifted to very high magnetic fields or there may be no magnetoresistance peak at all in these thinner underlayer films. Unfortunately, from our data we are not able to clearly distinguish which is true. On the other hand, the AFM scan in Section 5.3 reveals that the films grown on thicker underlayers have significant thickness variations on a mesoscopic length scale. This fact may contribute to the existence of the magnetoresistance peak and make the difference of between these two films.

5.7 Summary

We now summarize the results presented in this chapter. We have investigated the resistance on the superconducting branch of SI transitions tuned by thickness and by magnetic field. We found the data to be consistent with a model of overdamped JJAs. At higher temperatures, the resistance vs. temperature in zero field is consistent with the form predicted for the BKT transition, while in non-zero field it is of the Arrhenius form. At lower temperatures, the resistances become temperature-independent, which suggests that the electrical transport is dominated by quantum tunneling of vortices in a tilted washboard potential model. The crossing temperature and the value of resistance are also consistent with a model of vortices moving in an overdamped JJA. These films may still have magnetoresistance peaks in perpendicular fields but they have been shifted to very high magnetic fields. The response of the resistance to perpendicular magnetic fields is different from that superconducting films grown with thinner underlayers.

These results support the idea of that these strongly disordered superconducting films break into islands near criticality. Atomic Force Microscope scans reveal that the films are continuous with a 13% of thickness variation on a mesoscopic length scale. These thickness variations may contribute to the formation of superconducting islands and lead to magnetic field response different from that of films with thinner underlayers.

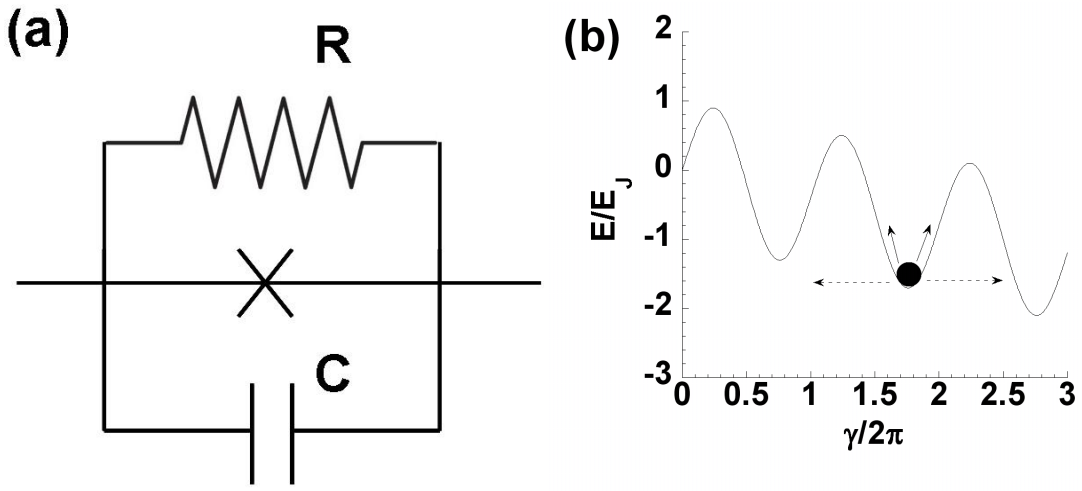

Figure 5.1: (a)A schematic of the equivalent circuit of the RCSJ model. The center cross represents a Josephson junction. (b) the "tilted washboard" potential described by Eq (5.5). The system point can escape from a well by thermal activation (solid arrows along the potential barrier) or by a quantum tunneling process (dashed arrows through the potential barrier).

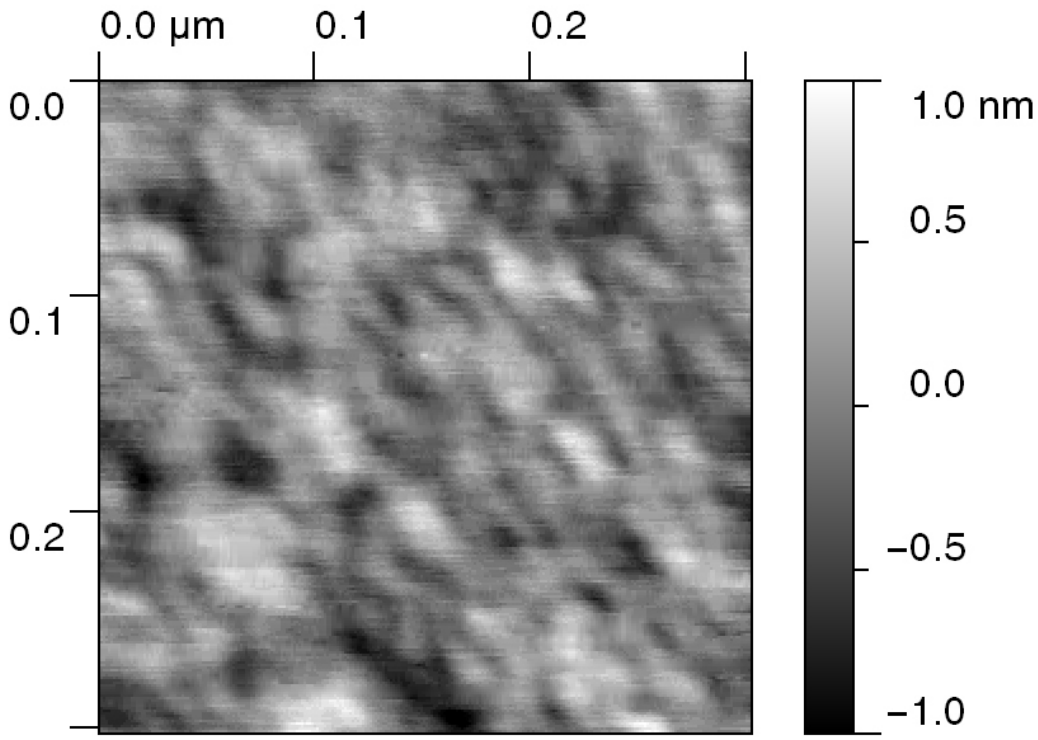

Figure 5.2: Surface height AFM scan of the 23.42Å thick *a*-Bi film. The scan is taken *ex situ* after a slow warming process.

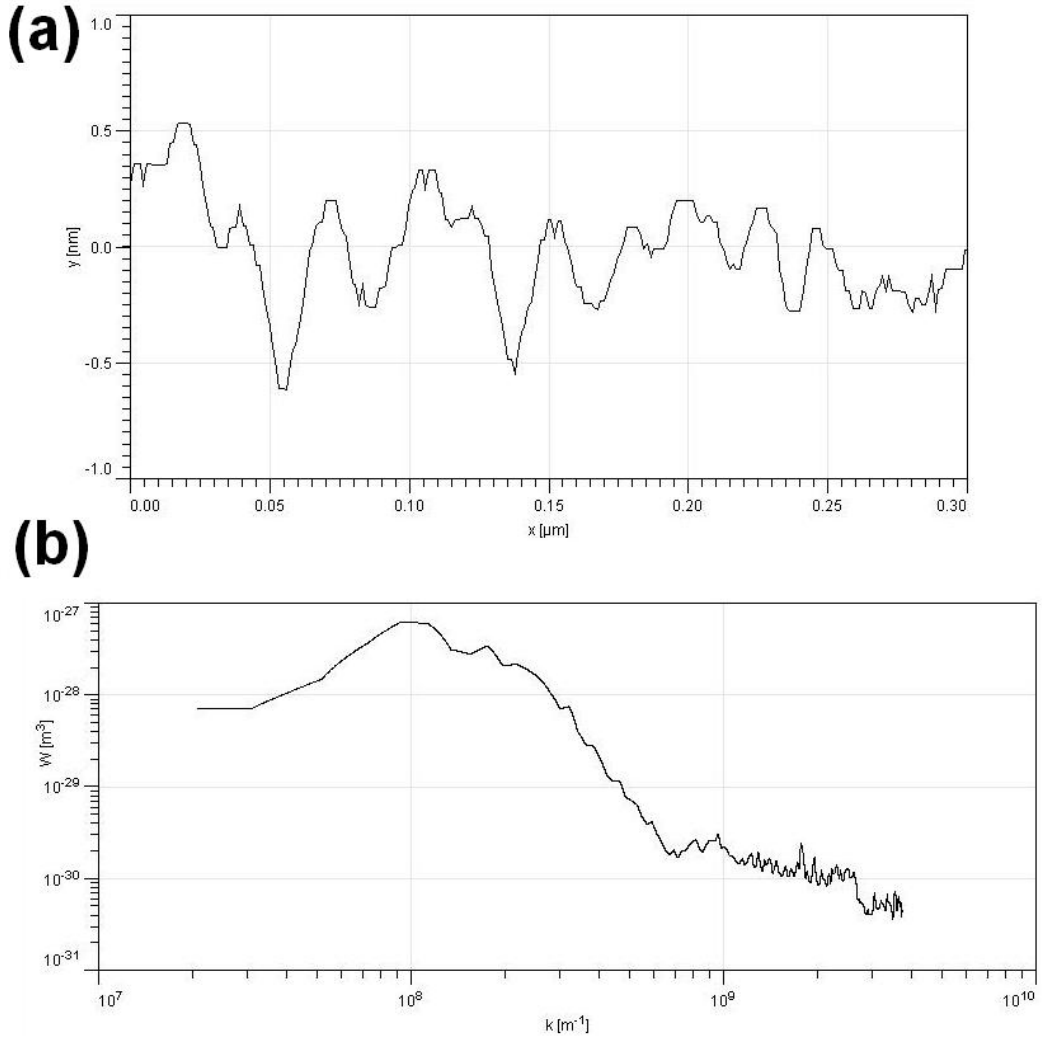

Figure 5.3: (a) Cross sectioned analysis of a horizontal cut in Fig. 5.2. It shows the surface has thickness variations but the film is well connected (b) The power spectral density of Fig. 5.2. It shows a peak at $k = 10^8 m^{-1}$, which represents a periodicity of the surface roughness.

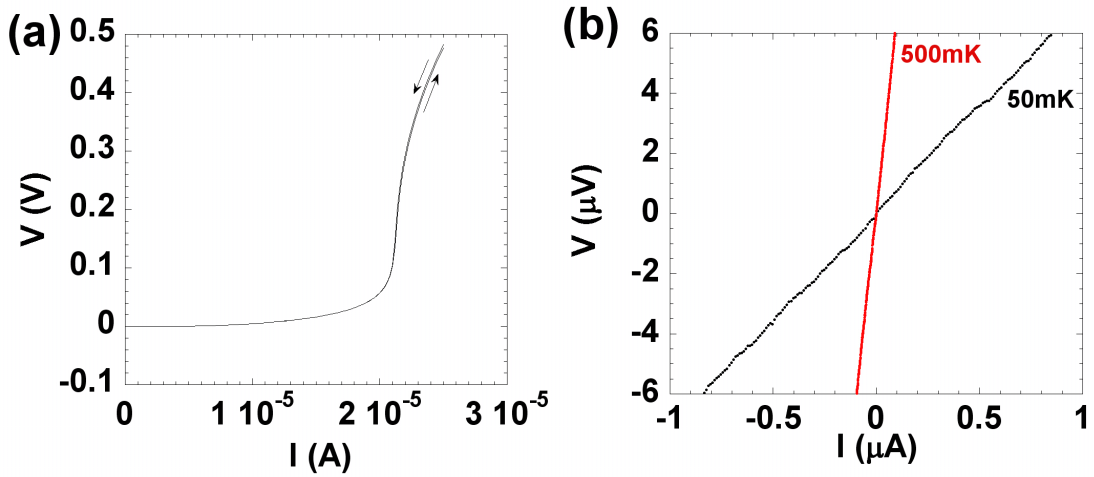

Figure 5.4: (a)The I-V characteristic of a 23.42Å thick film at 50mK in zero magnetic field. The arrows emphasize that the measurements were conducted sweeping back and forth between high and low currents. The I-V characteristic is not hysteretic. (b) The I-V characteristic of a 23.42Å thick film at 50mK and 500mK in zero magnetic field with a smaller scale. This shows that the I-V characteristic is linear in the small current limit.

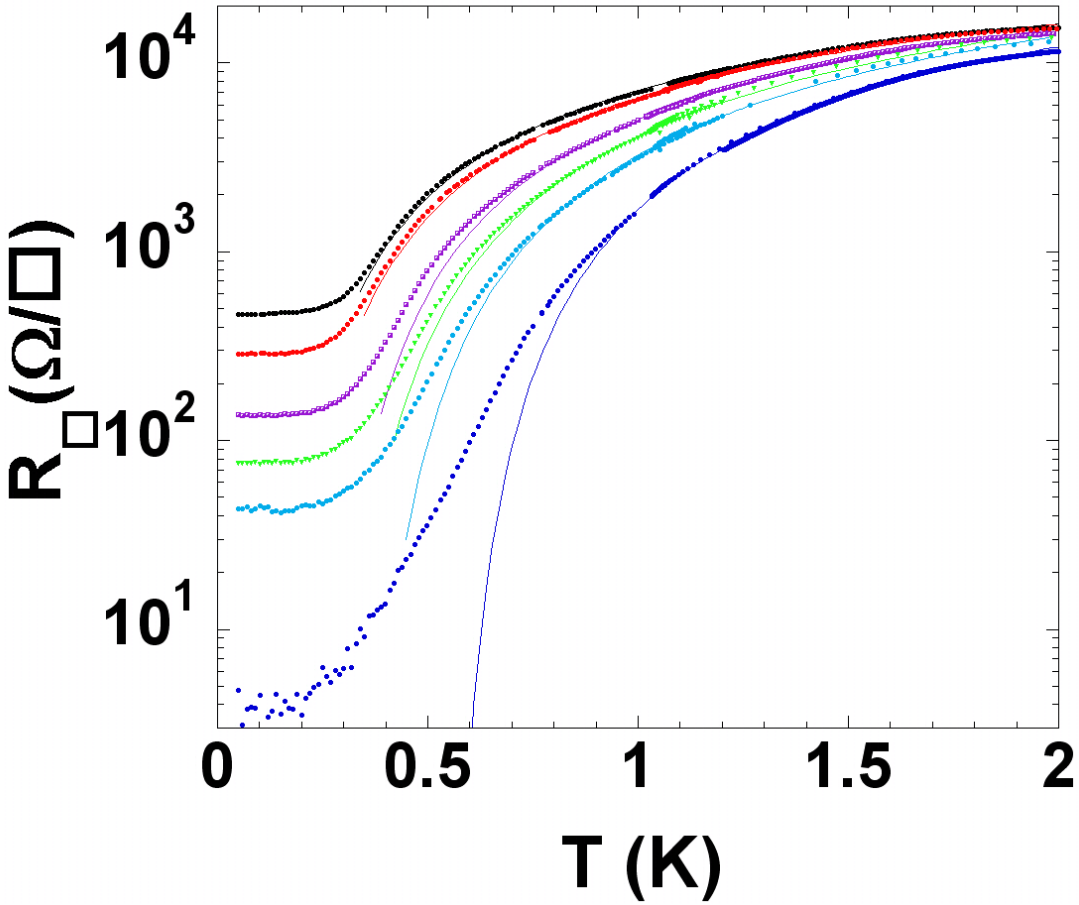

Figure 5.5: Sheet resistance vs. temperature of 22.24Å (top), 22.36Å, 22.63Å, 22.89Å, 23.15Å, and 23.42Å (bottom) *a*-Bi films in zero magnetic field. The solid lines are a fit by the Halperin-Nelson form (Eq (5.7)). The resistance is plotted on a logarithmic scale to emphasize the deviation between the data and the Halperin-Nelson form at low temperatures.

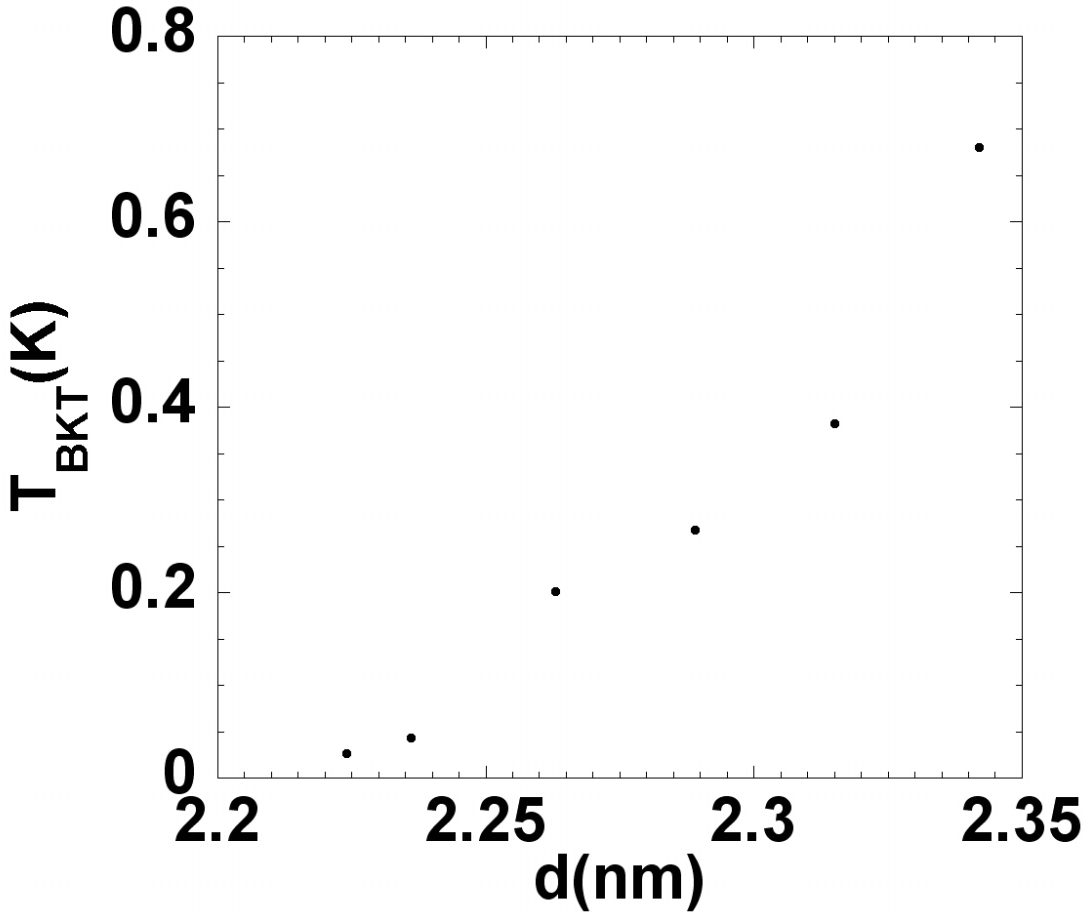

Figure 5.6: Brzezinski-Kosterlitz-Thouless transition temperature versus thickness of sequentially quenched-deposited a-Bi films in zero field. The transition temperature T_{BKT} is obtained by fitting the resistances with Eq. (5.7).

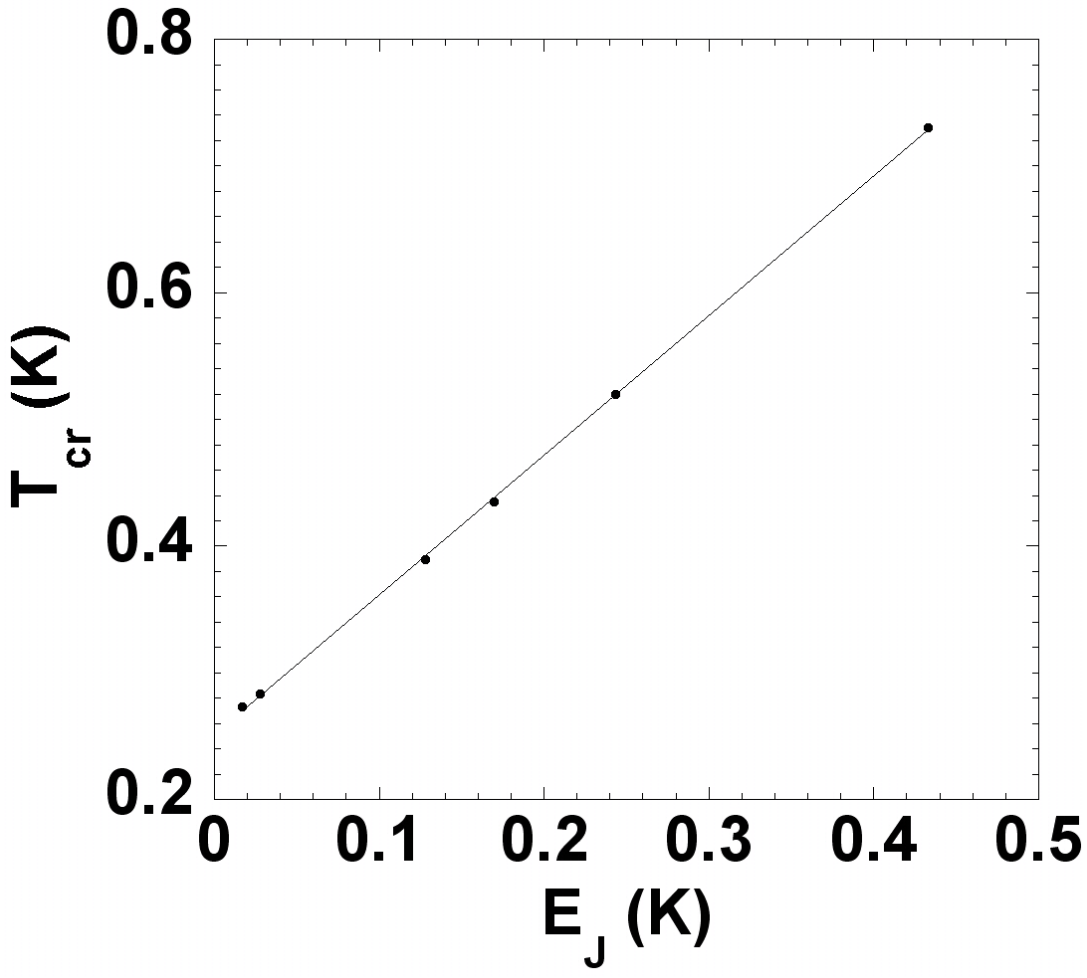

Figure 5.7: Crossing temperature plotted vs. the BKT temperature. The crossing temperature is obtained by inserting the value of the flattening resistance into Eq. (5.7).

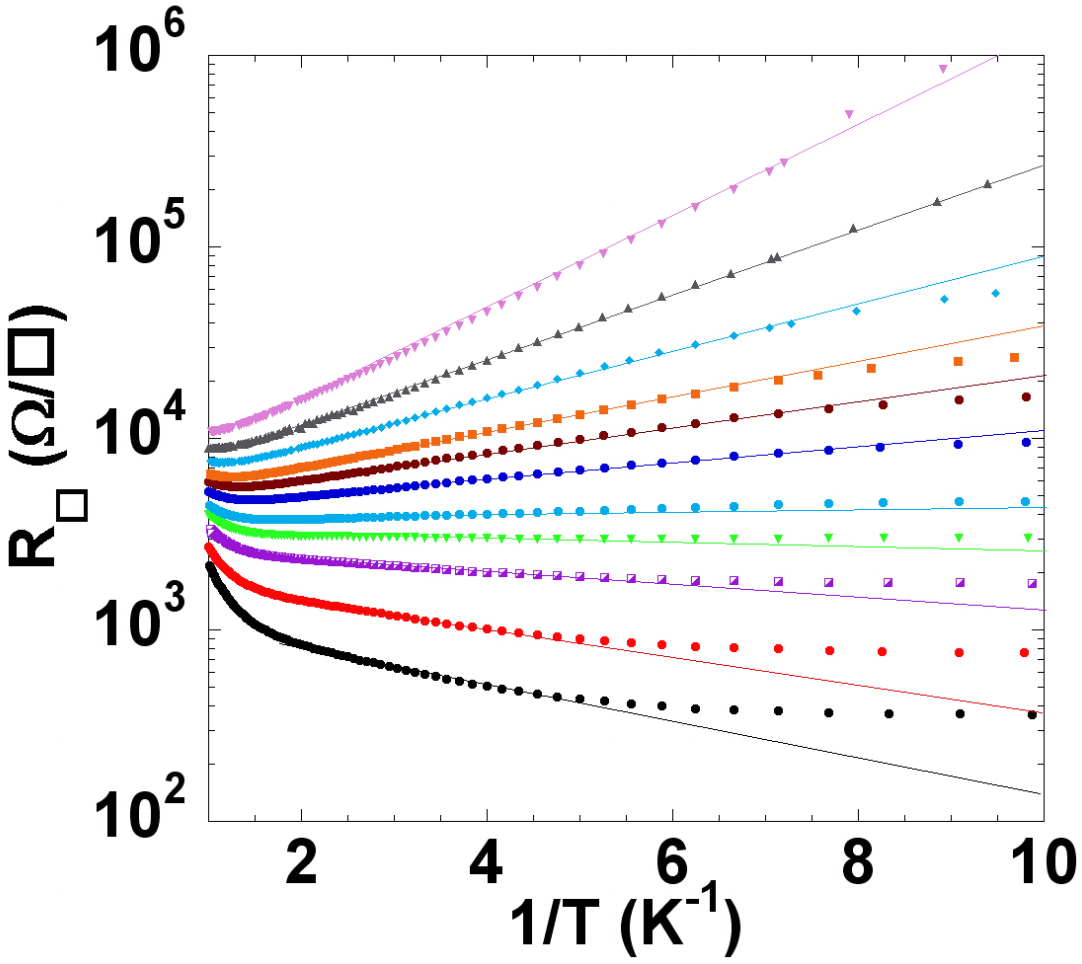

Figure 5.8: Arrhenius plot of the 23.42Å thick film in a perpendicular magnetic field. The magnetic fields applied are (bottom) 0.05, 0.1, 0.2, 0.3, 0.4, 0.6, 0.8, 1, 1.4, 2, 3T (top). The straight lines are the Arrhenius type fit. One can see that in the low fields, the resistance flattens out at low temperature.

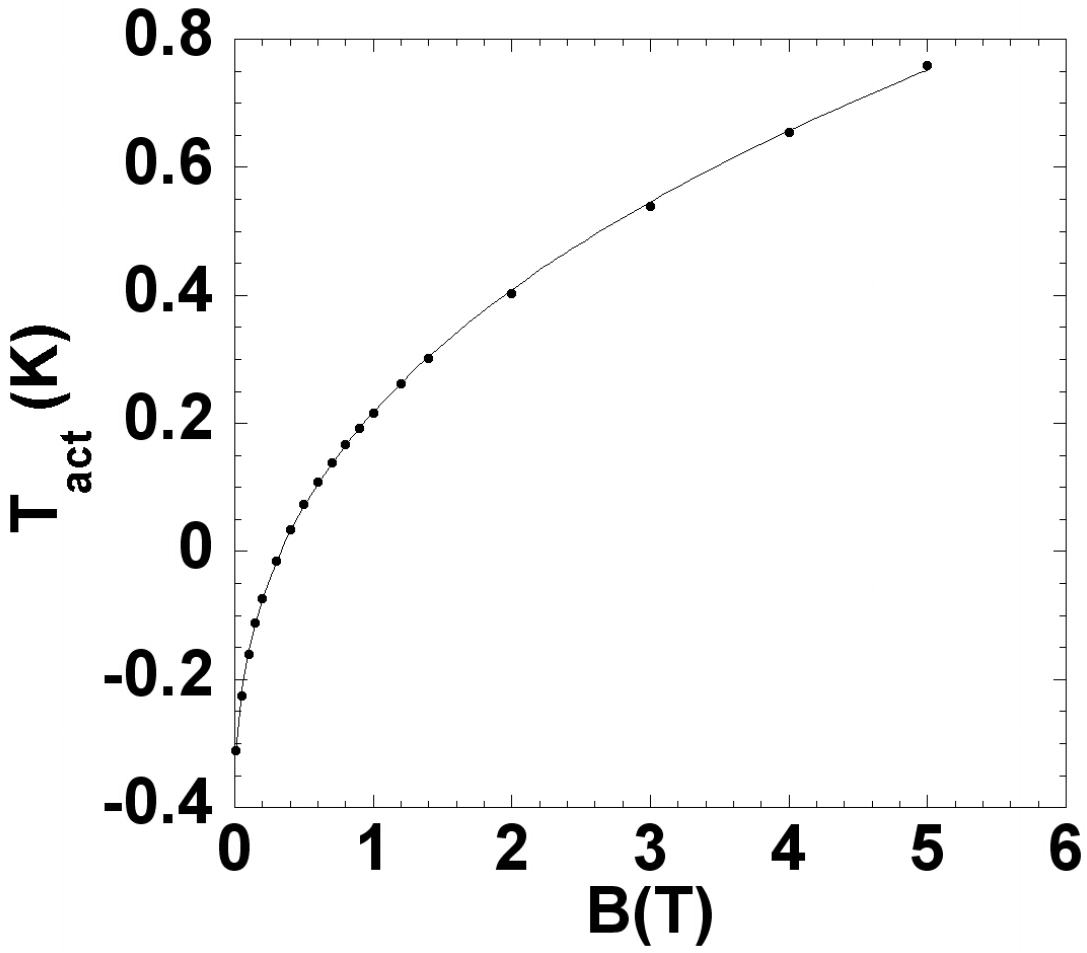

Figure 5.9: Activation energy of Arrhenius conduction of the 23.42Å film vs magnetic field. The fit is carried out in the temperature range from 200mK to 500mK. The solid curve shows that the activation energy can be described by $T_{act} = T_0 + a_0 B^b$, where $T_0 = -0.43$, $a_0 = 0.647$, $b = 0.374$ for this film.

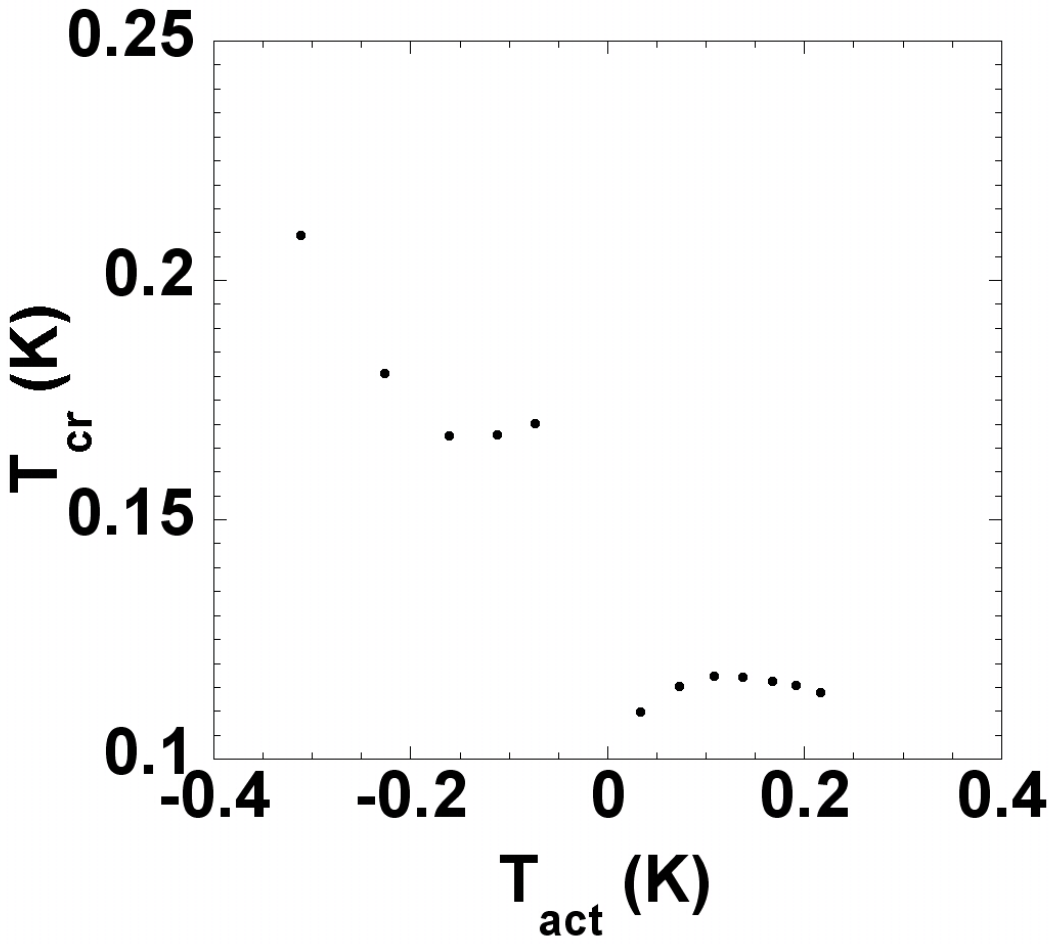

Figure 5.10: The crossing temperature vs the activation energy during the magnetic field tuning of the 23.42Å thick *a*-Bi film. The crossing temperature is the temperature of which the resistance changes from thermally activated behavior to temperature independent behavior.

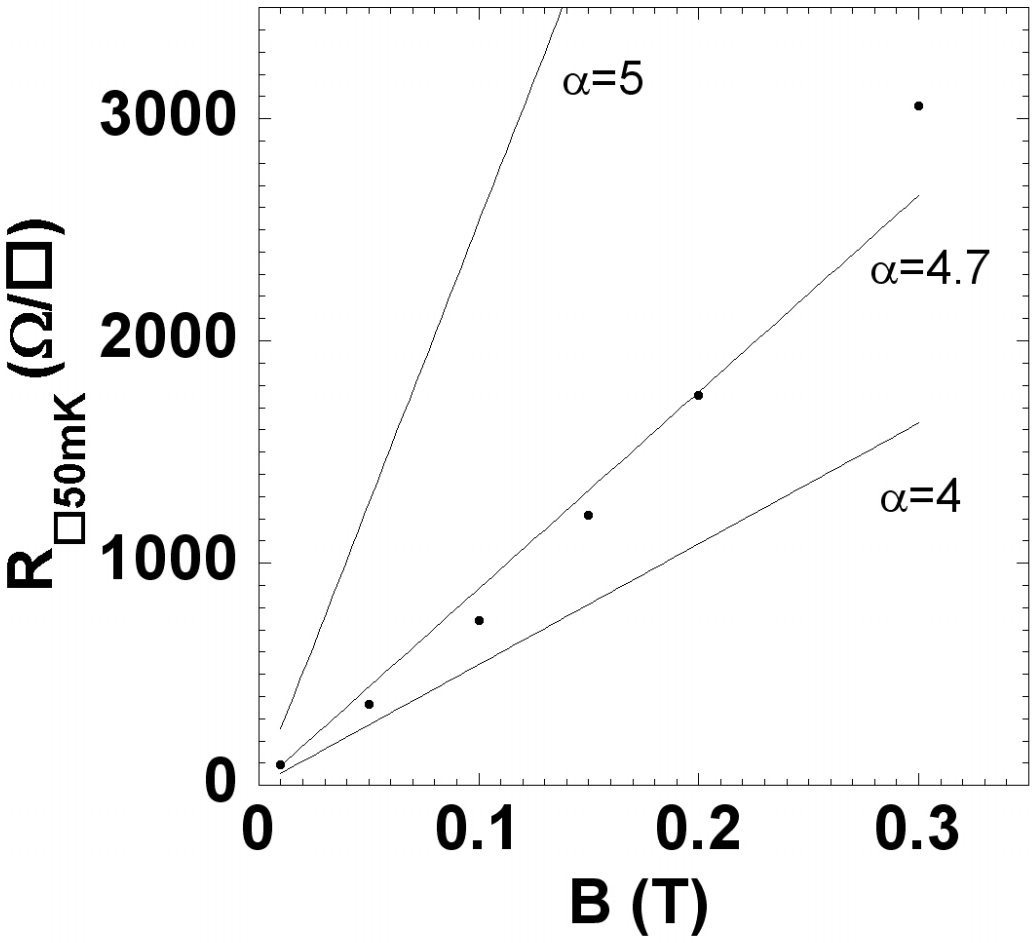

Figure 5.11: The resistances at 50mK vs magnetic fields the 23.42Å a-Bi film. The solid lines are calculated values base on Eq (5.18) with different α. The calculation based on the assumption that the damping parameter α and shunt resistance R are constant in different magnetic fields.

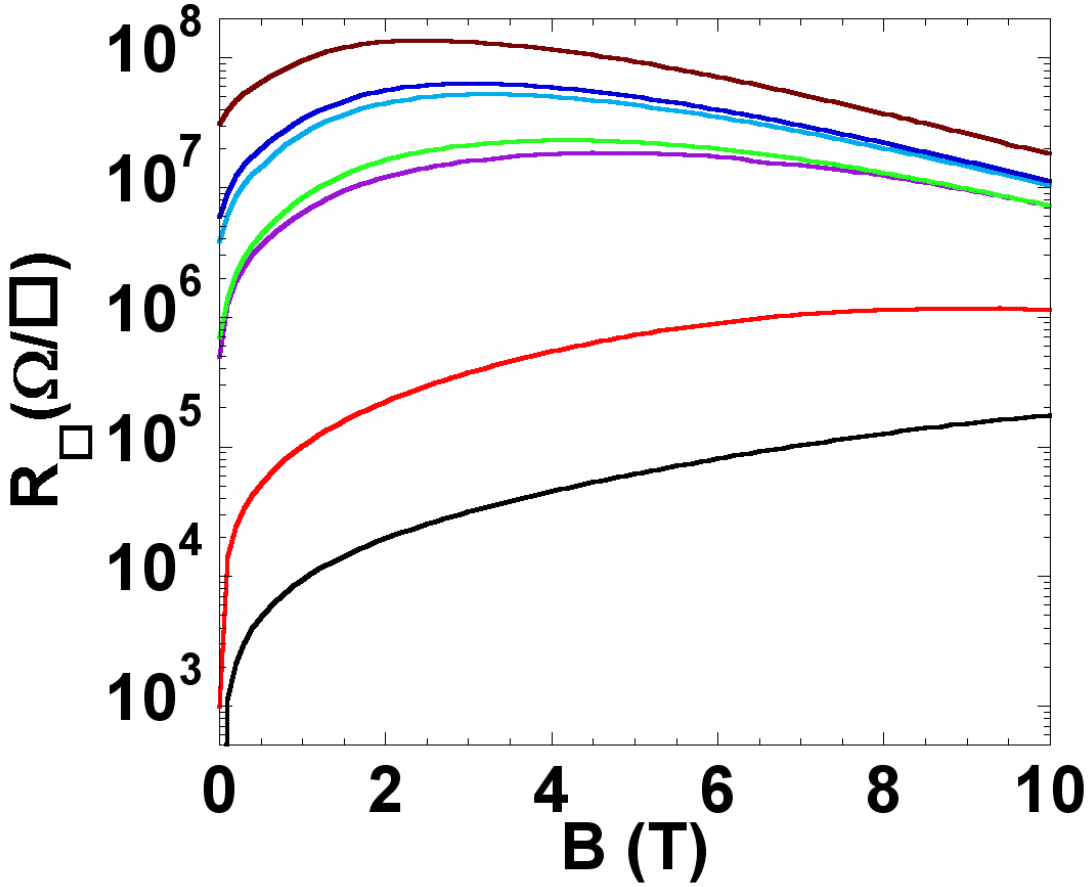

Figure 5.12: The resistances of different film thicknesses at 300mK as a function of magnetic field. The Thicknesses of the films are 21.12Å(top), 21.38Å, 21.58Å, 21.80Å, 22.01Å, 22.24Å, 23.42Å(bottom).

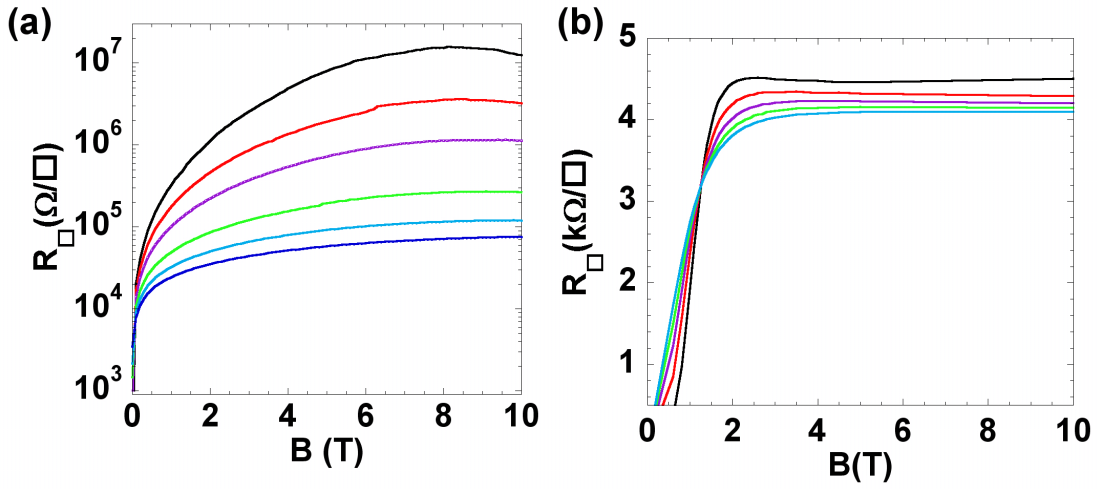

Figure 5.13: (a) resistance of the 22.24Å thick a-Bi film at temperatures of 200mK(top), 250mK, 300mK, 400mK, 500mK, and 600mK vs magnetic field. This film grown on top of 14.67 a-Sb underlayer and $R(T)$ in zero field is shown in Fig. 5.5. (b) Resistance of the 11.20Å thick a-Bi film at temperatures of 200mK(top), 300mK, 400mK, 500mK, and 600mK vs magnetic field. This film grown on top of 14.67 a-Sb underlayer and has global superconductivity at 0.8K in zero field[78].

Chapter 6

Hard Gap in the Insulating Regime of Nominally Granular Films

6.1 Introduction

Despite extensive investigations, generally accepted models of the SI transitions have not emerged, in part because the precise mechanisms may be material and tuning-parameter dependent in an unknown manner.[3]

Until recently there have been two principal approaches to SI transitions. In the first, a film is modeled as an array of Josephson junctions with the transition resulting from the competition between the charging and the Josephson coupling energies.[79] This picture involves the Mott-Hubbard localization of Cooper pairs. If one assumes that there is electromagnetic duality between vortices in the superconductor and charges in the insulator then the SI transition in two dimensions is characterized by a universal resistance $h/4e^2$.[25] In the second approach the Coulomb repulsion is enhanced in highly disordered films, weakening the net effective Cooper attraction.[80] This model has been referred to as fermonic, whereas

the first is usually referred to as bosonic. Studies of the insulating regime have emerged as a means of distinguishing between these two approaches. Paalanen, Hebard and Ruel were the first to report a *peak* in the magnetoresistance of InO_x films on the insulating side of the SI transition which they interpreted as a crossover between a Bose and a Fermi insulator .[26] This feature has been the subject of numerous investigations in recent years. For a review see Gantmakher and Dolgopolov.[81]

A new element in the theory has been the emergence of several models of the SI transition which include pairing on the insulating side of the SI transition, but emphasize the role of spatial inhomogeneity of the order parameter and predict the presence of a hard gap in the insulating regime, which is observed in experiments including those carried out in a magnetic field.[31, 32, 9] Ghosal, Randeria, and Trivedi[36] showed that with increasing disorder the system breaks up into localized superconducting islands exhibiting a finite spectral gap in the density of states. Muller [39] developed a Bose glass picture and predicted that in the insulating regime purely electronically activated transport occurs at asymptotically low temperatures. Feigel'man *et al.* developed an approach involving the localization of single electron eigenstates.[17, 82]

The latter theory predicts activated transport by generalizing the work of Matveev and Larkin[83] who introduced the idea of a parity effect in ultrasmall superconducting grains, which would result in a hard gap in the electrical transport properties. In the work of Feigel'man *et al.*, the local attractive interaction is considered within the standard BCS theory with the eigenstates treated as fractal. The localization of the eigenstates at strong disorder leads to the appearance of an

energy scale $\delta_L = 1/\nu_0 L^3$, where L is the localization length and ν_0 is the single-spin density of states. Here the localization is considered to be three-dimensional. The quantity δ_L is the average level spacing inside the volume in which the wave function is localized. Superconductivity survives if $T_c \gg \delta_L$, which is essentially Anderson's theorem.[84] Then in the range $T_c \ll \delta_L \ll \omega_D$, where ω_D is the Debye frequency, pairing correlations lead to the formation of a hard-gap insulator instead of one described by variable range hopping. The multifractal character of the single-electron eigenfunctions near the mobility edge is taken into account and the theory makes specific predictions of physical properties of the system dependent upon the proximity of the Fermi energy, E_F, to the localization edge, E_c, where $|E_F - E_C| \ll E_F$. The systematic behavior of the insulating state of nominally granular amorphous quench-condensed Bi, Ga, and Al films, reported here appear to be consistent in remarkable detail with the theory of Feigel'man *et al.*[17, 82]

Of particular interest in the present context are observations of Arrhenius activated behavior, *i.e.*, a hard gap in zero field and in magnetic fields on the insulating side of the SI transition in two-dimensional, nominally homogeneous amorphous systems.[31, 32, 9] It also been observed in this study, which has been presented in the previous chapters. These results are a challenge for theories of the insulating regime. In this chapter, we report a systematic study of Arrhenius behavior in the insulating regime, in zero magnetic field, of a different type of system exhibiting a SI transition. Surprising quantitative agreement with the theory of Feigel'man *et al.* [17, 82]has been found for nominally granular, monatomic, quench-deposited, amorphous quench-condensed films of Bi, Ga, and Al.

6.2 Thickness Tuning of Granular Films

Most previous research on quench-condensed films has been focused on nominally homogeneous, films grown by deposition onto substrates pre-coated *in situ* with a 10 Å thick underlayer of either *a*-Ge or *a*-Sb.[1] These underlayers have unmeasurable conductance. Films grown without the underlayer are thought to be granular and exhibit resistance vs. temperature curves, $R(T)$, which are nonmonotonic at values of thicknesses that are close to the threshold for superconductivity. They also achieve measurable conductances at greater thicknesses than nominally homogeneous films.

The data presented here were obtained by cycles of deposition and measurement that were all carried out *in situ* employing two different deposition systems using different refrigerators and separated in time by several decades. The nominally granular and nominally homogeneous *a*-Bi films were grown on (100) $SrTiO_3$ (STO) single-crystal substrates, while the nominally granular Ga and Al films were grown on silica-glazed alumina substrates. Typical examples of the evolution of Bi film resistances with thickness are shown in Fig. 6.1.

Recently we found that it is possible to stabilize the structure of quench-condensed films by encapsulating them with a thin layer of *a*-Sb. After doing this, slow warming does not result in their crystallization. This can be monitored by tracking the resistance. Amorphous Bi is a metal, whereas its crystallization results in a dramatic increase in resistance and the loss of superconductivity and metallic behavior. A comparison of the structures of two *a*-Bi films, one nominally homogeneous and one nominally granular as determined by atomic force microscopy (AFM) is shown in Fig. 6.2. The total thicknesses of the two films differ only by 5Å. However the magnitude and length scales of their surface roughnesses

differ significantly. For the nominally homogeneous film, thickness variations are small and occur over relatively long distances, whereas for the nominally granular film the variations are larger and are over shorter distances. The root mean square roughness R_{rms} for homogeneous films is 1.3Å with maximum thickness difference around 9Å, while R_{rms} is around 7Å and with maximum thickness difference around 20Å in granular film. In addition analysis of the surfaces' power spectra of the two configurations suggest that nominally granular films are of fractal dimensionality, whereas nominally homogeneous films are two dimensional.[78] These images suggest that nominally granular films do not consist of grains coupled by tunneling junctions, but are directly connected. This is a new approach to the understanding of nominally granular quench-evaporated films. Both nominally homogeneous and nominally granular configurations are noncrystalline as a consequence of being quench deposited. Note that these AFM scans are from films at the final stage of thickness tuning and in both examples the films exhibited global superconductivity at low temperature. However, given the very small variations of nominal thickness of both types of films traversing the transition from insulator to superconductor the two images may be representative of the insulating regimes of both types of sequences. An important caveat is that we have not carried out similar studies on the Ga and Al films, and their growth modes may be different from that of Bi.

The relatively large spatial variations in thickness of nominally granular films can result in local variations of the pairing amplitude as well as bring about a shortening of the localization length.[87] The latter is quite critical to the observation of a hard gap which is determined by the level spacing of single particle excitations within the localization length. A large localization length implies a

small level spacing, which could lead to an unobservable parity effect. Indeed, data of $R(T)$ of nominally homogeneous a-Bi films with thicknesses close to the critical thickness do not exhibit a hard gap. They can be fit by a 2D Mott variable range hopping form as shown in Fig. 6.3.[20]

6.3 Data and analysis

The prediction of Feigelman *et al.*[17, 82] is that in the insulating state the conductivity obeys an Arrhenius form

$$R \sim \exp\left[T_0/T\right] \tag{6.1}$$

and that the activation energy T_0 can be written in the form

$$T_0 = A(1-\sigma/\sigma_c)^{\nu D_2} \tag{6.2}$$

Here A is conductivity-independent constant, σ is the high-temperature conductivity, and σ_c is the value of the conductivity at which the hard gap first develops. Here ν is the localization critical exponent, and D_2 is the fractal dimension of the eigenfunctions. This exponent product is asserted to be 1.3, a result which follows from numerical work associated with the fractal character of the eigenfunctions associated with the 3D Anderson transition.[88, 89]

Figures 6.4, 6.5, and 6.6 show the variation of the logarithm of the resistance with the reciprocal of temperature for the sequences of films of nominally granular a-Bi, a-Ga, and a-Al in the insulating regime. Arrhenius conduction is found in the temperature regime below the local minimum of $R(T)$. This implies that local superconductivity is present although the films are insulating. At temperatures below the minimum in $R(T)$ there may be superconducting regions in the films, but the transport is dominated by an activated process.

To demonstrate that Arrhenius conduction is the best fit in these rather limited temperature ranges, we have compared the values of χ^2 determined for fits by several possible conduction mechanisms. Representative examples of the comparison are listed in table 6.1. Using this statistical analysis, Arrhenius conduction is found to fit better than either Efros-Shklovskii variable range hopping, or Mott variable range hopping in 2D or 3D for all three sequences presented here.

Figure 6.7 shows the activation temperature of the Arrhenius conduction plotted as a function of the high-temperature conductivity σ, which was chosen at 10K for Bi, 8K for Ga, and 14K for Al. From the plot, we determine by extrapolation the normal state conductivity σ_c at which the activation energy vanishes. The activation temperature can be fit by power law in $\sigma_c - \sigma$ with power close to 1.3, as shown in Fig. 6.8. This result is agreement with the predictions of the theory of Feigel'man *et al.*[17, 82] The localization length has been shown to depend upon film thickness, Fermi energy level, and film roughness.[87] Thus increasing the thickness of rough films and reducing their roughness, should increase their localization lengths, increase their conductances, and decrease the size of the activation energy.

Finally, we present our results of the series of a-Bi films with 14.67Å a-Sb underlayer. On the insulating side of SI transition, the $R(T)$ for these films are all of the Arrhenius type , which has been shown in Chapter 3. Here, we use the conductivity at 9K as normal conductivity σ. The average normal conductivity of two films on two sides of the SI transition is the critical conductivity σ_c. The activation energy T_0 of the films in zero field vs $\sigma_c - \sigma$ is plotted in Fig. 6.9. It is clear to see that the activation energies varies in a different way than the ones in Fig. 6.8. This suggests that the model may not be able to explain the behavior

in this series of films.

6.4 Discussion

These measurements demonstrate that there exists a hard gap in the insulating regime of these nominal granular films. The size and the evolution of the gap cannot be attributed to the superconducting gap of a superconductor-insulator-superconductor (SIS) tunneling model. The largest activation energies (temperatures) in these three film systems are all much larger than the bulk T_c, and the value of the activation energy decreases with increasing thickness, whereas the superconducting gap which would determine the activation energy in an SIS model would remain the same or increase with increasing thickness. In the presence of perpendicular magnetic field, films with properties close to the SI transition exhibit positive magnetoresistance and the value of activation energy increases with magnetic field. This is opposite to what would be expected for the superconducting gap in a magnetic field. In the temperature regime above the Arrhenius activated regime, the conductivities of these films are all consistent with Efros-Shklovskii variable range hopping. This further supports the view that the Arrhenius activated behavior is not due to Coulomb effects associated with nearest neighbor hopping, which might be the case if there were weakly coupled grains. As mentioned, similar activated behavior has also been reported for InO_x and TiN films both in zero field, and in the presence of magnetic fields.[31, 32, 9] The zero-field activation energy of InO_x appears to roughly follow the same power law with power 1.3 by tuning disorder.[17] The TiN data is not sufficiently detailed to draw any conclusions.

The other theoretical models predicting Arrhenius activated behavior in the insulating side of the SI transition such as those of Ghosal, Randeria, and Trivedi [36]and Muller[39] do not make specific predictions of the dependence of the activation energy on conductivity. Ghosal, Randeria, and Trivedi do show that the hard gap is inversely dependent upon the localization length. Muller's Bose glass model in which activation is a purely electronic process predicts that the prefactor of the activation form is of order h/e^2. Experimentally determined prefactors fluctuate around $h/4e^2$ but can be as large as h/e^2 for the most resistive films. The theory of Feigel'man *et al.[17, 82]* models the demise of superconductivity with increasing disorder as a competition with localization rather than a Coulomb effect.[80] The validity of such a picture is supported by early tunneling data on similarly prepared, nominally granular films, in which the superconducting gap remains nonzero through the superconductor-insulator transition.[90] In these experiments, which were planar tunneling studies, the gap edge broadened until its width became comparable to its average value. This was interpreted as a lifetime broadening effect, but the changes in the gap edge could very well have been produce by a spatial distribution of gap values which were averaged or summed in a planar tunneling experiment. Such behavior would not be inconsistent with what is found in scanning tunneling microscope studies of disordered TiN films in which the gap parameter varies with position and persists above the transition.[61]

6.5 Conclusion

In conclusion, we have found using a statistical analysis that Arrhenius activated conduction is the best description of data in the insulating regime of the SI transition of nominally granular quench condensed films of three different metals (Bi,

Ga and Al). An analysis to the structure of a Bi film demonstrates that nominally granular films may not be described as clusters connected by Josephson junctions but appear to be fully connected and quite rough. The systematic dependence of the activation energy on the high temperature conductance of nominally granular films has been found to be consistent with the theory of Feigel'man *et al.*[17, 82] The fact that consistency is found in films of three different metals measured at different times suggests that this agreement is not accidental, which is of course a possibility. This agreement further suggests that the picture of localization of single-particle wave functions and their fractal nature dominate the conduction mechanism of nominally granular quench-condensed films. An important puzzle is the apparent success of a model based on 3D localization for systems of films which are quasi-two dimensional. Also, the activation energy of homogeneous a-Bi with 14.67Å a-Sb underlayer does not follow the prediction of this model. This suggests that the theory of Feigel'man *et al.* may not be the complete explanation for this phenomenon.

Films	T^{-1}	$T^{-1/2}$	$T^{-1/3}$	$T^{-1/4}$
Bi 21.40Å	0.0132	0.0133	0.0148	0.0159
Bi 21.75Å	0.0053	0.0061	0.0120	0.0159
Bi 21.83Å	0.0088	0.0134	0.0188	0.0222
Bi 21.94Å	0.0030	0.0084	0.0113	0.0130
Bi 22.04Å	0.0186	0.0301	0.0349	0.0375
Bi 22.10Å	0.0402	0.0501	0.0537	0.0555
Ga 13.09Å	0.0299	0.1085	0.1477	0.1697
Ga 13.21Å	0.0145	0.0510	0.0696	0.0801
Ga 13.31Å	0.0125	0.0377	0.0523	0.0607
Ga 13.36Å	0.0124	0.0201	0.0260	0.0296
Ga 13.41Å	0.0086	0.0088	0.0101	0.0109
Ga 13.51Å	0.0085	0.0087	0.0087	0.0088
Al 51.64Å	0.0005	0.0014	0.0020	0.0023
Al 52.15Å	0.0055	0.0060	0.0098	0.0123
Al 52.23Å	0.0035	0.0040	0.0056	0.0067
Al 52.32Å	0.0054	0.0115	0.0149	0.0169
Al 52.40Å	0.0163	0.0218	0.0238	0.0249

Table 6.1: Here we list the comparison of the of the χ^2 fits of lnR to T^{-1}, $T^{-1/2}$, $T^{-1/3}$, and $T^{-1/4}$ for the four functional forms ($lnR \backsim T^{-1}$, $lnR \backsim T^{-1/2}$, $lnR \backsim T^{-1/3}$, and $lnR \backsim T^{-1/4}$). The definition of χ^2 is:$\chi^2 = \sum [(x_i - x_{fit}(T_i))/\sigma_i]$,where the x_i are the data points, $x_{fit}(T_i)$ is the fitted function, and the σ_i are the errors of the data points. The temperature ranges of the fits are 1.43K to 770mK for Bi, 4.5K to 3K for Ga, and 2.2K to 1.25K for Al. Despite the limited range of temperatures, the fit by T^{-1} is the best fit.

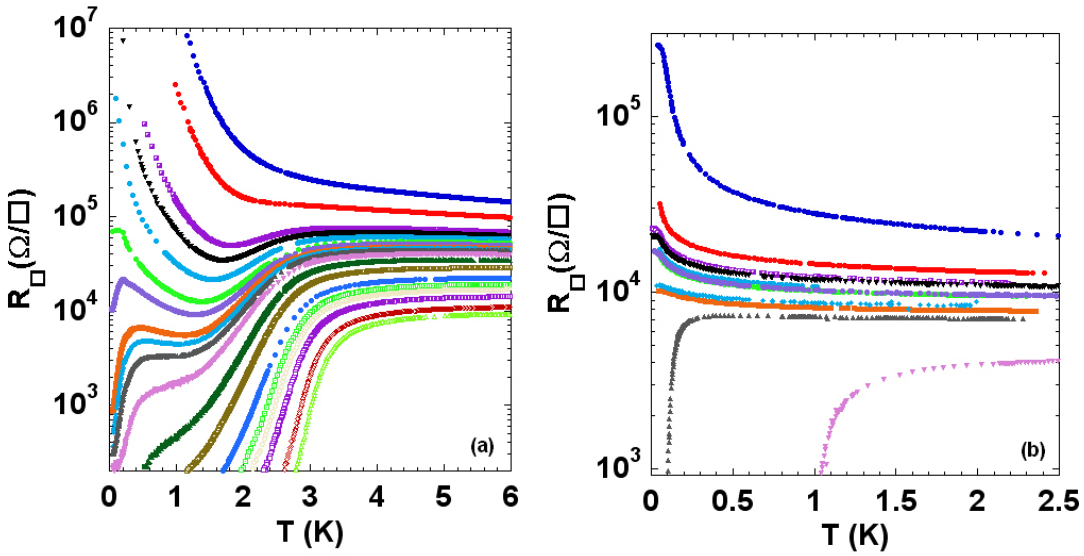

Figure 6.1: Sheet resistance vs. temperature of (a) a sequence of nominally granular $a-$Bi films with nominal thicknesses from 21.11Å (top) to 26.07Å (bottom) in average increments of 0.27Å and (b) of a sequence of nominally homogeneous $a-$Bi films with thicknesses from 8.89Å (top) to 10.40Å (bottom) in average nominal increments of 0.1Å.

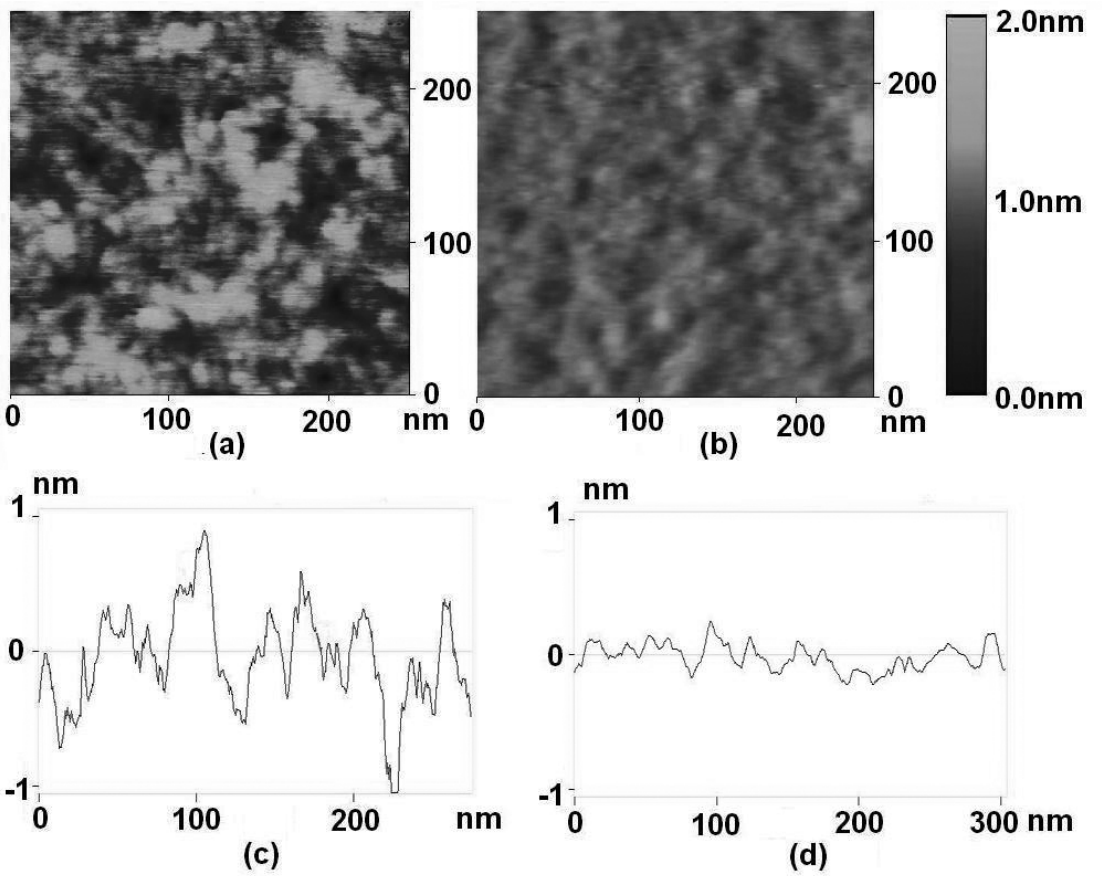

Figure 6.2: Atomic force microscopy images of (a) a 25.1Å thick nominally granular a-Bi film with a 15Å Sb capping layer and (b) a 10.4Å thick nominally homogeneous Bi film with a 10Å Sb underlayer and a 15Å Sb capping layer. These two scans share the same color scale. (c) is the cross section analysis of (a), and (d) is the cross section analysis of (b).

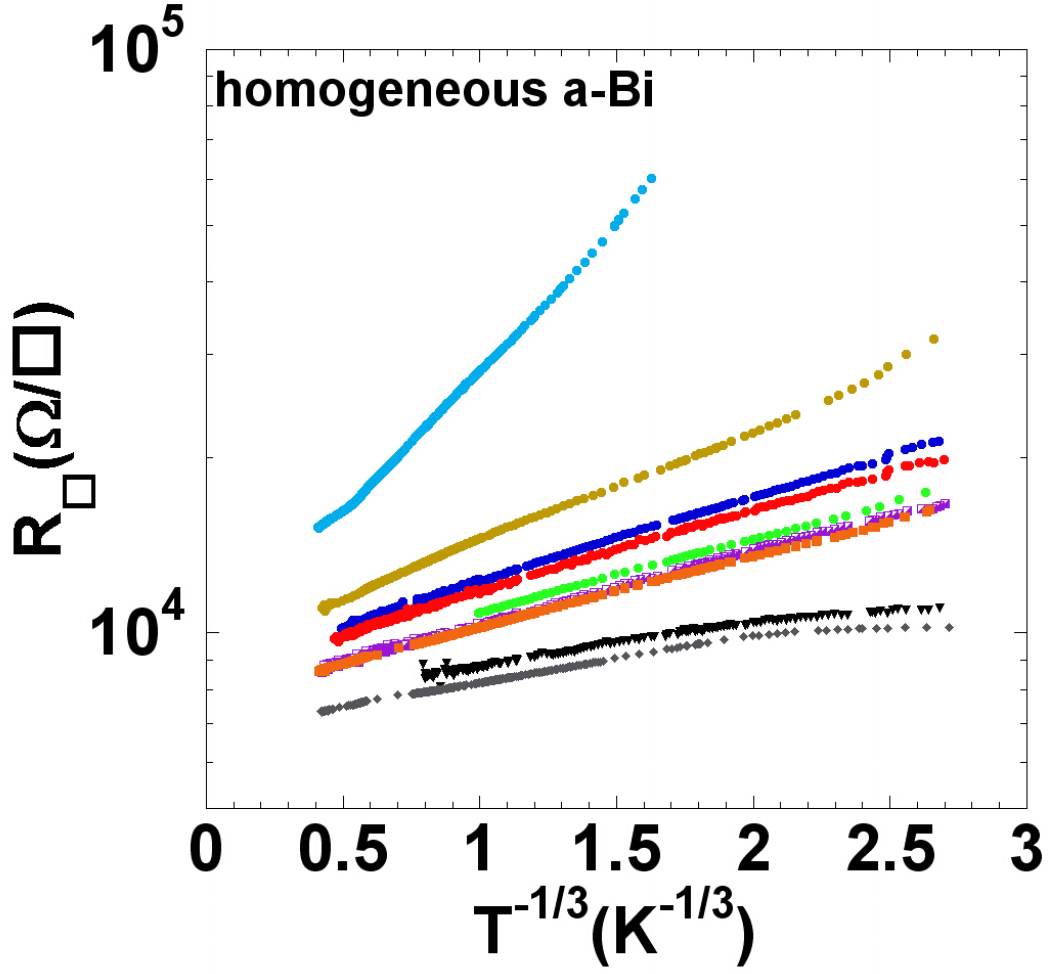

Figure 6.3: Sheet resistance versus $T^{-1/3}$ of a sequence of homogeneous a-Bi films of different thicknesses. The data used is that displayed in Fig. 6.1(b). This data can be fit by 2D Mott variable range hopping even for thicknesses very close to the critical thickness.

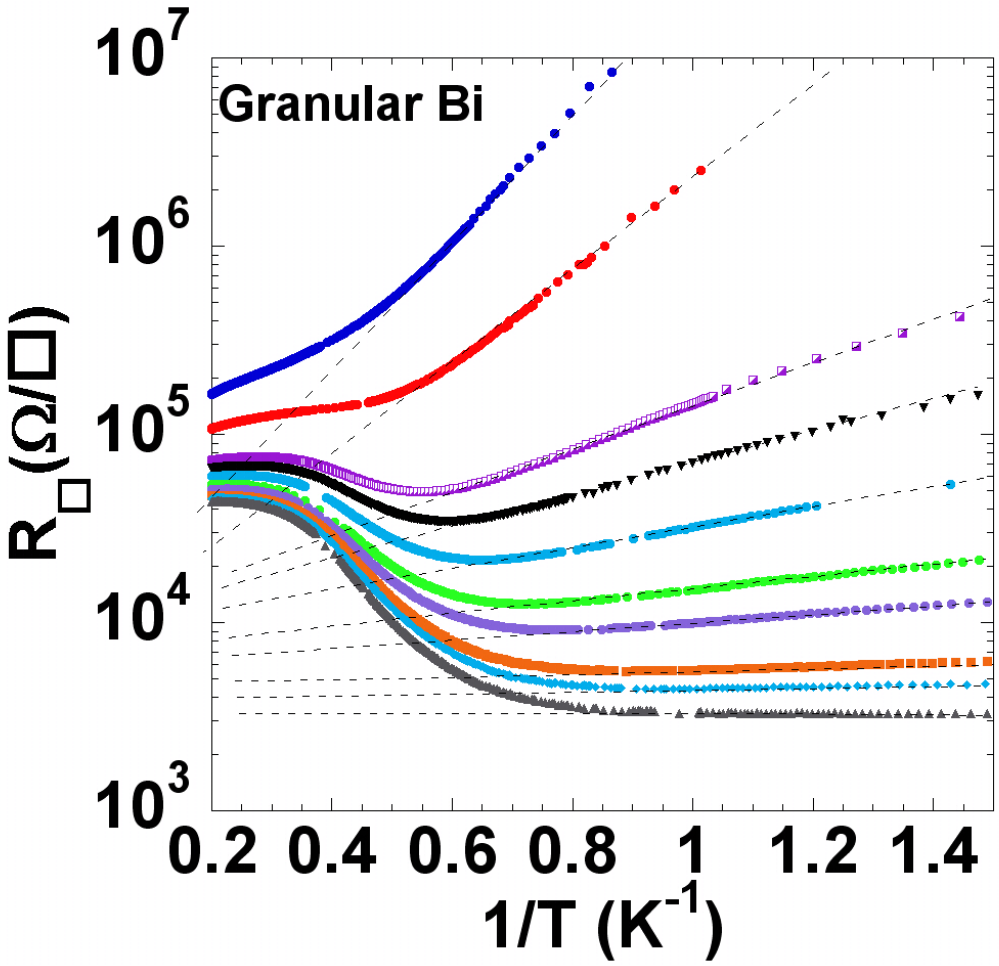

Figure 6.4: Arrhenius plots of granular Bi films with different thicknesses. The dash lines are guides to the eye. The thicknesses are from 21.11 to 22.23Å for the films. The data is from the work of Parendo *et al.* [86].

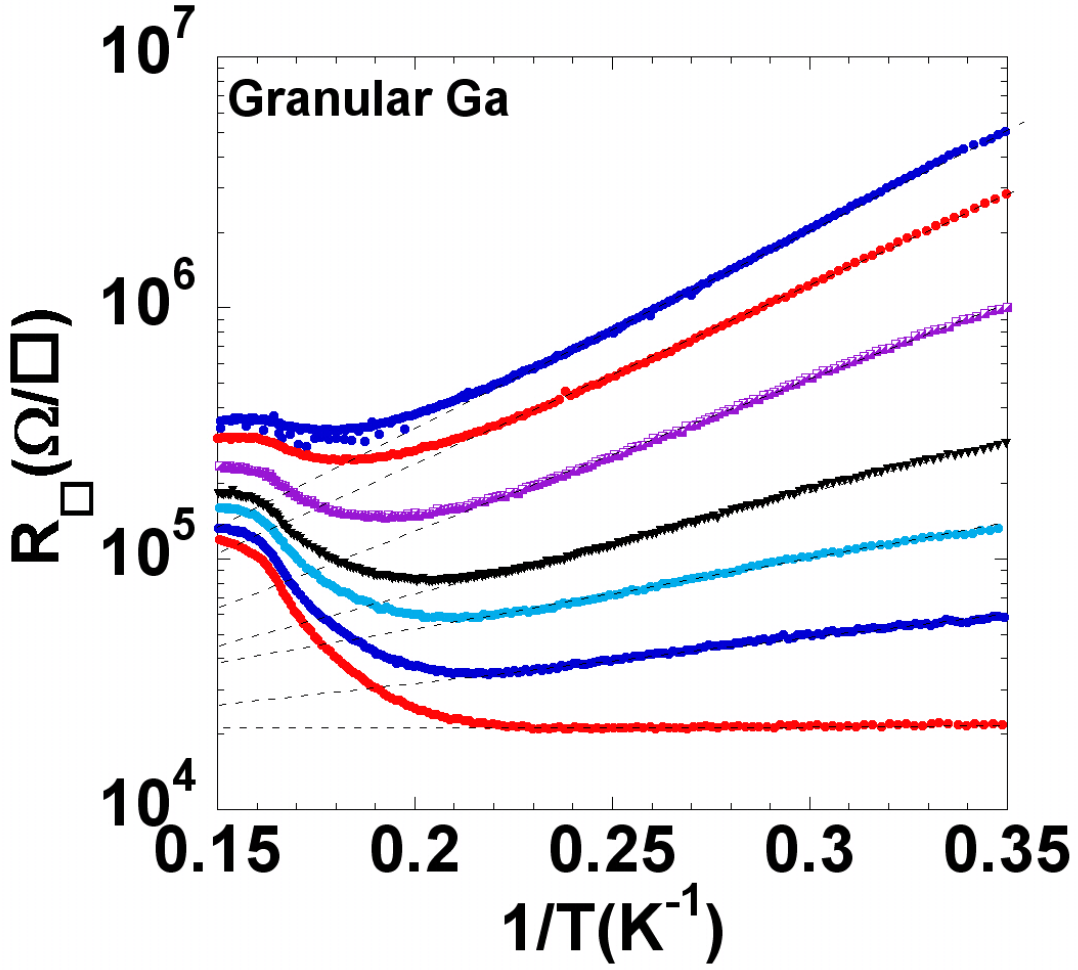

Figure 6.5: Arrhenius plots of granular Ga films with different thicknesses. The dash lines are guides to the eye. The thicknesses are from 13.09 to 13.51Å for the Ga films. The data is from the work of Jaeger *et al.* [?].

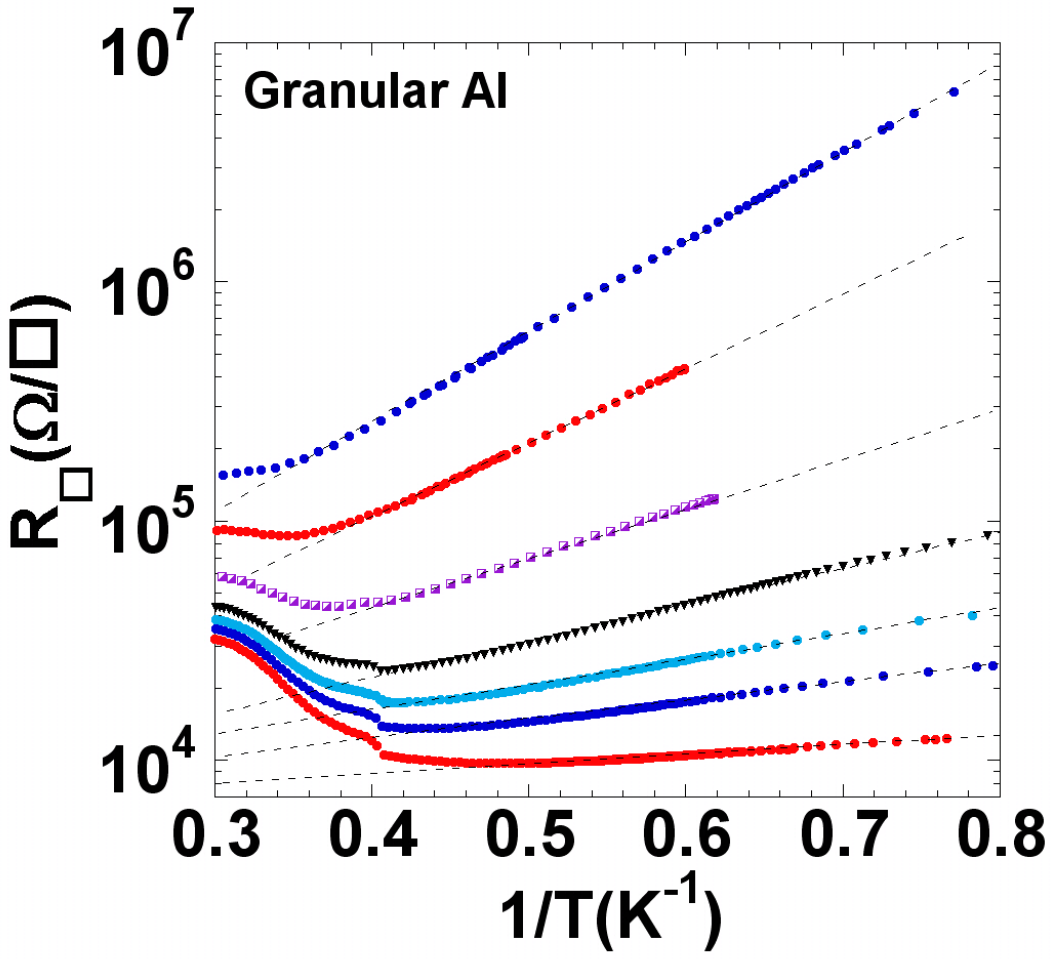

Figure 6.6: Arrhenius plots of granular Al films with different thicknesses. The dash lines are guides to the eye. The thicknesses are from 51.27 to 52.40Å for the Al films. The data is from the work of Jaeger *et al.* [**?**].

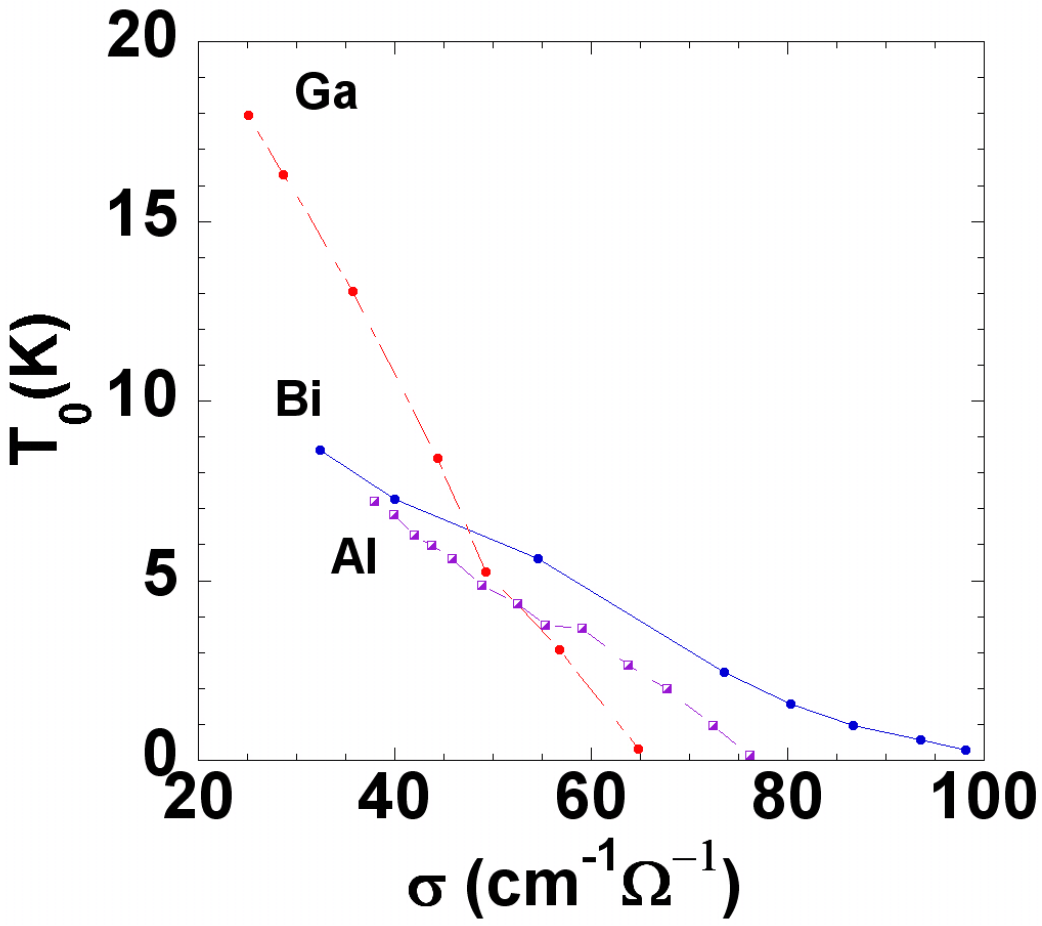

Figure 6.7: The activation temperature of three different materials versus conductivity σ in the normal state.

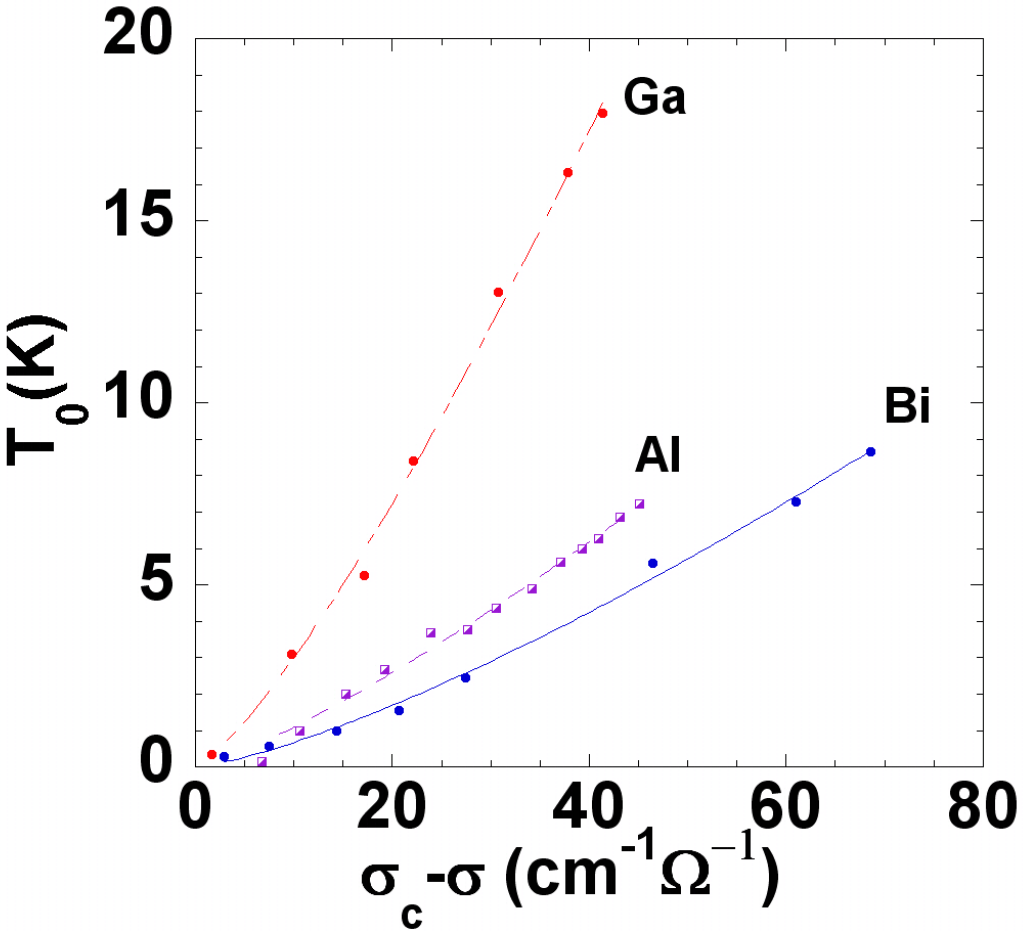

Figure 6.8: The activation temperature versus (σ_c-σ). The lines are fits by a power law with a power of 1.329 ± 0.062 for Bi, 1.272 ± 0.056 for Ga, and 1.254 ± 0.058 for Al.

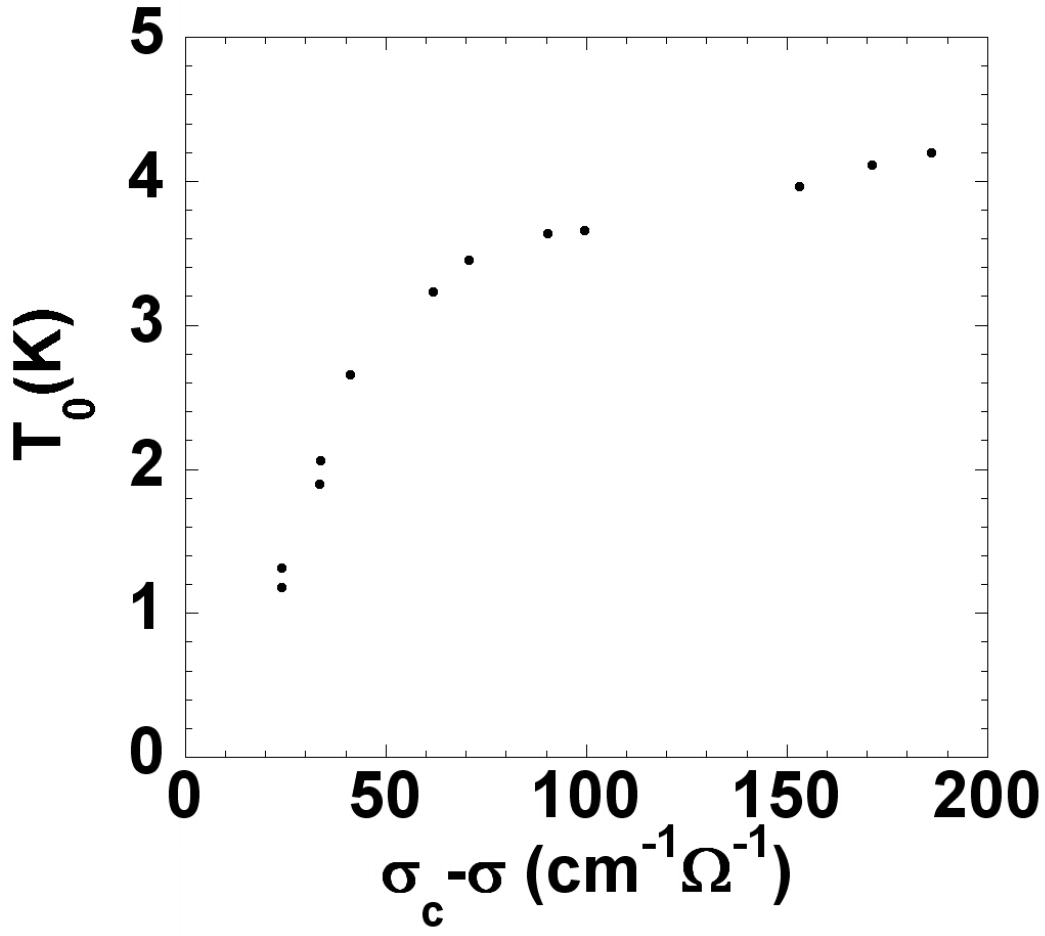

Figure 6.9: The activation energy T_0 of the films with 14.67Å a-Sb underlayer in zero field vs $\sigma_c - \sigma$. The film thicknesses are from 19.74Å to 22.01Å with an average 0.2Å increment.

Chapter 7

Conclusions

A combination of thickness and perpendicular magnetic field tuning of SI transitions has been performed on a series sequentially quench-deposited homogeneous a-Bi thin films with a 14.67Å a-Sb underlayer. Transport properties, including measurements of resistance and of I-V characteristics have been studied in both the insulating and superconducting regimes. In the insulating regime, in perpendicular magnetic fields, the resistance exhibits an Arrhenius type of conduction rather than variable range hopping at low temperatures. For the films with an Arrhenius prefactor smaller than $h/4e^2$ in zero magnetic field, the magnetoresistance (MR) exhibits a peak as a function of perpendicular magnetic field. Furthermore, isotherms of MR cross over at values of magnetic field higher than those at which the MR peak is found at different temperatures. At this crossing field, the prefactor of the Arrhenius conduction form is equal to $h/4e^2$. The MR can be scaled around this crossing field with a critical exponent product of $\nu z = 0.7$, which corresponds to the universality class of the (2+1)D XY model. This reveals a possible quantum phase transition in the insulating regime, presumably the transition is between the Bose and Fermi insulators discussed extensively in the literature.

The I-V characteristic exhibits strong non-linearity in the insulating regime at low temperatures in both the zero and non-zero field regimes. It has been found that these non-linear I-V curves can be well described by a heating model involving the decoupling of the electron and phonon temperatures at low temperatures. This may not be related to the superconductivity but the model provides a quantitative way to estimate the heating effect due to power dissipation by the measuring current.

On the conductive or superconducting side, the transport properties are found to be remarkably similar to those of an overdamped random Josephson junction array and vortex dynamics dominates the conductive behavior in both zero and non-zero magnetic fields. At high temperatures, the resistances of films can be described by the Halperin-Nelson form but deviate and flattening out at different finite values of temperature in zero magnetic field. This suggests that a Berezinsky-Kosterlitz-Thouless transition never occurs in these films at low temperatures perhaps as a consequence of quantum fluctuations and quantum tunneling which combine to generate non-zero resistance[76]. When an external field is applied, the resistance is again fit by an Arrhenius form at high temperature with the activation energy changing smoothly from negative to positive as a function of magnetic field. The Arrhenius conduction with negative energy is consistent with the model of vortex motion in a tilted washboard potential due to thermal excitation. At lower temperatures, quantum effects dominate the transport. The resistance flattens out as a function of temperature, a phenomenon which can be explained by macroscopic quantum tunneling of vortices through a tilted washboard potential.

The magnetoresistance peaks of this series film shift to higher magnetic field with increasing thickness. However, the magnetoresistance is still different from previous work on homogeneous *a*-Bi films with thinner *a*-Sb underlayers, which has no magnetoresistance peak at all.

The observed phase transition in the insulating regime and similarity of the behavior to that of a random Josephson junction array in the superconducting regime suggest that isolated superconducting islands or localized Cooper pairs exist in both regimes. However, an AFM scan of the last film has revealed that this series of films although continuous, has a 13% thickness variation on a mesoscopic length scale. Therefore, it is not surprising that there may be superconducting islands in the presence of strong disorder or magnetic fields[36, 38].

On the other hand, the AFM scan also suggests that some of the thick nominal granular films grown by quench condensed deposition do not consist of grains, but are directly connected. which may be similar to the present results, but with larger thickness variations. These insulating granular films also exhibit an Arrhenius type conduction at low temperatures, which reveals the existence of a hard gap in the electronic density of states. The evolution of this hard gap with increasing film thickness is consistent with the theory of Feigel'man *et al.*[17], which suggests that this hard gap is the parity gap due to the localization of Cooper pairs. However, the activation energy of the Arrhenius type conduction found in the thickness tuning homogeneous a-Bi films doesn't follow this model. Therefore, the model may not completely explain this phenomenon.

The morphology of thin films can affect the transport properties in a significant way. In this study, a thickness variation on mesoscopic length scales was found by an AFM scan. The roughness of *a*-Bi films with a thicker underlayer is also larger

than those with thinner underlayers but is smaller than that of nominal granular films. The transport properties also has been found to be different. The insulating regime of films with thicker underlayers has an Arrhenius type conduction and exhibits a magnetoresistance peak while films with thinner underlayers exhibit variable range hopping in the insulating regime. The magetoresistance response in in the superconducting regime is also different in these two types of films. On the other hand, these films with thicker underlayers don't have a local minimum in $R(T)$ in zero field, which is different from typical granular films. Also, the hard gap behaves differently in this two types of films.

In InO_x, TiN, or high-Tc superconductors, there may also be mesoscopic length scale disorder due to variations in chemical composition of the compounds. Therefore, some features in this study such as the magnetoresistance peak and the Arrhenius type of conduction may be similar to what is found in studies of those materials. It is still not clear if an a-Bi film with only atomic level disorder would also exhibit the same features in its transport properties very close to criticality. A systematic and quantitative study is required to investigate how the disorder on a mesoscopic length scale affects the transport properties.

The present study was conducted using DC techniques to probe the transport properties of the films. Although it strongly supports the existence of localized Cooper pairs, measurements with methods that directly probe Cooper pairs or vortices, such as the Ernst effect, are still required. The comparison of the results of different methods may deepen our understanding of localized Cooper pairs and the Bose insulator.

Bibliography

[1] M. Strongin, R. S. Thompson, O. F. Kammerer, and J. E. Crow, Phys. Rev. B **1**, 1078 (1970).

[2] D. B. Haviland, Y. Liu, and A. M. Goldman, Phys. Rev. Lett. **62**, 2180 (1989).

[3] Allen M. Goldman and Nina Markovic, Physics Today, November 1998 p. 39.

[4] Parendo, Kevin A., K.H. Sarwa B. Tan, A. Bhattacharya, M. Eblen-Zayas, N. Staley, and A. M. Goldman, 2005, Phys. Rev. Lett. **94**, 197004.

[5] M. A. Steiner, G. Boebinger, and A. Kapitulnik, Phys. Rev. Lett **94**, 107008 (2005).

[6] V. F. Gantmakher, M. V. Golubov, V. T. Dolgopolov, G.E. Tsydynzhapov, and A. A. Shashkin, Physica B **284-288**, 649 (2000).

[7] G. Sambandamurthy, L. W. Enlgel, A. Johansson and D. Shahar, Phys. Rev. Lett. **92**, 107005 (2004).

[8] Myles Steiner and Aharon Kapitulnik, Physica C **422**, 16 (2005).

[9] T. I. Baturina, A. Yu. Mironov, V. M. Vinokur, M. R. Baklanov, and C. Strunk, Phys. Rev. Lett. **99**, 257003 (2007).

[10] M. A. Palaanen, A. F. Hebard, and R. R. Ruel, Phys. Rev. Lett **69**, 1604 (1992).

[11] G. Sambandamurthy, L. W. Engel, A. Johansson, E. Peled, and D. Shahar, Phys. Rev. Lett. **94**, 017003 (2005).

[12] Valerii M. Vinokur, Tatyana I Baturina, Mikhail V. Fistul, Aleksey Yu. Mironov, Mikhail Baklanov, and Christoph Strunk, Nature **452**, 613 (2008).

[13] M. D. Stewart, Jr., Aijun Yin, J. M. Xu, and J. M. Valles, Jr., Phys. Rev. B **77**, 140501(R) (2008).

[14] N. Markovic, C. Christiansen, A. M. Mack, W. H. Huber, and A. M. Goldman, Phys. Rev. B **60**, 4320 (1999).

[15] L.M. Hernandez and A. M. Goldman, Review of Scientific Instruments **73**.162 (2002).

[16] Kevin A. Parendo, Ph. D. Thesis, University of Minnesota (2006).

[17] M. V. Feigel'man, L. B. Ioffe, V. E. Kravtsov, and E. A. Yuzbashyan, Phys. Rev. Lett. **98**, 027001 (2007).

[18] A. I. Shal'nikov, Nature (London) **142**, 74 (1938).

[19] H. M. Jaeger, D. B. Haviland, B. G. Orr, and A. M. Goldman, Phys. Rev. B **40**, 182 (1989).

[20] Kevin A. Parendo, K. H. Sarwa B. Tan, and A. M. Goldman, Phys. Rev. B **73**, 174527 (2006).

[21] W. Buckel, and R. Hilsch, Z. Phys. **138**, 109 (1954).

[22] M. Kawasaki, K. Takahashi, T. Maeda, R. Tsuchiya, M. Shinohara, O. Ishiyama, T. Yonezawa, M. Yoshimoto, and H. Koinuma, Science **266**, 1540 (1994).

[23] G. Koster, B. L. Kropman, G. J. H. M. Rijnders, D. H. A. Blank, and H. Rogalla, Applied Physics Letters **73**, 2920 (1998).

[24] Melissa Eblen-Zayas, Ph. D. Thesis, University of Minnesota (2006).

[25] M. P. A. Fisher, Phys. Rev. Lett. **65**, 923 (1990).

[26] M. A. Paalanen, A. F. Hebard, and R. R. Ruel, Phys. Rev. Lett. **69**, 1604 (1992).

[27] V. F. Gantmakher *et al.*, JETP Lett **68**, 363 (1998).

[28] Y. J. Lee, Y. S. Kim, E. N. Bang, H. Lim, and H. K. Shin, J. Phys: Condens Matter. **13**, 8135 (2001).

[29] T. I. Baturina, A.Yu. Mironov, V. M. Vinokur, M. R. Baklanov, and C. Strunk, Phys. Rev. Lett. **99**, 257003 (2007), T. I. Baturina, D. R. Islamov, J. Bentner, C. Strunk, M. R. Balkanov, and A. Satta, JETP Lett. **79**, 337 (2004).

[30] M. Steiner and A. Kapitulnik, Physica C **422**, 16 (2005); Myles A. Steiner, Nicholas P. Breznay, and Aharon Kapitulnik, Phys. Rev. B **77**, 212501 (2008).

[31] D. Shahar and Z. Ovadyahu, Phys. Rev. B **46**, 10917 (1992).

[32] D. Kowal and Z. Ovadyahu, Solid State Commun. **90**, 783 (1994).

[33] Yen-Hsiang Lin and A. M. Goldman, unpublished.

[34] H. Q. Nguyen, S. M. Hollen, M. D. Stewart, Jr., J. Shainline, Airjun Yin, J. M. Xu, and J. M. Valles, Jr. Phys. Rev. Lett. **103**, 157001 (2009); M. D. Stewart, Jr., A. Yin, J. M. Xu, and J. M. Valles, Jr., Science **318**, 1273 (2007).

[35] N. Markovic, A. M. Mack, G. Marines-Arizala, C. Christiansen, and A. M. Goldman, Phys. Rev. Lett. **81** 701 (1998).

[36] Amit Ghosal, Mohit Randeria, and Nandini Trivedi, Phys. Rev. B **65**, 014501 (2001).

[37] Victor M. Galitski, G. Refael, Matthew P. A. Fisher, and T. Senthil, Phys. Rev. Lett. **95** 077002 (2005).

[38] Y. Dubi, Y. Meir, and Y. Avishai, Nature **449**, 876 (2007).

[39] M. Muller, Ann. Phys. (Berlin) **18**, 849 (2009).

[40] A. Kramer and S. Doniach, Phys. Rev. Lett. **81** 3523 (1998).

[41] W. Wu, and P. W. Adams, Phys. Rev. B **50**, 13065 (1994).

[42] E. Bielejec, J. Ruan, and W. Wu, Phys. Rev. B **63**, 100502(R) (2001).

[43] C. Christiansen, L. M. Hernandez, and A. M. Goldman, Phys. Rev. Lett. **88**, 037004 (2002).

[44] R. P. Barber, Jr., Shih-Ying Hsu, J. M. Valles, Jr., R. C. Dynes, and R. E. Glover III, Phys. Rev. B **73**, 134516 (2006).

[45] M. Ovadia, B. Sace´pe´, and D. Shahar, Phys. Rev. Lett. **102**, 176802 (2009).

[46] Kevin A. Parendo, K. H. Sarwa B. Tan, and A. M. Goldman, Phys. Rev. B **74**, 134517 (2006).

[47] Keithley 2182A nanovoltmeter user manual, Keithly Instruments Inc., Cleveland (2004).

[48] M.Yu. Reizer, Phys. Rev. B **40**, 5411 (1989).

[49] F. C. Wellstood, C. Urbina, and John Clarke, Phys. Rev. B **49**, 5942 (1994).

[50] A. Sergeev and V.Mitin, Phys. Rev. B **61**, 6041 (2000).

[51] F.Giazotto *et al*., Rev. Mod. Phys. **78**, 217 (2006).

[52] M.Yu. Reizer and A.V. Sergeev, Sov. Phys. JETP **63**, 616 (1986).

[53] B. Altshuler, V. Kravtsov, I. Lerner, and I. Aleiner, following Letter, Phys. Rev. Lett. **102**, 176803 (2009).

[54] A. Schmid, Z. Phys. **271**, 251 (1974).

[55] D. Kalok, A.Bilu˘si´c, T. I. Baturina, V.M. Vinokur, and C. Strunk, unpublished, arXiv1004.5153 (2010).

[56] D. Ephron, A. Yazdani, and M. R. Beasley, Phys. Rev. Lett. **76**, 1529 (1996).

[57] J. A. Chervenak and J. M. Valles, Jr., Phys. Rev. B **61**, R9245 (2000).

[58] W. R. White, A. Kapitulnik, and M. R. Beasley, Phys. Rev. Lett. **70**, 670 (1993).

[59] N. Mason, and A. Kapitulnik, Phys.Rev. Lett. **82**, 5341 (1999).

[60] Yongguang Qin, Carlos L. Vicente, and Jongsoo Yoon, Phys. Rev. B **73**, 100505 (2006).

[61] B. Sacepe, C. Chapelier, T. I. Baturina, V. M. Vinokur, M. R. Baklanov, and M. Sanquer, Phys. Rev. Lett. **101**, 157006 (2008).

[62] Y. Imry, M. Strongin, and C. C. Homes, Physica C **468**, 288 (2008).

[63] B. D. Josephson, Phys. Lett. **1**, 251 (1962); Adv. Phys. **14**, 419 (1965).

[64] Michael Tinkham, " Introduction to Superconductivity", 2nd Edition, McGraw-Hill Inc., New York, (1996).

[65] J. M. Kosterlitz and D. J. Thouless, J. Phys. C **6**, 1181 (1973).

[66] M. R. Beasley, J. E. Mooij, and T. P. Orlando, Phys. Rev. Lett. **42**, 1165 (1979).

[67] B. I. Halperin and David R. Nelson, Journal of Low Temp. Phys. **36**, 599 (1979).

[68] H.S.J. van der Zant, F. C. Fritschy, T. P. Orlando, and J. E. Mooij, Phys. Rev. Lett. **66**, 2531 (1991).

[69] C. J. Lobb, David W. Abraham, and M. Tinkham, Phys. Rev. B **27**, 150 (1983).

[70] M. Iansiti, M. Tinkham, A.T. Johnson, Walter F. Smith, and C. J. Lobb, Phys. Rev. B **39**, 6465 (1989).

[71] Hermann Grabert, Peter Olschowski, and Ulrich Weiss, Phys. Rev. B **36**, 1931 (1987).

[72] M. Iansiti, A. T. Johnson, C. J. Lobb, and M. Tinkham, Phys. Rev. B **40**, 11370 (1989).

[73] M. Buttiker, E. P. Harris, and R. Landauer, Phys. Rev. B **28**, 1268 (1983).

[74] T. S. Tighe, A. T. Johnson, and M. Tinkham, Phys. Rev. B **44**, 10286 (1991).

[75] H. S. J. van der Zant, W. J. Elion, L. J.Geerligs, and J. E. Mooij, Phys. Rev. B **54**, 10081 (1996).

[76] Aleksandra Petkovic, Valerii M. Vinokur, and Thomas Nattermann, Phys. Rev. B **80** 212504 (2009).

[77] Lit-Deh Chang and Sudip Chakravarty, Phys. Rev. B **29** 130 (1984).

[78] Yen-Hsiang Lin, A. M. Goldman, arXiv 1002.1720 (2010).

[79] S. Doniach, Phys. Rev. B **24**, 5063 (1981).

[80] A. M. Finkel'stein, Physica B **197**, 636 (1994).

[81] V. F. Gantmakher and V. T. Dolgopolov, Uspekhi Fizicheskikh Nauk **180**, 3 (2110); arXiv:1004.3761.

[82] M. V. Feigel'man, L. B. Ioffe, V. E. Kravtsov, E. Cuevas, arXiv:1002.0859v2 (2010).

[83] K. A. Matveev and A. I. Larkin, Phys. Rev. Lett. **78**, 3749 (1997).

[84] P. W. Anderson, J. Phys. Chem Solids **11**, 26 (1959).

[85] Yen-Hsiang Lin and A. M. Goldman, unpublished. M. F. Barnsley, R. L. Devaney, B. B. Mandelbrot, H.-O. Peitgen, D. Saupe, and R. F. Voss,with contribution by Y. Fisher, and M. McGuire, *The Science of Fractal Images*, page65-70 (Springer-Verlag, New York, 1988).

[86] Kevin A. Parendo, K. H. Sarwa B. Tan, and A. M. Goldman, Phys. Rev. B **76** 100508 (2007).

[87] Arthur R. Mcgurn and Alexei A. Maradudin, Phys. Rev. B **30**, 3136 (1984).

[88] D. A. Parshin and H. R. Schober, Phys. Rev. Lett. **83**, 4590 (1999).

[89] A. Mildenberger, F. Evers, and A. D. Mirlin, Phys. Rev. B **66**, 033109 (2002).

[90] Alice E. White, R. C. Dynes and J. P. Garno, Phys. Rev. B **33**(R) 3549 (1986).